12-2022

Multi-Criteria Performance Evaluation and Control in Power and Energy Systems

Payam Ramezani Badr
Clemson University, prameza@clemson.edu

Multi-criteria Performance Evaluation and Control in Power and Energy Systems

---

A Dissertation
Presented to
the Graduate School of
Clemson University

In Partial Fulfillment
of the Requirements for the Degree
Doctor of Philosophy
Electrical Engineering

---

by
Payam Ramezani Badr
December 2022

Accepted by:
Dr. Christoper Edrington, Committee Chair
Dr. Zheyu Zhang
Dr. Robert Prucka
Dr. Johan Enslin
Dr. Gokhan Ozkan

Abstract

The role of intuition and human preferences are often overlooked in autonomous control of power and energy systems. However, the growing operational diversity of many systems such as microgrids, electric/hybrid-electric vehicles and maritime vessels has created a need for more flexible control and optimization methods. In order to develop such flexible control methods, the role of human decision makers and their desired performance metrics must be studied in power and energy systems. This dissertation investigates the concept of multi-criteria decision making as a gateway to integrate human decision makers and their opinions into complex mathematical control laws. There are two major steps this research takes to algorithmically integrate human preferences into control environments:

- MetaMetric (MM) performance benchmark: considering the interrelations of mathematical and psychological convergence, and the potential conflict of opinion between the control designer and end-user, a novel holistic performance benchmark, denoted as MM, is developed to evaluate control performance in real-time. MM uses sensor measurements and implicit human opinions to construct a unique criterion that benchmarks the system's performance characteristics.

- MM decision support system (DSS): the concept of MM is incorporated into multi-objective evolutionary optimization algorithms as their DSS. The DSS's role is to guide and sort the optimization decisions such that they reflect the best outcome desired by the human decision-maker and mathematical considerations.

A diverse set of case studies including a ship power system, a terrestrial power system, and a vehicular traction system are used to validate the approaches proposed in this work. Additionally, the MM DSS is designed in a modular way such that it is not specific to any underlying evolutionary optimization algorithm.

Dedication

I dedicate this work to my mother who had to write her own Ph.D. dissertation while raising two difficult children. My efforts pale in comparison to her sacrifice and unwavering determination.

-Payam

Acknowledgments

I would like to thank my academic adviser and first professional mentor, Dr. Christopher S. Edrington, for his expertise and guidance that made my Ph.D. experience and this dissertation possible.

I would also like to thank the other members of the committee for agreeing to review this dissertation and provide their invaluable insights.

Contents

List of Tables

List of Figures

Chapter 1

Introduction

Nomenclature

MCDM	Multi-Criteria Decision Making
MOO	Multi-Objective Optimization
EMO	Evolutionary Multi-objective Optimization
SOO	Single-Objective Optimization
DM	Decision-Maker
DSS	Decision Support System
PF	Pareto optimal Front
EED	Environmental/Economic Dispatch
VEGA	Vector-Evaluated Genetic Algorithm
AHP	Analytic Hierarchy Process
MACBETH	Measuring Attractiveness by a Categorical Based Evaluation TecHnique
MOGA	Multi-Objective Genetic Algorithm
NPGA	Niched Pareto Genetic Algorithm
NSGA	Non-dominated Sorting Genetic Algorithm
SPEA	Strength Pareto Evolutionary Algorithm
PAES	Pareto Archived Evolutionary Strategy
EM	Energy Management
MG	Micro-Grid
CQGA	Chaotic Quantum Genetic Algorithm
MLCDE	Multi-cross Learning based Chaotic Differential Evolution
PSO	Particle Swarm Optimization
MOPSO	Multi-Objective Particle Swarm Optimization
CSA	Crow Search Algorithm
MOCSA	Multi-Objective Crow Search Algorithm
MADS	Mesh Adaptive Direct Search
SPS	Ship Power System
EV/HEV	Electric and Hybrid Electric Vehicles

1.1 Overview

This chapter is about motivating the dissertation, literature review, introduction of some fundamental definitions/terminologies and presenting the intended research contributions and their value to the existing literature. More specifically, Section 1.2 motivates the research by introducing some preliminary facts and generic examples. Section 1.3 introduces MOO and some of its relevant fundamental concepts and definitions. Section 1.4 expands on a MOO sub-category called EMO, and the specific terminologies and literature that are behind it. Section 1.5 investigates the primary application focus of this dissertation, i.e., autonomous control, and presents the relevant research gaps in the area that motivated the studies herein. Section 1.6 breaks down the intended state-of-the-art and why they are a useful addition to the existing literature.

1.2 Motivation

The task of decision making is one of the fundamental actions in life. An average adult person makes approximately 2,000 to 35,000 decisions per day [79]. Decisions are made based on the available information and their processing to achieve some desired objective(s). Although everyday decisions such as where to eat lunch do not involve complex information processing, there are high-stake decisions that should be made with maximum precision to achieve optimal outcomes. For example, a multi-billion dollar hedge fund cannot afford to make investment decisions without analyzing the alternatives using mathematical models and scientific approaches. However, mathematical models are not the only determinant in decision making, because psychological preferences also play a role in the ultimate outcome. The relationship between mathematical and psychological convergence in MCDM has been extensively studied in the literature [14, 94, 93, 136, 139]. MCDM is the science of studying decision making problems with multiple conflicting objectives (or goals or criteria). MCDM covers both discrete problems with a finite set of alternatives, also denoted as actions or solutions, and continuous problems, i.e., MOO. Preference models that articulate the "opinions" of DMs are used to support the underlying substantive process and select the most preferred optimal outcome. MOO can also be used in autonomous controllers that implement some type of optimization in power and energy systems. Additionally, there are usually multiple conflicting goals in MOO which adds to the complexity of finding the optimal outcome due to performance trade-offs. In this dissertation, there are two general areas where performance trade-offs are investigated with respect to power and

energy systems: 1) performance evaluation (benchmark), and 2) autonomous control.

1.3 Multi-objective optimization

Optimization is the process of finding one or more solutions that minimize (or maximize) one or more objectives subjected to the applied constraints (if any). A SOO problem, as the name suggests, includes a single objective function with usually a single optimal solution. On the other hand, a MOO simultaneously considers several conflicting objectives. There is usually no single optimal solution in MOO, rather a set of solutions resulting in different performance trade-offs, called "Pareto optimal" solutions, or "non-dominated" solutions. Despite having several Pareto optimal solutions, in practice, usually only one must be chosen at the end for a given MOO problem. Therefore, there are two equally important tasks in MOO: 1) an optimization process to find the Pareto optimal solutions, and 2) a DSS to choose the single most preferred solution. The latter task typically necessitates DM preference articulation [14]. The general form of a MOO and some background definitions are provided as follows [10, 14].

$$\begin{cases} \min \mathbf{f}(\mathbf{x}) := \min\{f_k(\mathbf{x})\} & k = 1 : K \\ g_p(\mathbf{x}) \geq 0 & p = 1 : P \\ h_q(\mathbf{x}) = 0 & q = 1 : Q \\ x_i^L \leq x_i \leq x_i^U & i = 1 : I \end{cases}$$

Where $\mathbf{f}$ is the objective functions vector, $\mathbf{x}$ is the solution vector, $g(\mathbf{x})$ are the inequality constraints, and $h(\mathbf{x})$ are the equality constraints. Also, each element of $\mathbf{x}$, i.e., x_i is subject to upper (x_i^U) and lower (x_i^L) bounds when applicable. All $\mathbf{x}$ that satisfy the applied constraints are said to belong to the "feasible region" ($\mathcal{S}$). Furthermore, the image of $\mathcal{S}$ in the objective space is called the "feasible objective region" ($\mathcal{Z}$), i.e., $\mathcal{Z} := \{\mathbf{f}(\mathcal{S})\}$. The following definitions or their representations in the objective space are shown for an arbitrary bi-objective convex problem in Figure 1.1

Definition 1.3.1 (Pareto dominance)**.** A solution $\mathbf{x}^1 \in \mathcal{S}$ is said to dominate another solution $\mathbf{x}^2 \in \mathcal{S}$ (denoted $\mathbf{x}^1 \succeq \mathbf{x}^2$), if and only if, $f_k(\mathbf{x}^1) \leq f_k(\mathbf{x}^2)$ for all $k = 1 : K$, and $f_k(\mathbf{x}^1) < f_k(\mathbf{x}^2)$ for at least one k.

Definition 1.3.2 (Pareto optimality)**.** A solution vector $\mathbf{x}^* \in \mathcal{S}$ is said to be Pareto optimal, if

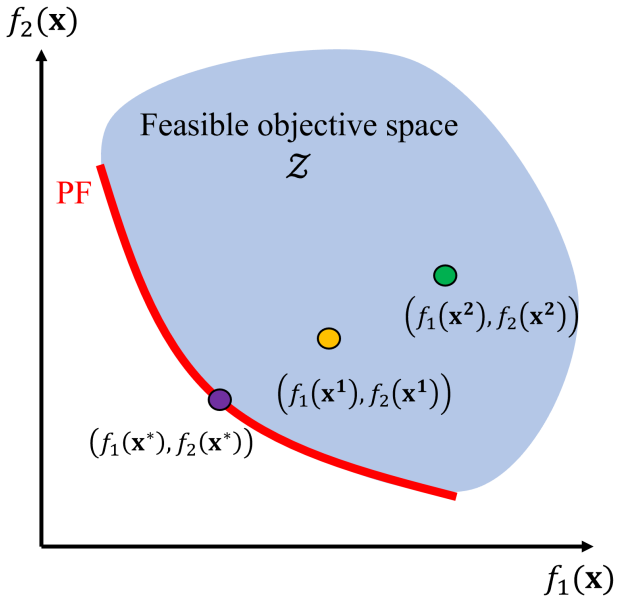

Figure 1.1: Key MOO definitions illustrated for an arbitrary bi-objective convex objective space example.

there does not exist another $\mathbf{x} \in \mathcal{S}$ such that $f_k(\mathbf{x}) \leq f_k(\mathbf{x}^*)$ for all $k = 1 : K$, and $f_k(\mathbf{x}) < f_k(\mathbf{x}^*)$ for at least one k.

Definition 1.3.3 (Pareto optimal set)**.** The set of all solution vectors that satisfy the Pareto optimality condition is the Pareto optimal set $\mathcal{P} := \{\mathbf{x}^* \in \mathcal{S} \mid \nexists\, \mathbf{x} \in \mathcal{S} \text{ s.t. } \mathbf{f}(\mathbf{x}) \leq \mathbf{f}(\mathbf{x}^*)\}$.

Definition 1.3.4 (Pareto optimal front)**.** The image of $\mathcal{P}$ in the objective space is the Pareto optimal front $PF := \{\mathbf{f}(\mathcal{P})\}$.

Realistically, most optimization problems have multiple often conflicting objectives. For example, in an electrical machine design problem, production cost is not the only objective, and other variables such as power output, reliability and quality must be considered. As a result, different objectives are often redefined to provide an equivalent cost, thereby artificially reducing the number of conflicting goals into a single goal. However, the correlation between different objectives is usually complex and dependent on the available alternatives. Also, various objectives are typically "non-commensurable", meaning they are not measured with the same unit, so aggregating them into one synthetic objective is not always straightforward. Additionally, it is difficult to guess the appropriate trade-off between different objectives *a priori*, that is before some or all Pareto optimal solutions are found. Thus, an appropriate DSS is necessary to help the DM find the most preferred

solution, such that the DM is convinced of its relative goodness. Arguably the biggest advantage of MOO compared to SOO is the addition of a DSS that can find better solutions, i.e., solutions that are optimal with respect to multiple objectives and DM preferences.

However, having a DSS comes with an increased complexity which can limit the extent of its integration in time-sensitive applications. In problems such as navigation, industrial design, urban planning, investment, etc. there is usually either no time limit or the time limit is large enough that it cannot interfere with the algorithm's execution. On the other hand, autonomous control applications are time-sensitive, such that DSS and DM participation should not interfere with the timing constraints. Historically, this practical issue has been an obstacle for researchers and engineers to fully utilize MOO in autonomous control of power and energy systems. This issue will be further investigated in Section 1.5.

MOO methods can be sorted into four general categories depending their DSS (or lack thereof): 1) no-preference, 2) *a priori*, 3) *a posteriori*, and 4) interactive [93]. Additionally, there are two basic MOO methods, i.e. the weighting method [145, 55], and the ϵ-constrained method [59, 21], which do not fall into any specific category since they do not have a well-defined DSS. The basic methods are commonly used in many problems without necessarily being recognized as MOO methods.

1.3.1 No-preference

As the name would suggest, no-preference MOO methods do not have a DSS that incorporates DM preferences into the optimization process. Therefore, the MOO task is simplified to find neutral compromise solutions and the ultimate decision is made based on some assumptions. This is the most commonly applied MOO in autonomous control applications due to its minimal complexity. The assumptions on which the compromise solutions are found are considered to be time-invariant by the control designer. This assumption is valid for power and energy systems that have invariable operational requirements such as factory assembly line machines. However, optimal trade-off performances are not time-invariant in systems that are expected to operate in versatile and unpredictable situations such as military vehicles or maritime vessels. The method of global criterion [147, 144], and the neutral compromise solution [140] are two of the most well-known MOO methods in this category.

1.3.2 *a priori*

In *a priori* methods, the DSS requests preference information from the DM before the mathematical task of the optimization begins. The DM is asked to articulate their opinions (or aspirations) in the form of intuitive or quantitative inputs. Then, the DSS guides the MOO to find Pareto optimal solutions that best satisfy DM preferences. This is a relatively straightforward DSS to model and implement, but the problem is that the DM is asked to make a judgment before knowing the alternatives. *a priori* methods put the DM at a disadvantage in expressing uninformed preferences that are either too optimistic or pessimistic. Uninformed preferences might guide MOO to converge to a Pareto optimal set that excludes solutions which could have been interesting to the DM. The value function method [75], Lexicographic ordering [50, 116], and goal programming [22, 23, 24] are examples of *a priori* MOO methods.

1.3.3 *a posteriori*

MOO algorithms that generate a representation of the Pareto optimal set and provide it to the DSS for DM preference input are called *a posteriori*. DM is tasked with selecting their most preferred solution based on the generated Pareto optimal set. The advantage of *a posteriori* methods is that they provide the DM with an overview of what is mathematically possible so the DM can make informed judgments. In MOO problems that have more than two objectives, it becomes harder and slower to generate a comprehensible representation of the Pareto optimal set for the DM. Higher the number of objectives in a given MOO problem, harder it is to visualize the information necessary for a DM to make a preference judgment. EMO algorithms typically belong to this category of MOO. However, EMOs have some distinctive features compared to other MOO methods; thus, they are introduced as a separate class in Section 1.4. Some methods belonging to *a posteriori* MOO category are: 1) weighted metrics [147, 126], 2) achievement scalarizing function [137, 138, 88], and 3) approximation methods [117, 87].

1.3.4 Interactive

The most extensive class of MOO are the interactive methods, which are also the most challenging to develop and implement. In interactive MOO, an iterative solution pattern is generated and repeated. After each iteration, some information is provided to the DM through the DSS to

specify their preferences. Thus, the DM is actively engaged with the MOO task as it is happening. Note that the DM can specify and adjust their preferences between each iteration and learn about the inter-dependencies of different objectives and preferences in the problem. Interactive methods are superior to others in maximizing DSS effectiveness in finding the most mathematically and psychologically optimal solution. The ordinal regression method [70], its augmentations [58, 49], AHP [118], and MACBETH [42] are some of the most well-known interactive MOO approaches.

The underlying assumption in interactive methods is that a DM is available at all times to engage with the MOO process, and that there is no time limit for the algorithm's execution. Interactive methods are not suitable for autonomous control applications unless there is an approach where the DSS manages the MOO task with DM preferences whenever they become available. Such an approach must have a DSS with no-preference, *a priori*, and *a posteriori* properties, as well as interactive properties whenever a DM is available to make judgments. This dissertation is primarily focused on motivating and developing such a DSS, first for performance evaluation, and then control in power and energy systems.

1.4 Evolutionary multi-objective optimization

EMO are technically a sub-category of MOO, but because of extensive research in this area throughout the years EMO are treated distinctively in the literature. EMO processes attempt to find a set of well-distributed discrete Pareto optimal points, such that the extent and shape of the PF can be obtained. EMO algorithms use a population-based approach where multiple initial solutions iteratively evolve into a new population of solutions. EMO methods are popular because: 1) they do not require any derivative information, 2) they are relatively simple to implement, and 3) they are flexible and have a wide range of applications [14, 31].

Usually, an EMO begins its search process with an initial population of solutions that are created at random within a specified constraint for each decision variable. If there are no constraints in the problem, some reasonable values can be assumed for the initialization. Then, the EMO starts an iterative operation of updating the population of solutions by using four main operators: selection, crossover, mutation, and elite-preservation. The operation stops only when one or more termination criteria are satisfied. If some knowledge of good solutions is available, it is better to use such information in creating the initial population [33]. Here are some fundamental definitions

specific to EMO literature.

Definition 1.4.1 (Evolutionary algorithm)**.** Algorithms that stochastically apply the evolutionary concept of Darwinian survival-of-the-fittest, and genetically motivated recombination/mutation principles to a population of solutions to iteratively generate a new and (hopefully) better population of solutions in the context of stationary or dynamic fitness landscapes such as optimization problems.

Definition 1.4.2 (Crossover/recombination)**.** An operator in evolutionary algorithms where two or more solutions are used to create, through recombination, one or more new solutions.

Definition 1.4.3 (Mutation)**.** An operator applied to a single solution to create a new modified solution. The fundamental difference with the crossover operator is that mutation is applied to a single solution, while crossover is applied to more than one.

Definition 1.4.4 (Niching)**.** Niching is an operator in evolutionary algorithms that controls the significance of population members so as to not allow a single solution to take over the entire population. Therefore, niching enables the generation of a diverse solution population.

Definition 1.4.5 (Elitism)**.** An operator in evolutionary algorithms which selects and preserves the better solutions among old and new populations in an archive.

Definition 1.4.6 (Fitness)**.** Fitness is a function created from objective function(s), applied constraint(s), and other information (e.g., DM preferences) which is used in the selection process of an evolutionary algorithm. A fitness function is usually the judge that determines which solution is better.

Similar to other *a posteriori* MOO methods, EMO works based on the following principles: 1) generating multiple non-dominated and well-distributed solutions that are as close to the PF as possible, and 2) select one of the generated solutions using the information obtained from the DSS. The main difference and advantage of EMO compared to classical *a posteriori* MOO methods is that many trade-off solutions can be found in a one simulation run, in contrast to several simulations in most *a posteriori* methods [14]. Historically, evolutionary algorithms, including EMO, are criticized for their lack of theoretical trustworthiness compared to classical gradient-based approaches. However, reference [34] shows that an EMO that starts from randomized non-optimal solutions can eventually progress toward solutions that satisfy the Karush-Kuhn-Tucker (KKT) optimality criteria [93, 109].

How well and how fast an EMO can generate solutions that meet the KKT criteria is dependent on: 1) the underlying evolutionary algorithm's performance, and 2) the DSS' ability to properly guide the process.

Generally, EMO are divided into two main categories of a) non-Elitist methods, and b) Elitist methods [10, 14]. Elitist methods include an elitism operator in their algorithm which means older but better solutions are preserved in an archive, and cannot be replaced by newer but worse solutions.

1.4.1 Non-Elitist methods

In the early days of MOO, researchers resorted to basic weighted-sum approaches to convert MOO into SOO and solve them via an evolutionary algorithm [113, 112, 51]. Later, a method named VEGA was proposed in [120]. VEGA modifies the original three operator GA, i.e., selection, crossover, and mutation, by performing independent selection cycles for each objective. More specifically, VEGA divides the solution population into multiple equally sized sub-populations. Then, the selection operation is done in each sub-population by only considering one objective at a time. Once the selection operation is finished, the sub-populations are combined to apply the other operators, i.e., crossover, and mutation. The biggest issue in VEGA is that it prefers the optimal solutions for each specific objective; thus, neglecting good trade-off solutions. However, this shortcoming in VEGA was later improved in [110], and it was also shown that VEGA has similar performance characteristics with the weighted-sum approach.

Another non-elitist method is the MOGA, which was originally introduced in [52]. MOGA was the first EMO algorithm that used ranking and niching techniques together to guide the search toward the true PF, and generate well-distributed solutions. The problem with MOGA is that it has a sometimes conflicting ranking/fitness criteria that causes the algorithm to prefer poorer but less densely populated solutions over better but more crowded ones. Thus, MOGA's performance is highly dependent on the specifics of the optimization problem.

NPGA [67], and NSGA [125] are two other well-known non-elitist methods. Although non-elitist methods differ from one another usually in one or two operator mechanics, their common trait of not memorizing suitable solutions from previous iterations negatively impacts their performance.

1.4.2 Elitist methods

Elitist methods memorize some solutions in each iteration such that they cannot be replaced by newer but weaker ones. Thus, elitist EMO algorithms have a monotonically non-degrading performance [14]. There are many different elitist EMO algorithms proposed throughout the years, but some notable ones are introduced in here. Note that essentially all evolutionary algorithms can be modified for EMO problems; however, some algorithms provide better overall performance than others.

SPEA [154] suggested the creation of an external archive to store all non-dominated solution found so far in each iteration. Then, a fitness score is assigned to the combination of the current non-dominated solutions with the ones stored in the archive. The fitness score of each non-dominated solution is proportional to the number of solutions they dominate. Diversity of solutions is maintained via clustering and a constant size archive.

PAES [78] is another elitist EMO algorithm that is based on the (1+1) evolution strategy [41]. PAES also uses an external archive with a pre-specified size to preserve previously found non-dominated solutions. After random initialization, a new solution (child) is generated from a previous one (parent); then, they are compared with each other. If the child dominates the parent, the child is accepted as the parent for the next iteration. If the parent dominates the child, the child is eliminated and a new mutation is performed to generate another child. However, if the child and the parent do not dominate one another, the survival choice is carried out using a crowding process. The non-dominated solutions found so far are stored in the archive to preserve diversity. Next, the child is compared with the members of the archive to check if it dominates any solution stored in there. If yes, the child is accepted as the new parent and the dominated solution(s) is removed from the archive. If the child does not dominate any member of the archive, both parent and child are checked for their Euclidean distance (in the objective space) with the archive members. If the child is in the least crowded area of the objective space compared to the archive members, it becomes a parent and is added to the archive.

The elitist augmentation of NSGA, named NSGA-II, was proposed in [32]. They key characteristics of NSGA-II are its elitist operator, explicit diversity preserving mechanic, and emphasis on non-dominated solutions. The idea behind NSGA-II is to merge the current population of solutions with the previous one; then, this pool of solutions is partitioned into multiple non-domination fronts

where the next iteration of solutions is sequentially filled by points from these fronts.

1.5 Multi-objective autonomous control

So far some of the most prominent theoretical developments of MOO (and EMO) in the literature was reviewed. In this section, the history of MOO in autonomous control of power and energy systems is investigated.

EM is a category of autonomous control in power and energy systems. EM is tasked with optimal dispatch and allocation of available energy resources in the system. Usually, EM is a SOO that is carried out with respect to the monetary cost of generating energy. Most of MOO research for EM is focused on EED in power distribution systems [4, 100, 143, 63, 96, 82]. However, there are some exceptions in the choice of objectives. For example, the authors in [151] considered power generation cost and battery health in MOO for EM in islanded MGs.

Reference [4] uses SPEA to solve the EED as a EMO problem with some modifications: 1) Addition of a feasibility check on the initial population of solutions to guarantee constraint requirements in each run. 2) A population merging procedure similar to NSGA-II is added to find more non-dominated solutions in the next generation. 3) A fuzzy logic DSS is used to find the best compromise solution. However, no details are provided on how the DM preferences are integrated into the DSS, and how these preferences would affect the outcome of their algorithm. If there are no DM preferences; then, the DSS will select the final solution based on the best mathematical compromise which will be always on the center of the PF. As previously discussed, no-preference assumption is not necessarily true depending on operational circumstances.

In [143], the EED problem of a MG is transformed into a Markovian process based around the intermittent nature of PV resources. Then, a mixed-integer MOO problem is formulated with energy cost and carbon tax objectives. The MOO problem is solved using branch-and-cut optimization algorithm. Additionally, the authors also propose a MG design MOO. Despite the comprehensive nature of this study with respect to operation and design of MGs, the authors do not address performance trade-offs that arise in MOO problems. Lack of context around the role of DM in the MG operation creates the assumption that only mathematical compromise was considered.

The work in [82] uses a quantum computing concept-based evolutionary algorithm named CQGA to solve the EED problem in MGs. CQGA combines the quantum probability vector encoding

mechanism and the GA crossover strategy to improve the global search ability and escape the local Pareto optimal regions by using chaotic algorithms [74]. The authors in this work also fail to investigate the DM's role and preferences in the MG's operation. Additionally, this research work used the word "best" often but do not give much information about what criteria determines the "best" solutions in their utilized fitness function. This hints that an underlying trade-off assumption is embedded in CQGA instead of a DSS; thus, there is no flexibility in modifying the preference options.

Hemmati *et al* [63] proposed a method named MLCDE to solve the EED problem in islanded MGs. MLCDE is shown to have superior search abilities in finding non-dominated solutions compared to some well-known algorithms such as PSO due to its chaotic operator and learning capabilities. Additionally, the authors included a binary handling process to distinguish between continuous and discrete decision variables, and reduce the optimization's computational time. However, the EED objective function is simply the summation of cost and emission (carbon tax) over a specified time period. Therefore, the proposed MLCDE algorithm is essentially a SOO.

MADS evolutionary optimization technique is another method that was employed in [96] to solve the EED problem. The authors claim that the MADS is suitable for non-linear, non-convex and discontinuous decision spaces which allowed them to include a comprehensive set of constraints and multi-order formulations into MADS. However, similar to [63], the MADS technique merely uses the summation of cost and emission objective functions and ignores performance trade-off customization and DSS.

The NSGA-II algorithm is employed by Zhao *et al* [151] to solve a bi-objective optimization in MGs with respect to operating costs and battery aging objectives. This study uses an intuitive *a posteriori* weighted-sum approach to select the final solution within the Pareto optimal set. The authors first generated five Pareto optimal solutions using NSGA-II; then, individually evaluated each solution in the objective space, and used equal weights to select one out of the available five options. There are some downsides to this approach: 1) The objective weighting combinations are explicit and infinite, but they are chosen implicitly by the DM. 2) The weighted objective is not integrated with the algorithm to guide its search space for the next cycle. The former item limits the justification for the choice of weights. For example, if the DM thinks both objectives are equally important; then, a 50-50 weighting split is justified, but if the DM favors one objective over the other, there is no DSS to process this intuitive thinking to appropriate explicit weights. Also, lack of a

feedback mechanism reduces the efficiency of the NSGA-II optimization as the preference information is not used to generate more desirable solutions in the next cycle.

1.6 State-of-the-art

Based on what was discussed in Section 1.5, there are some research gaps in MOO/EMO research in autonomous control of power and energy systems. The most notable missing element between the control application and MOO/EMO theories is the effective incorporation of DM preferences into the optimization process through a DSS. The lack of interest to utilize DM preferences in autonomous control can be summarized into two reasons: 1) The assumption that the most balanced mathematically optimal operation is desired at all times in all power and energy systems. 2) Additional computational burden and programming that can jeopardize the timely execution of control decisions. However, the first assumption is not valid in many applications that have dynamic operational requirements such as Navy SPS, and vehicular power trains. It can also be argued that the solution to the EED problem in MGs is not necessarily balanced at all times. For example, a MG operator may desire to reduce more energy production cost at the expense of more emission in certain times of the day, or vice versa.

Power and energy systems and their autonomous control are designed to ultimately service human customers. Many consumer products such as smart phones and cars already include a certain level of customization that usually appear in the form of performance options. For example, many modern cars allow the driver to choose between standard, economy, and high-performance driving experiences. Assuming that the human end-user is also the DM[1], it must be considered that their opinion is implicit and non-expert. This means that a preference interface must be able to infer implicit opinions to make the necessary adjustments without damaging the technical performance of the system.

Therefore, this dissertation capitalizes on the missing elements of MOO/EMO research in autonomous control of power and energy systems in two steps:

- Development of a *in-situ* benchmark for non-expert human DMs to assist them in monitoring and evaluating the performance of power and energy systems.

[1]DM is not necessarily the end-user. An artificial intelligence, sometimes dubbed an "analyst" can also be the DM. This topic is out-of-scope, so the assumption is made that the DM and the end-user are one and the same.

- Developing a new DSS and integrating it into different EMO algorithms in several applications, e.g., terrestrial power systems, Navy SPS, and traction motors of EV/HEV.

The scope of this research work is not limited to a certain optimization algorithm nor any specific system, that is why the proposed DSS is validated for two different EMO algorithms, i.e., MOCSA and MOPSO, in different power/energy systems. However, the dissertation is focused on the EMO category instead of classical MOO due to their popularity in autonomous control. It must be noted that with certain modifications, the contributions of this dissertation can be extended to classical MOO which is a potential subject for future research.

Chapter 2

MetaMetric: A Holistic Multi-Objective Criterion

Nomenclature

DIWA	Dynamic Implicit Weighting Approach
MOO	Multi-Objective Optimization
EMO	Evolutionary Multi-objective Optimization
DSS	Decision Support System
ROI	Region Of Interest
PF	Pareto optimal Front
DM	Decision-Maker
MM	MetaMetric
NSGA	Non-dominated Sorting Genetic Algorithm

2.1 Overview

This chapter starts by familiarizing the readers with "metrics" and "normalized metric" based on some of the existing works in the literature (Section 2.2). Next, "preference articulation" is introduced as a fundamental part of DSS, and a new method, denoted DIWA, is presented after reviewing some of the well-known methods in Section 2.3. Relevant discussions are made on how DIWA compares to other preference articulation methods, and why it is better suited for autonomous control applications. The MM benchmark methodology is presented in Section 2.4.

2.2 Normalized metrics

Performance metrics are observable criteria with which a system's performance can be quantified[1]. There are a variety of performance metrics in power and energy systems depending on the application. For example, mean-squared error of the desired speed and the actual speed in a traction motor is a potential performance metric. Voltage deviation, i.e., the absolute difference between the nominal voltage level and the measured voltage level is another performance metric in power systems. There are also process evaluating metrics such as the distance between generated PF to the real PF, or the diversity of solutions (quantified using distribution indices) in MOO/EMO algorithms [155].

Different objective functions are usually measured with different units and are thus "incommenusurable". Therefore, it is beneficial to normalize objectives with respect to a reference value such that they become comparable with one another [69]. The most common normalization technique in power and energy systems for variables with different units is per-unitization. Another method is to create a relative rate-of-improvement/deterioration metric that is inherently normal. For instance, if as a result of power system optimization, the costs were reduced by 100 $ and power losses were decreased by 100 W, although both values are 100, they have different meanings and are not comparable. Now, if cost was quantified as a percentage improvement metric to the initial cost (e.g. without optimization) to be 2%, and similarly for power loss to be 25%; then, cost and power loss become commensurable.

There has been a multitude of research to normalize the objective space in EMO algorithms to solve the issue of commensurability [62]. The basic goal of most research in this particular topic is to somehow estimate the so-called "nadir" and "utopian" (or "ideal") values, and normalize different objectives based on relative metrics with respect to those values. Additionally, reference points can be chosen based on the DM's "aspiration" or "reservation" preference values [130]. Aspiration can be defined as what the DM hopes to see in a particular objective. Similarly, a reservation is an arbitrary limit set by the DM indicating their desire that an objective does not get worse than that limit. Using aspiration and reservation points as references to generate normal metrics for incommensurable objectives is a convenient and flexible approach; however, uninformed and too optimistic or pessimistic choices reduce their effectiveness.

[1] In mathematics, "metrics" are specifically defined as distance functions between different points of a given set [19]. However, other disciplines have more general definitions of metrics.

In power and energy systems, there are usually certain standards and performance limits that can be used by the DM as aspiration or reservation points. For example, the standard voltage deviation limit in power distribution systems is defined to be 5% based on IEEE Std 1159-2019 [2]. So, the 5% band around the nominal voltage is a suitable reservation point to be chosen as reference for a voltage metric. If no standards exist to choose a suitable reference point from; then, the DM can select one based on their own judgment.

If the goal is performance evaluation and benchmarking, the choice of reference to form normal metrics does not impact the system/process, but rather serves as a baseline for assessment. However, if the metrics are to be integrated into the system/process to change their outcome or guide their actions; then, the reference choice for the DM is more subtle. Therefore, two normalization techniques are considered based on whether the DM is only interested in performance benchmarking or they intend to guide the autonomous control process with their preferences:

1. *a priori* normalization: The DM is asked to provide references for metrics before the operation begins. Since it was assumed (see Chapter 1) that the DM is non-expert, this approach is only effective for performance benchmarking.

2. Dynamic normalization: References for metrics are dynamically and automatically selected through the DSS based on the best and worst values (extremums) found for each objective.

a priori normalization is somewhat *ad-hoc* and depends on what the DM considers relevant for performance evaluation. Examples of this method will be shown on a case-by-case basis in Chapter 3. The dynamic normalization, also dubbed as "straightforward normalization" in the literature [62], is described as follows.

$$M_k := \tilde{f}_k(\mathbf{x}) = \frac{f_k(\mathbf{x}) - Z_k^{lo}}{Z_k^{up} - Z_k^{lo}} \tag{2.1}$$

Where M_k is the normal metric, and $\{f_k(\mathbf{x}) \mid k \in \{1, \ldots, K\}\}$ are the objective functions in the optimization problem. Z_k^{up} and Z_k^{lo} are the worst and best solutions found for the problem in the objective space. Z_k^{up} and Z_k^{lo} in an iterative and elitist EMO are found in the archive. If the EMO algorithm is non-elitist; then, Z_k^{up} and Z_k^{lo} are selected based on the current population of solutions. In classical derivative-based optimization techniques, Z_k^{up} and Z_k^{lo} correspond to nadir and utopian/ideal values and must be calculated by separately optimizing each objective.

2.3 Preference articulation

One of the most overlooked and yet important aspects of a DSS is preference articulation. Let's start by investigating different methods of preference articulation and incorporation that are popular in the literature; then, introduce the proposed approach and compare it with (relevant) existing works.

In most EMO applications, such as autonomous control, the DM is not interested in the entire PF since the final solution is usually unique. An important role of DSS in EMO is to help the DM to select the Pareto optimal solution that best satisfies their preferences. DM preferences are used to guide the EMO algorithm's search toward specific parts of the Pareto front, i.e., ROI. There are eight general categories of preference articulation commonly used in the literature [11].

- **Weighting**: Each objective function is assigned a coefficient or weight by the DM. Higher the weight is, more important is its corresponding objective function.
- **Solution ranking**: The DM is asked to perform pairwise comparisons between pairs of solutions among a subset of solutions generated by the EMO.
- **Objective ranking**: Similar to solution ranking but the DM is asked to make comparisons in the objective space.
- **Aspiration point**: The DM provides the values which they want to achieve for each objective to the DSS.
- **Reservation point**: The DM provides the worst values for which they are still satisfied with for each objective to the DSS.
- **Trade-off functions**: The DM infers their preferences in form of relative trade-off functions that specifies how much gaining (or losing) one unit of each objective is worth compared to other objectives.
- **Outranking approaches**: The DM inputs the necessary parameters to design a fuzzy modeling that measures the truth level of statements like "solution $\mathbf{x}^1$ is at least as good as solution $\mathbf{x}^2$."
- **Desirability thresholds**: The DM specifies "Absolutely Satisfying", and "Marginally Infeasible" objective values that are used to classify the desirability of their corresponding solutions.

Many of the preference articulation methods belonging to the mentioned categories are not useful for dynamic applications; because they require an expert DM which violates the fundamental assumption made in Chapter 1 (trade-off, desirability and reference point categories), and are intrinsically static (ranking categories)[2]. However, weighting methods (most common) and implicit outranking approaches fit the basic requirements for an autonomous application with the end-user being the DM. Therefore, the existing literature of weighting and outranking preference articulation methods is surveyed in detail to provide the background for the proposed novel approach.

2.3.1 Weighting approaches

The biased sharing approach [30], the biased crowding-based approach [15], and the weighted hypervolume-based approach [153] are three of the most prominent preference articulation methods belonging to this category.

In [30], the relative importance of each objective is expressed in form of explicit weights. More specifically, the Euclidean distance computation in the sharing mechanism of NSGA is weighted to ensure (solution) population diversity by penalizing the fitness values of solutions present within the proximity of a particular solution. Thus, the "weighted Euclidean distance" is introduced as follows.

$$d(\mathbf{x}^1, \mathbf{x}^2) = \sqrt{\sum_{k=1}^{K} w'_k \left(\frac{f_k(\mathbf{x}^1) - f_k(\mathbf{x}^2)}{Z_k^{up} - Z_k^{lo}} \right)} \tag{2.2}$$

$$w'_k = \frac{1 - w_m}{\max_{k=1}^{K}(1 - w_m)} \tag{2.3}$$

$$\text{s.t.} \quad w_k \in [0, 1] \quad \text{and} \quad \sum_{k=1}^{K} w_k = 1 \tag{2.4}$$

Where w_k is the weight designated by the DM to the k-th objective. This preference articulation method was assessed for two biobjective problems with convex Pareto fronts and only two weight sets, i.e., (0.9,0.1) and (0.1,0.9). The problem of restricted weight sets applies to all preference articulation methods that require the DM to provide explicit values from an infinite number of possible combinations.

[2]Examining every preference articulation category and their respective literature is outside the purview of this dissertation; so, interested readers are encouraged to review the provided references for more details.

The biased crowding-based approach augments the crowding distance calculation in NSGA-II to focus its search on the ROI. Given an objective vector $\mathbf{z}$ from a specific PF, biased crowding distance is defined as follows.

$$D(\mathbf{z}) = d(\mathbf{z})\left(\frac{d'(\mathbf{z})}{d(\mathbf{z})}\right)^{\theta} \tag{2.5}$$

Where $d(\mathbf{z})$ and $d'(\mathbf{z})$ are the original crowding distance and the crowding distance computed based on the locations of the solutions projected onto a hyper-plane that is defined via a direction vector (η). η is a DM-specified direction vector determining the most probable or central linearly weighted utility function. θ is the bias intensity/pressure parameter (also specified by the DM). Solutions with larger crowding distance are preferred, allowing solutions near the tangent point to survive. The parameter θ controls the extent of the generated solutions, and larger θ means narrower solution extent. The main advantages of this approach are its scalability with the number of objectives, and insensibility to the non-convexity of the PF. However, its convergence was later questioned and proven to be inferior [16].

The hypervolume indicator is a performance metric that computes the surface of the objective space dominated by a solution set and bounded by a reference point. The main feature of the hypervolume performance metric is that it does not contradict the order induced by the Pareto dominance relation [154]. Zitzler *et al* [153], proposed a weighted version of the hypervolume metric in order to guide the search based on the DM's preferences expressed by either weighting coefficients or a reference point. Three different weighting scenarios were proposed for a bi-objective case study: 1) a weight distribution that favors extreme solutions, 2) a weight distribution that emphasizes one objective over the other, and 3) a weight distribution based on a reference point. The ordinary hypervolume metric (I_H) and its weighted counterpart (I_H^w) are given in (2.6) and (2.7), respectively.

$$I_H(\mathcal{A}) = \int_{(0,\ldots,0)}^{(1,\ldots,1)} \alpha_{\mathcal{A}}(\mathbf{z})\ d\mathbf{z} \tag{2.6a}$$

$$\alpha_{\mathcal{A}}(\mathbf{z}) = \begin{cases} 1 & \text{if } \mathcal{A} \succeq \{\mathbf{z}\} \\ 0 & \text{else} \end{cases} \tag{2.6b}$$

$$\text{s.t.} \quad \alpha_{\mathcal{A}}(\mathbf{z}) : [0,1]^K \rightarrow \{0,1\} \tag{2.6c}$$

Where $\alpha_{\mathcal{A}}(\mathbf{z})$ is called the "attainment function" of objective vector set $\mathcal{A}$ with respect to objective vector $\mathbf{z}$ [53]. Note that $I_H(\mathcal{A})$ is calculated over a normalized objective space from the origin.

$$I_H^w(\mathcal{A}) = \int_{(0,\ldots,0)}^{(1,\ldots,1)} w(\mathbf{z}).\alpha_{\mathcal{A}}(\mathbf{z})\ d\mathbf{z} \tag{2.7}$$

$w(\mathbf{z})$ is the weight distribution function of objective vector $\mathbf{z}$. The main idea behind the weighted hypervolume approach is to give different weights to different regions in the objective space such that the ROI is emphasized in the algorithm. The biggest disadvantage of the weighted hypervolume method is its dependence on the lower integration bound of $I_H^w(\mathcal{A})$ (chosen by DM) and the need to define a complex and explicit weight distribution functions. The weight distribution function's complexity compounds as the number of objectives increase.

2.3.2 Outranking approaches

The most notable work in this category was done by Fernandez *et al* [47]. The authors used the outranking concept [115] in order to create a preference articulation method for NSGA-II. Each objective[3] $f_k(.)$ is assigned a preference (pr_k) and indifference (I_k) relation such that for each pair of

[3]Metric in normal space

objective vectors, i.e., $(f_k(\mathbf{x}^1), f_k(\mathbf{x}^2))$ one of the following will apply:

$$f_k(\mathbf{x}^1)\ pr\ f_k(\mathbf{x}^2) \tag{2.8a}$$

$$f_k(\mathbf{x}^2)\ pr\ f_k(\mathbf{x}^1) \tag{2.8b}$$

$$f_k(\mathbf{x}^1)\ I\ f_k(\mathbf{x}^2) \tag{2.8c}$$

For each pair of objective vectors $(f_k(\mathbf{x}^1), f_k(\mathbf{x}^2))$, the DSS creates a fuzzy predicate that models the truth degree of the predicate "$f_k(\mathbf{x}^1)$ is at least as good as $f_k(\mathbf{x}^2)$" as indicated by the DM. For example, Assuming $\mathbf{z}^1 = f(\mathbf{x}^1)$ and $\mathbf{z}^2 = f(\mathbf{x}^2)$, the proposition "$\mathbf{z}^1$ outranks $\mathbf{z}^2$" which means "$\mathbf{z}^1$ seems at least as good as $\mathbf{z}^2$" holds if and only if the combination of criteria in agreement with this proposition is strong enough and there is no important dissident criteria. More information on the outranking logic can be found in [52, 114].

In another work [48], more preferential relationships are considered in addition to strict preference or indifference relations as follows:

- Weak preference: There exist clear and positive reasons to favor one objective over the other, but they are not sufficient to justify strict preference.
- Incomparability: None of the relations of indifference, strict preference nor weak preference applies. In other words, there are no clear and positive reasons to justify any relations.
- k-preference: There are clear and positive reasons to justify strict preference in favor of one of the two objectives or establish incomparability, but there are no clear distinction between strict preference and incomparability.

The addition of these new outranking relationships are reported by the authors to enhance the performance of their case study which was the multi-objective knapsack problem.

2.3.3 Dynamic implicit weighting approach

This section has so far established the concept of preference articulation and its role in DSS. A thorough overview of the most prominent and relevant works in this area shows that a lot of attention has been invested in theoretically developing preference articulation methods with

various degrees of performance effects. However, as previously discussed in Chapter 1, there are none or very few practical researches (particularly in autonomous control of power and energy systems) that utilized sophisticated DSS methods including preference articulation. Most multi-objective autonomous control research works use basic weighting methods and ignore the complexities of more difficult, albeit better DSS.

Therefore, a new preference articulation method, denoted as DIWA, is introduced that aims to bridge explicit preference information and implicit human DM opinion. DIWA is specifically developed considering dynamic time-constrained applications such as autonomous control. DIWA is a two criteria process:

1. DM opinion: the human DM is given four preference options to choose for each available objective/metric. The preference options are "low", "medium", "high" and "very high" importance. These preference options divide the normal weighting range [0,1] into corresponding quartiles. The DM can express an indifference opinion by choosing the same preference option for the associated objectives/metric.

2. Dynamic factor: a dynamic coefficient that is inversely related to the performance "goodness" of each objective/metric determines the final weight within the DM-specified preference quartile.

The idea behind dividing the weighting range into quartiles is inspired by human psychology, and desire for symmetrical subdivision of numbers that are divisible by four. Examples of this preference can be found in various currencies, annual and even daily planning patterns (for instance, companies breakdown their goals into quarterly objectives). Additionally, four options should be sufficient to cover implicit preference opinions of a human DM. The DM preference options and their corresponding quartile weight ranges are shown in Table 2.1.

Table 2.1: DM preference options and their corresponding quartile weight ranges.

Options	Range $\{\mu^{\min}, \mu^{\text{avg}}, \mu^{\max}\}$ (pu)
Low Importance	{0, 0.125, 0.25}
Medium Importance	{0.25, 0.375, 0.50}
High Importance	{0.50, 0.625, 0.75}
Very High Importance	{0.75, 0.875, 1}

The dynamic coefficient is a function of normalized metrics representing each objective's state at any given time/iteration such that the least performing metrics are prioritized for the highest

weight. Looking back at the normal metric (2.1), the dynamic coefficient can be defined as follows.

$$c_k(t) = \frac{1 - M_k(t)}{\text{mean}(1 - M_k(t))} \tag{2.9}$$

It is evident in (2.9) that $c_k(t)$ is a relative ratio and not an absolute value. This approach is necessary for better generalization and scalability in different problems. Note that t either represents the iteration of an evolutionary algorithm or a real-time measurement depending whether the dynamic coefficient is integrated into an optimization algorithm's search process or is only utilized for online performance evaluation. These different utilizations will be further clarified in future chapters of this dissertation. The final weights for each objective/metric are selected in DIWA as follows.

$$W'_k(t) = \min\left(\mu_k^{\max}, \max\left(\mu_k^{\min},\ c_k(t).\mu_k^{\text{avg}}\right)\right) \tag{2.10a}$$

$$W_k(t) = \frac{W'_k(t)}{\sum_{\forall k} W'_k(t)} \tag{2.10b}$$

2.4 MetaMetric benchmark

There are various measurements and performance indices in power and energy systems such as voltage, current, power loss, energy resource efficiency, and power generation cost. System-level control designers typically consider one primary objective for optimization (cost for example) and incorporate a series of operational constraints in their control law formulation. Thus, autonomous controllers and their benefits are subjective to their designers' opinion on what constitutes performance "goodness" and the fidelity of their modeling.

If the control designer is not the end-user (which is usually the case); then, the DM is a different person with potentially different opinions about performance goodness. It can be argued that in reality a control system is designed based on specific needs of an application, so there must be some level of consensus between the end-user and the designer. This argument is only partially true, because it is difficult to consider all potential operational circumstances. Additionally, it is useful to develop a diverse performance evaluation benchmark with respect to varying DM preferences and metrics. Such benchmarking framework, especially if it is *in-situ*, allows for a comprehensive understanding of the control system's impact on the underlying plant.

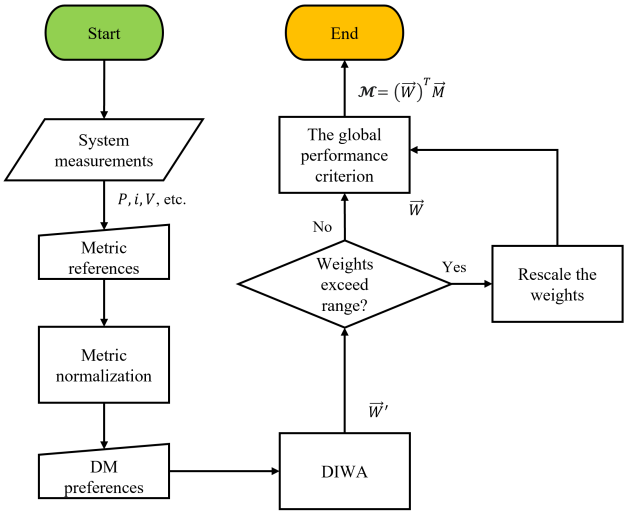

Figure 2.1: The MM performance benchmark methodology flowchart.

Therefore, the normalized metrics and DIWA concepts which were introduced earlier in this chapter are utilized to develop a performance evaluation framework, denoted as the MM benchmark. The name MetaMetric is inspired from the fact that this framework generates one holistic (meta-)metric from multiple sub-metrics as follows.

$$\mathcal{M}(M_k, W_k) = \sum_{k=1}^{K} W_k(t) M_k(t) \tag{2.11a}$$

$$\text{s.t.} \quad 0 \leq W_k \leq 1 \tag{2.11b}$$

Where W_k is calculated based on (2.10). As mentioned before, M_k are normal metrics formulated *a priori* on a case-by-case basis considering the application and DM's interests. The MM benchmark's flowchart is illustrated in Figure 2.1.

Chapter 3

MetaMetric Benchmark Case Studies

Nomenclature

DIWA	Dynamic Implicit Weighting Approach
MOO	Multi-Objective Optimization
EMO	Evolutionary Multi-objective Optimization
DSS	Decision Support System
PF	Pareto optimal Front
DM	Decision-Maker
MM	MetaMetric
RES	Renewable Energy Sources
MG	Micro-Grid
DG	Distributed Generation/Generator
EM	Energy Management
PM	Power Management
ADMM	Alternating Direction Method of Multipliers
WT	Wind Turbine
HMI	Human-Machine-Interface

UDP	User Datagram Protocol
DDS	Data Distribution Service
IPS	Integrated Power System
SPS	Ship Power System
PGM	Power Generation Module
EMRG	Electro-Magnetic Rail-Gun
ES	Energy Storage
ESM	Energy Storage Management
EEM	Efficiency Energy Management
MVDC	Medium Voltage DC
LVDC	Lowe Voltage DC
SWBD	SWitch BoarD
PMM	Propulsion Motor Module
IPNC	Integrated Power Node Centers
N_g	Number of DG
N_r	Number of RES
N_b	Number of buses
t_s	Simulation (model) time-step
P, P^L	Active power output and demand, respectively
$\mathcal{C}_{grid}$	Cost of purchasing power from utility
$\mathcal{C}_{fuel}$	Fuel cost
$\mathcal{C}_{res}$	RES power generation cost
$\mathcal{E}$	Emission profile
$\mathcal{U}$	ON/OFF status
$V\angle\delta$	Phase-to-ground rms voltage
$Z\angle\theta$	Impedance magnitude and angle
M	Normal metrics
W	Metric weights
$\mathcal{M}$	The MM variable

3.1 Overview

Two power systems are used for the MM benchmark case studies, which are thoroughly presented in this Chapter. The first case study is the IEEE 33-bus distribution system configured as a MG with multiple DGs and RES (Section 3.2). The next case study detailed in Section 3.3 is a 4-zone DC Navy SPS which was virtually tested in real-time in engagement and cruising modes of operation.

3.2 IEEE 33-bus distribution system

3.2.1 Introduction

The rising popularity of RES and electrification of infrastructures has increased the demand for more affordable, efficient and smarter power distribution systems. The MG concept was introduced as a solution to mitigate the adverse effects of DG and provide flexibility in service [81]. Application of MG in various sectors: residential, commercial and military has created a diverse demand for system management and control strategies that can provide reliable and resilient performance that specifically meet their application's requirements. For example, in a nuclear power plant MG, safe and reliable service is the top priority, while in a residential application, priorities are shifted toward cost saving and sustainability; priorities can also change with time regardless of the application. Hierarchical control strategies, including primary, secondary (PM) and tertiary (EM) levels, with diverse objective functions are utilized in MG systems to achieve their varying priorities. The diversity of objective functions and performance trade-offs in system control necessitates a need for proper performance metrication to derive control systems' properties and their underlying modeling assumptions. Therefore, having a holistic performance evaluation helps to better understand existing control methods, especially from a DM's standpoint, who wants to test the system without prior comprehensive information. The 12.66 kV 33-bus AC MG is shown in Figure 3.1.

3.2.2 Candidate control system

Generally, EM incorporates an optimization algorithm that searches for optimal power sharing combinations for a given objective functional and a set of system constraints [25, 90, 108]. In non-convex applications such as in MG, speed of convergence and guarantee of global optimality

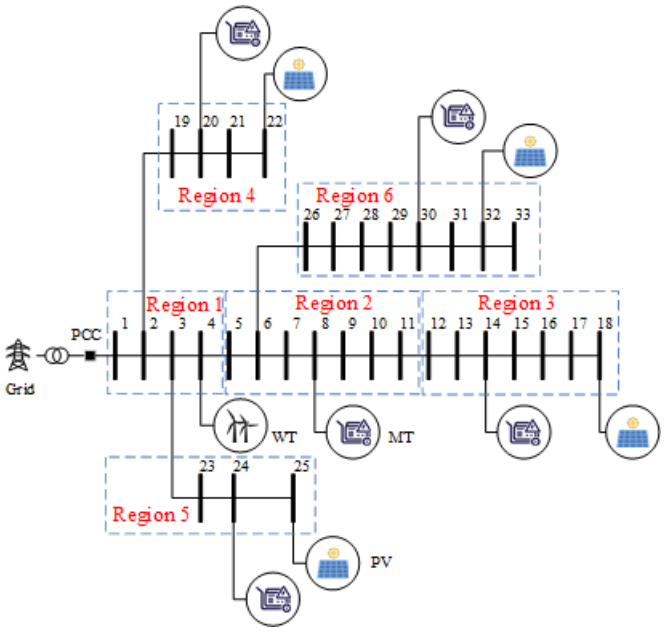

Figure 3.1: IEEE 33-bus system configured as a notional MG with DG and RES, which is used for MM benchmark case study.

becomes an issue. The control strategy studied for performance analysis in this case study is a distributed dual-step EM based on the single perturbation theory [66, 65] and the ADMM [13]. The proposed EM breaks down the optimization process into two steps. The first step solves the optimization problem with relaxed constraints using the singular perturbation theory, thus narrowing the search space. Then, the second step solves the full optimization problem with the reconfigured search space via ADMM to find the optimal power sharing solution.

The EM strategy is assumed to be pre-existing in this case with a proven theoretical background, guarantee of convergence, and stability. A general overview of this example EM strategy is given in Appendix A, but interested readers are encouraged to visit the provided references for more information.

3.2.3 Benchmark metrics

The MM benchmark is used for *in situ* performance evaluation by formulating normalized metrics. As indicated in Chapter 2, the metrics must be defined *a priori* by the DM with the desired performance references (i.e., aspiration, reservation, or boundary points). Assuming the DM in charge of the 33-bus test system is interested in four criteria: monetary cost, emission cost, voltage

quality, and power loss; the following metrics are defined to be used in the MM benchmark.

3.2.3.1 Cost

One of the most important concepts in a MG is cost management. There are many ways of modeling a cost metric. In this case study, the cost metric is based on the financial expense of generating real power. The financial effects of DG and RES turn ON/OFF maneuvers, maintenance, infrastructural charges, utility fees or government dues (tax) and energy sales to the grid, are also neglected. Therefore, the cost metric as a function of DG, RES and utility real power injection into the MG at time t can be given as (3.1).

$$\begin{aligned} m_1 = \frac{1}{\|\vec{P}\|_1} \Bigg[& \sum_{i=1}^{N_g} \Big(\mathcal{U}_i(t) f_i(P_i(t)) \Big) \\ & + \sum_{j=1}^{N_r} \Big(\mathcal{U}_j(t) f_j(P_j(t)) \Big) + \mathcal{C}_{grid}(t) P_{grid}(t) \Bigg] \end{aligned} \tag{3.1}$$

The cost performance reference (m_1^*) is chosen *a priori* by the DM as the cost of operating the system without the RES and DG, i.e., legacy distribution system configuration. Since the DM expects the cost to improve from the designated reference, m_1^* is a reservation value, and the normal metric is formulated as follows.

$$M_1 := \cos\Big(\frac{m_1}{m_1^*}(\frac{\pi}{2})\Big) \tag{3.2}$$

3.2.3.2 Emission

Recent interest in transforming energy sectors from fossil fuel dependency to more sustainable and environmentally friendly solutions, signifies monitoring emissions such as: carbon-dioxide (CO2), sulfur-dioxide (SO2) and nitrogen-oxides (NOx). Governmental institutions periodically collect and release general emission reports. For example, the Energy Information Administration (EIA) documents energy statistics, including average emission profile of utilities and industries, at state and national level in the United States [3]. Table 3.2 shows the average emission profile data for U.S. utilities and three other sources, assuming NOx and SO2 emissions are negligible for PV and WT [101, 54].

The emission metric for a notional MG is formulated in (3.3). Emission is composed of operational (power generation), upstream (manufacturing, assembly and transportation), and

Table 3.2: Emission profile of some power generation sources including U.S. utility average

Source	Emission profile (Kg/MWh)			Total (Kg/MWh)
	CO2-eq	SO2-eq	NOx-eq	
Micro Turbine	720	0.0036	0.1	720.10036
PV	0.4941	-	-	0.4941
WT	0.03411	-	-	0.00713
Utility	449	0.376	0.356	449.732

downstream (decommissioning and recycling/disposal) elements [135, 39, 101]. To make relevant comparisons, specific pollutants like cadmium poisoning in CdTe PV panels [54] are neglected in (3.3). Other assumptions include, 1) only CO2 (green house gas), SO2 and NOx (poison gases with adverse health effects) emissions are significant, 2) utility, DG and RES are assumed to be the only emission sources.

$$m_2 = \frac{1}{\|\vec{P}\|_1}\Bigg[\sum_{i=1}^{N_g}\Big(\mathcal{U}_i(t)\mathcal{E}_i P_i(t)\Big) + \sum_{j=1}^{N_r}\Big(\mathcal{U}_j(t)\mathcal{E}_j P_j(t)\Big) + \mathcal{E}_{grid}P_{grid}(t)\Bigg] \tag{3.3}$$

m_2 is normalized similar to m_1, with its reference (m_2^*) being the legacy distribution system's emission reservation level, that is the emission metric with only the grid providing power.

$$M_2 := \cos\Big(\frac{m_2}{m_2^*}(\frac{\pi}{2})\Big) \tag{3.4}$$

3.2.3.3 Voltage deviation

Assuming voltage drops and surges are equally undesired, a per-unit voltage deviation metric is formulated in (3.5).

$$m_3 = \sum_{i=1}^{N_b}\Big|1 - V_i(t)\Big| \tag{3.5}$$

The reservation level for m_3 is chosen by the DM based on IEEE Std 1547 [1] to be the 5% margin of the nominal voltage. Thus, the normalized voltage metric (M_3) is defined as follows.

$$M_3 := \cos\Big(\frac{m_3}{m_3^*}(\frac{\pi}{2})\Big) \tag{3.6}$$

3.2.3.4 Line power loss

Power loss is an important metric to monitor in a system. Assuming shunt-capacitance is negligible for an AC MG at distribution voltage level, the line power loss metric can be quantified as (3.7).

$$m_4 = \sum_{i=1}^{N_b} \sum_{j=1}^{N_b} \frac{(V_i(t) - V_j(t))^2}{Z_{ij}} \cos\theta_{ij} \tag{3.7}$$

Because PM control must apply EM optimal commands to the sources and maintain steady bus voltages across the system, a steady line power loss metric during each optimization cycle is an indication of good PM performance. Considering this relationship, in cases where PM action is assumed to be ideal, the line power loss metric is expected to remain relatively constant in each EM cycle. Thus, the normalization process for m_4 is slightly different such that m_4^* is measured at the beginning of each EM cycle and that the DM expects m_4 to not deviate from the reference. The following normalization sufficiently captures the described logic.

$$M_4 := \left| \sin\left(\frac{m_4}{m_4^*}(\frac{\pi}{2})\right) \right| \tag{3.8}$$

3.2.4 Experimental setup

The 12.66 kV 33-bus AC MG is modeled in MATLAB/Simulink and deployed in an OPAL-RT OP4510 simulator using the RT-LAB software. The CHIL experimental configuration layout is illustrated in Figure 3.2. The MG model time-step is $t_s = 83\mu$s and it is solved for electromagnetic dynamics using ode4 (Runge-Kutta). Eight ARTEMiS nodal solvers from RT-LAB Simulink library are used to sub-divide the model into eight parts to reduce the computational load. With respect to the controllers, the distributed EM algorithm is implemented in six sbRIO 9627 controller devices, each corresponding to one of the respective six regions of the MG. The MM performance analysis module runs in one sbRIO device that operates in parallel with the EM. All sbRIOs are programmed via the National Instruments LabVIEW software. The HMI performs as a synchronizer between the OP4510 and sbRIO controllers. UDP is used to send regional active power, reactive power and bus voltage data from the OPAL-RT to each respective sbRIO. Also, the distributed EM formulation requires information exchange (bus voltages and Lagrangian multipliers) between neighboring controllers which is achieved using DDS communication protocol. Note that all physical communication lines are Ethernet cables.

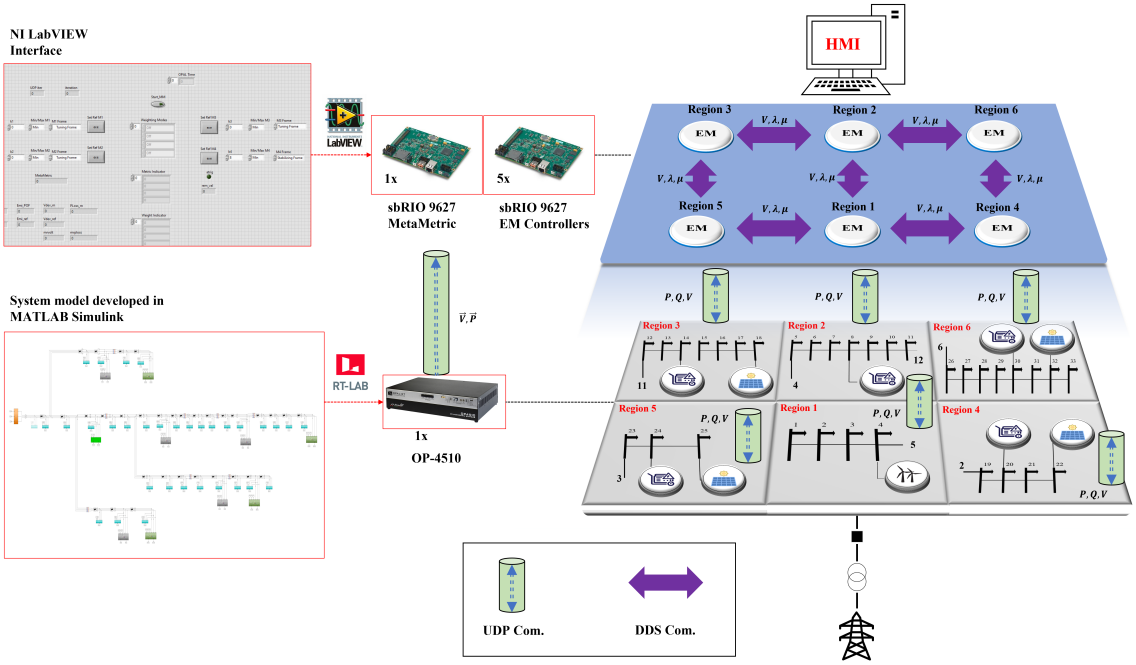

Figure 3.2: The CHIL experiment layout for the IEEE 33-bus AC MG case study.

3.2.5 Test scenarios

From 16 possible DM weight preference combinations, five scenarios are selected for experimentation (Table 3.3). The selected scenarios are sufficient to showcase the effect of changing DM preferences on the performance benchmark.

3.2.6 Results and discussion

The experiment data was recorded for every second in a 24-hour test. The total power generation and the furthest bus voltage (bus 18) from the substation is given in Figure 3.3. The total

Table 3.3: IEEE 33-bus AC MG CHIL test scenarios

Metrics	Reference value	DM weight preferences				
		Scenario 1	Scenario 2	Scenario 3	Scenario 4	Scenario 5
Cost	Legacy system	Medium	High	Medium	Medium	Medium
Emission	Legacy system	Medium	Medium	High	Medium	Medium
Voltage	5% deviation	Medium	Medium	Medium	High	Medium
Power loss	Measured value every 15 min.	Medium	Medium	Medium	Medium	High

Table 3.4: Summary of the MM benchmark results in the IEEE 33-bus AC MG

Metrics (%)	Scenario 1			Scenario 2			Scenario 3			Scenario 4			Scenario 5		
	min.	avg.	max.	min.	avg.	max.	min.	avg.	max.	min.	avg.	max.	min.	avg.	max.
$\hat{m}_1$	7.32	21.96	59.75	7.32	21.96	59.74	7.32	21.96	59.74	7.29	21.96	59.71	7.32	21.96	59.71
$\hat{m}_2$	13.09	42.35	100	13.09	42.35	100	13.09	42.35	100	12.95	42.36	100	13.09	42.36	100
$\hat{m}_3$	30.87	32.66	92.53	30.87	32.66	92.53	30.87	32.66	92.53	30.87	32.66	92.53	30.87	32.66	92.53
$\hat{m}_4$	98.47	99.97	100	96.81	99.96	100	97.89	99.96	100	99.21	99.97	100	99.37	99.97	100
$\mathcal{M}$	**28.93**	**44.7**	**91.96**	**25.88**	**41.42**	**86.90**	**27.11**	**44.36**	**92.09**	**29.54**	**42.94**	**91.97**	**38.89**	**52.93**	**93.10**

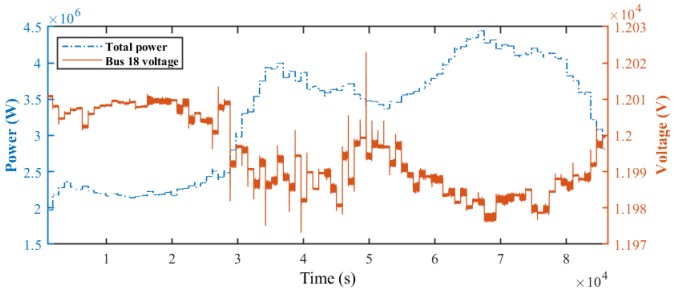

Figure 3.3: Total power generation and the bus voltage profile in the IEEE 33-bus AC MG case study.

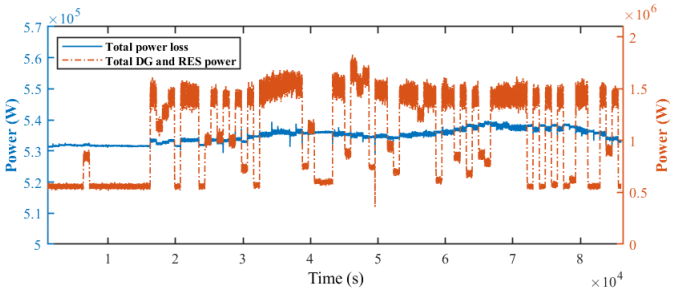

Figure 3.4: Total DG and RES power generation and the total power loss in the IEEE 33-bus AC MG.

power generation of the DG and RES sources and the total line power loss are shown in Figure 3.4. The overall MM analysis data from each case study are summarized in Table 3.4. The quarter-hourly and hourly $\mathcal{M}$ scores for different weighting scenarios are shown in Figure 3.5 (a), (b) and (c). Also, the average metric weights for two of the five scenarios are illustrated in Figure 3.6 (a) and (b).

3.2.6.1 MG operation

As it can be seen from Figure 3.3, the furthest bus line-line rms voltage from the substation (bus 18) is 12001.9 V on average, with a minimum of 11973.15 V, which is within the 5% margin. As expected, because of DG/RES ancillary service in the MG, the total line power loss is maintained

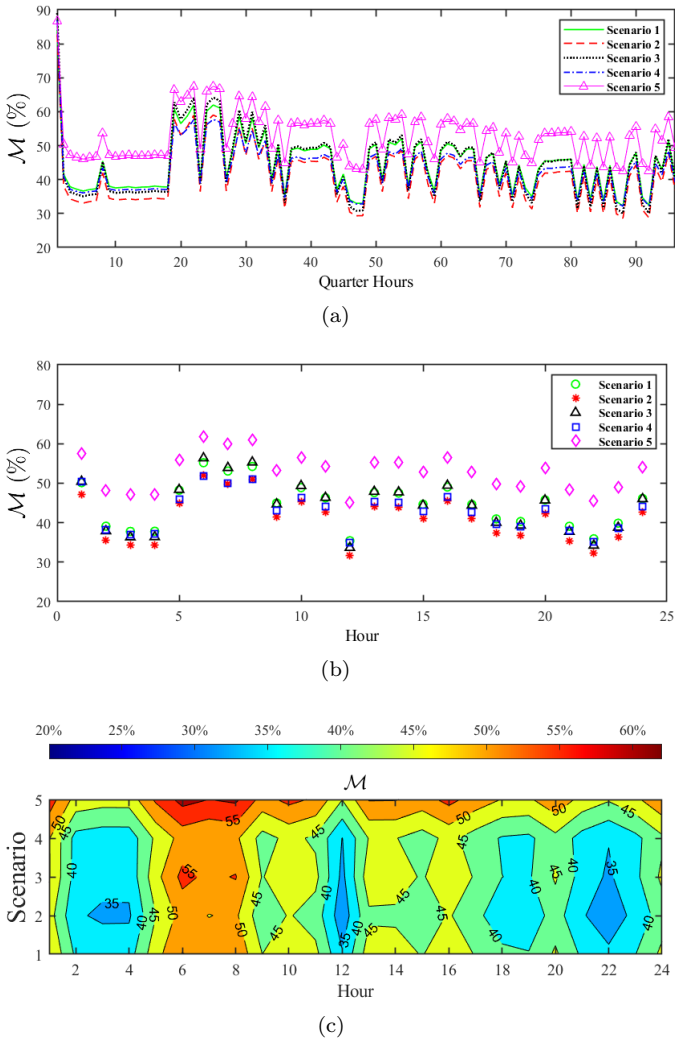

Figure 3.5: Average $\mathcal{M}$ scores representing the global performance benchmark of the IEEE 33-bus AC MG. (a) Quarter-hourly, (b) hourly, and (c) colored contour, results.

in the 530-540 kW range for the entire operation (Figure 3.4). Also, because the power loss metric was normalized using the Ψ option, its performance is graded at 99.97% as shown in Table 3.4. However, two factors must be considered to explain the power loss metric's performance: 1) the deviation tolerance was assumed 6% in each EM cycle, so smaller tolerance choices would have adversely affected M_4. 2) The candidate control under study is EM only and the MG's PM is ideal. Generally, the results show that M_4 is a neutral metric in the studied system, mostly because of the ideal PM. Neutral in this context means metrics that are relatively invariant and consistently satisfy their intended objective. The presence of neutral metrics can give a biased understanding of overall

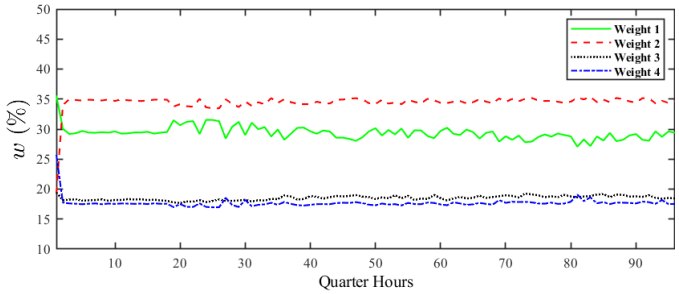

(a)

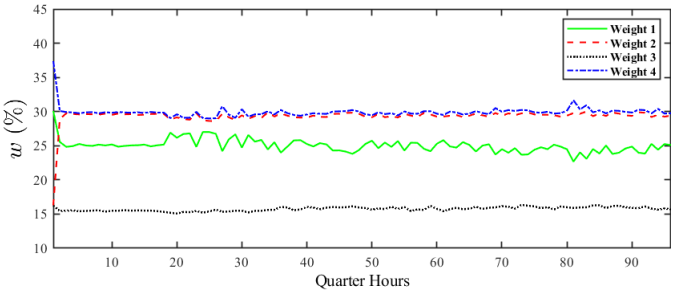

(b)

Figure 3.6: MM benchmark adaptive weighting behavior in the IEEE 33-bus MM benchmark case study, demonstrating the relationship between DM opinions, dynamic performance and metric weights. (a) scenario 1, (b) scenario 5.

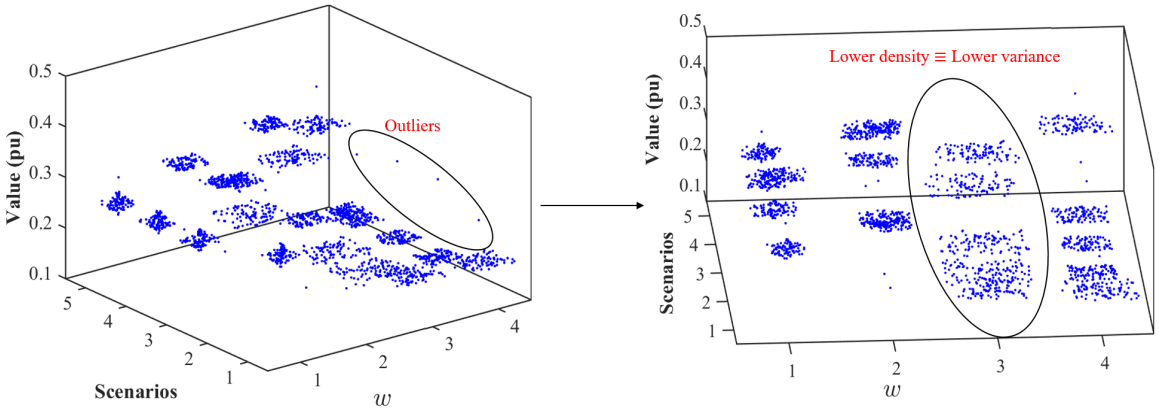

Figure 3.7: The weighting distribution swarm chart of each metric's weight for each scenario in the IEEE 33-bus MM benchmark case study. These statistical figures show how much metric weights vary in different scenarios.

performance goodness; thus, the adaptive metric weighting and $\mathcal{M}$ help to mitigate this bias.

3.2.6.2 MM benchmark

The 5th scenario with an average of 52.93% is the setting that produces the highest MM score compared to other scenarios (Figure 3.5). This is because the DM weight preference in scenario 5 biases the MM algorithm toward M_4 which is neutral as previously discussed. However, as shown in Figure 3.6 (b), the adaptive metric weighting reduces w_4 as much as possible without violating the DM weight preference. As a result, the difference between MM scores in different scenarios are not as salient as the difference between each individual metric.

The weighting distributions in Figure 3.7 show that weight variances are directly proportional to metric variances. There are some weight outliers in Figure 3.7, especially for less variant metrics, which are a result of transient dynamics. Presence of many outliers in the weight distribution is a sign of problematic performance as it pertains to the presence of many transients in the system. Furthermore, Figure 3.6 (a) shows that when there is no bias in the DM weight preferences, the weighting focuses on the metric with the relatively higher variation, which in this case is M_2 (Figure 3.8). The variations in M_2 is indicative of sudden changes in the power share of available sources, and the difference between DG, RES and the utility emission profiles.

Generally, the adaptive weighting behavior: 1) reduces the impact of neutral metrics on $\mathcal{M}$, and 2) compensates for poor DM judgments that emphasize on neutral metrics. The advantage in monitoring $\mathcal{M}$ instead of metrics individually, is that it provides a holistic viewpoint over the entire system.

3.2.6.3 Discussion

The IEEE 33-bus AC MG with distributed dual optimization EM tested using the MM performance analysis. The following performance characteristics were detected for the system under-test.

- The PM is ideally modeled; therefore, issues like transient stability do not appear in the system.
- The system is not aggressive in optimizing M_3 and settles around 35% score during the operation.
- Lack of energy storage and trade with the utility negatively affects the global performance in the early and late hours of the day (Figure 3.5).

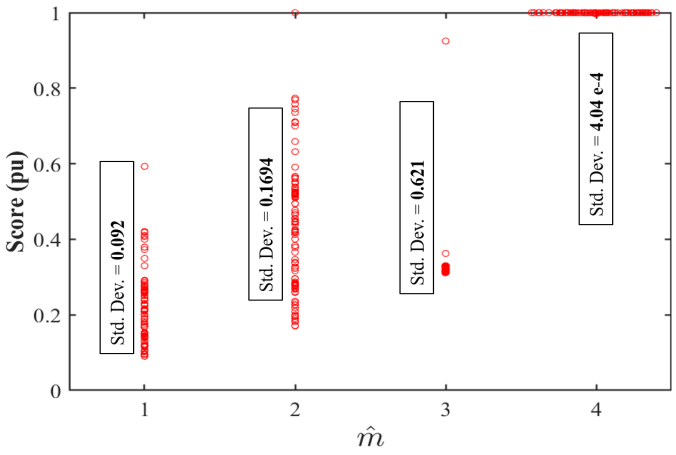

Figure 3.8: IEEE 33-bus MM benchmark normalized metric performance data distribution. Higher variance indicates performance volatility, while low variance shows robustness.

- There is a performance drop at noon which was traced back to dynamic transients due to sudden changes in power shares.
- Figure 3.5 (c) illustrates that the highest performing hours of the day are in the morning where the utility prices are the lowest and the load demand is minimum. This fact indicates that the MG is still reliant on the purchased power from the utility.

Furthermore, the data distribution for different metrics shown in Figure 3.8, demonstrate that power set-points, thus M_1 and M_2, had more than 50% distribution range. This observation relates to the non-convexity of the EM objective functional. Overall, although there were no violations (negative scores), there is room to expand and improve the control system based on the MM performance analysis results.

3.3 4-zone DC ship power system

3.3.1 Introduction

Advancements of electrical technologies in the 20th century increased the demand for maritime vessel electrification, which led to the development of SPS [105, 17, 27, 61, 124, 28]. Furthermore, all-electric power architectures known as IPS are considered to be the future of SPS, especially in military applications. IPS reduces the number of PGM and increases reliability through integrating electrical and non-electrical loads such as the navigational systems, lighting, propulsion, and weapons in one holistic electrical network [37, 156, 122, 38, 134]. Some of the challenges facing IPS in Navy ships are: 1) safety of the ship and its personnel, 2) operational longevity and survivability, 3) robust response to weapon discharge loads and battle maneuvers, and 4) reduced refueling and maintenance intervals. Additionally, the U.S. Navy road maps and other research about the future generation of battle ships show that the DC technology is more advantageous in SPS applications [36, 72].

Similar to terrestrial MGs, SPS require autonomous control and management systems to achieve their goals. Control engineers and researchers consistently propose new methods to achieve certain objectives. For example, pulse load demands imposed by EMRG and LASER guns prompted the need to incorporate ES such that they operate as spinning-reserve [132, 131, 56, 43, 80, 77]. For example, in [43] the authors proposed an ESM to reduce ramp-rate stress on PGM by optimally charging/discharging the ES using a two-step optimization methodology. In another work by the authors in [77], a fuzzy logic-based ESM is proposed for hybrid ES configurations with high power density super-capacitors and high energy density batteries to support peak demands and pulse loads in Navy SPS. Also, Navy ships often operate in cruising mode to patrol large areas, so it is important that they reduce cost by maximizing operational efficiency. Some researchers [122, 73, 146, 44, 150, 9, 128, 6] approached the operational cost problem for Navy and commercial ships by introducing power and energy management methods that increase the efficiency of several components. For instance, the authors in [44] propose an efficiency energy management (EEM) using a distributed evolutionary algorithm to optimize the PGM cost function. In [128], particle swarm optimization is leveraged to dispatch renewable sources, diesel generators and ES in commercial SPS to minimize the ship's overall cost.

The concepts of mathematical and psychological convergence and their relationships in multi-criteria decision making processes are extensively studied in the literature [139, 136, 94, 14, 93]. These

works show that preference and intuition models can be used in parallel to substantive processes in various applications. Furthermore, preference models are sometimes in conflict with their substantive counterparts, thus creating trade-offs between the mathematical and psychological convergence of a given problem. The same convergence conflict can also be studied in the performance evaluation of energy systems such as SPS. Two perspectives are considered for performance evaluation: 1) control designers', and 2) end-users' (i.e., DM). The increasing number of different power and energy management methods for SPS, complicates the performance goodness criteria. In other words, some performance metrics that are interesting to a particular DM may not necessarily align with the control designer's objectives. Therefore, a metric evaluation strategy that incorporates a DM preference model in parallel to the substantive control process is essential to properly evaluate the SPS control-performance.

3.3.2 SPS model

The schematic diagram of the DC 4-zone SPS is shown in Figure 3.9. Zones are separated by medium voltage DC (MVDC) lines (L), and two switch boards (SWBD) connected to either side of the ship. Also, the system has a 100 MW power rating, and consists of 12 kV MVDC and 1 kV low voltage DC (LVDC) power networks. The other electrical components include PGM, propulsion motor modules (PMM) and the armaments which are connected to the MDVC bus (Port or Starboard), and integrated power node centers (IPNC) are supplied in the LVDC areas. IPNC represent various service loads lumped into one node; for example, IPNC 1 is the combined radar and navigational systems. In addition to the four ES shown in Figure 3.9, another ES is embedded in the EMRG that exclusively supports its operation.

3.3.3 Candidate control system

The control system in this case study is consisted of three distributed hierarchical "layers". The distributed control system has five ESM, five EEM and 10 PM controller agents as shown in Figure 3.10 (see Appendix B for more details). The MM benchmark module is implemented in parallel to the hierarchical control paradigm, and directly communicates with the SPS model. Then, MM sends the performance data back to the HMI for online monitoring purposes. Aside from online monitoring, the performance data are periodically logged for later evaluation.

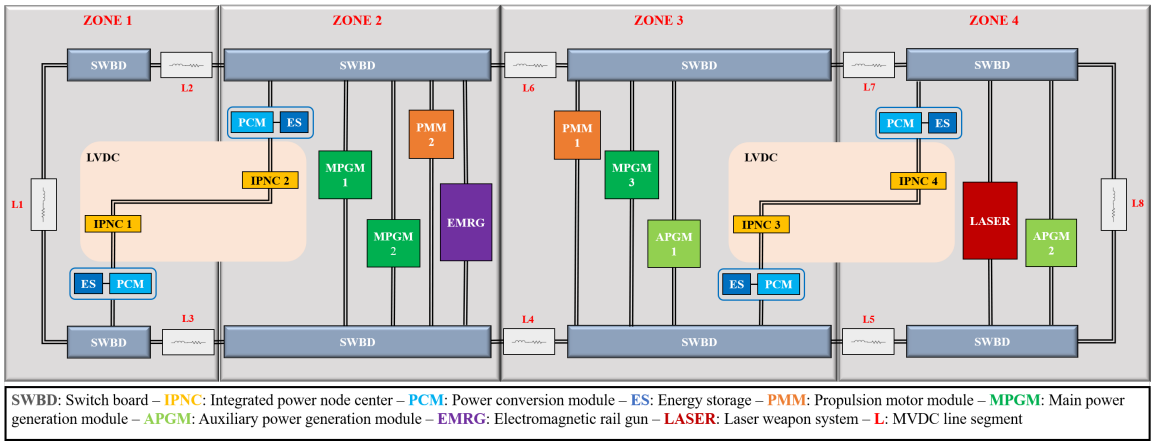

Figure 3.9: The 4-zone DC Navy SPS schematic diagram.

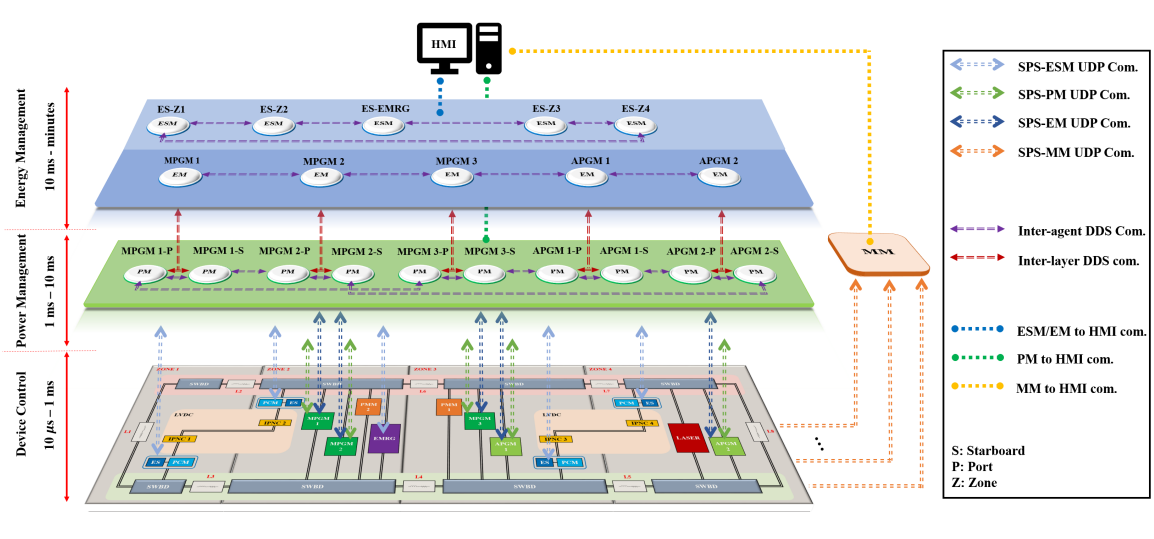

Figure 3.10: The distributed hierarchical control structure of the DC Navy SPS.

3.3.3.1 Test scenarios

A 45 minutes long test with a notional load profile as shown in Figure 3.11 is used to demonstrate the capabilities of the candidate control system and evaluate its performance. The MM performance benchmark is conducted with respect to six metrics as shown in Table 3.5; where:

- Essential voltages (index n) are the node voltages connected to the EMRG, Laser, IPNC 1 (i.e., radar and navigation), and both PMM.

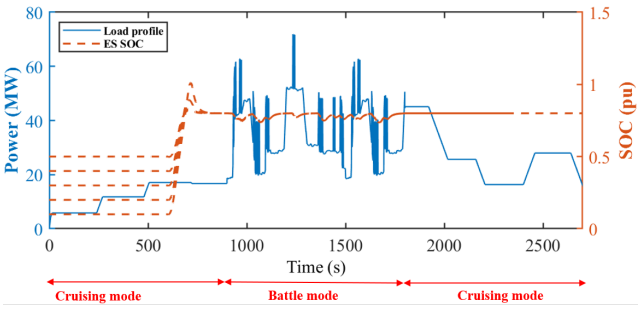

Figure 3.11: The load profile and the ES modules' SOC in the 4-zone DC Navy SPS case study.

Table 3.5: Metrics considered for MM benchmark in the 4-zone DC Navy SPS case study.

Metrics				DM weight preference		
				Naval test stages		
$\hat{M}_n$	Name	Formula	Normalization reference	Stage 1	Stage 2	Stage 3
1	Essential voltage	$\sum_{\forall n} \lvert 1 - V_n \rvert$	0.25 pu	Medium	Very high	Medium
2	Non-essential voltage	$\sum_{\forall n'} \lvert 1 - V_{n'} \rvert$	0.15 pu	Medium	Low	Medium
3	Avg. PGM efficiency	mean($\eta(k)$)	18.24%	Very high	Low	Very high
4	PGM ramp rate	$\sum_{\forall i} \lvert r_i^{GEN}(k) \rvert$	5 MW/s	Medium	High	Medium
5	Maximum line current	max($I_L(k)$)	500 A	Low	Medium	Low
6	ES ramp rate	$\sum_{\forall j} \lvert r_j^{ES}(k) \rvert$	5 MW/s	-	Medium	-

- Non-essential voltages (index n') are the node voltages connected to IPNC 2, 3 and 4.
- $\eta_i \mid \forall i \in \{1, 2, 3, 4, 5\}$ is the PGM efficiency, including the gas turbine and the synchronous generator.

After the experiment is completed, the logged metric data are used to conduct the MM benchmark for 26 additional DM preference scenarios (Table 3.6). For demonstration convenience in Table 3.6, very high, high, medium, and low preference options are replaced with A, B, C, and D characters, respectively. Note that the first two scenarios in Table 3.6 were used for the experiment. The MM benchmark is useful in better understanding the strengths and weaknesses of the candidate control approach considering additional performance viewpoints.

Table 3.6: MM benchmark DM preference scenarios used in the 4-zone DC Navy SPS case study.

no.	Scenario	no.	Scenario	no.	Scenario	no.	Scenario
1	$\{C, C, A, C, D, -\}$	8	$\{A, C, D, B, A, D\}$	15	$\{B, D, A, C, B, A\}$	22	$\{C, D, B, A, C, B\}$
2	$\{A, D, D, B, C, C\}$	9	$\{A, D, B, C, A, B\}$	16	$\{B, D, C, A, B, C\}$	23	$\{D, A, B, C, D, B\}$
3	$\{D, C, A, C, D, D\}$	10	$\{A, D, C, B, A, C\}$	17	$\{C, A, B, D, C, B\}$	24	$\{D, A, C, B, D, C\}$
4	$\{C, C, C, C, C, C\}$	11	$\{B, A, C, D, B, C\}$	18	$\{C, A, D, B, C, D\}$	25	$\{D, B, A, C, D, A\}$
5	$\{A, B, C, D, A, C\}$	12	$\{B, A, D, C, B, D\}$	19	$\{C, B, A, D, C, A\}$	26	$\{D, B, C, A, D, C\}$
6	$\{A, B, D, C, A, D\}$	13	$\{B, C, A, D, B, A\}$	20	$\{C, B, D, A, C, D\}$	27	$\{D, C, A, B, D, A\}$
7	$\{A, C, B, D, A, B\}$	14	$\{B, C, D, A, B, D\}$	21	$\{C, D, A, B, C, A\}$	28	$\{D, C, B, A, D, B\}$

3.3.4 Results and discussion

The DC SPS is tested using the example distributed control system, and a "base" scenario where the SPS has a fixed droop control. The base scenario provides a bottom-line performance reference to better demonstrate the MM benchmark. The distributed control operation for each layer is as follows.

Each ES starts with different SOC; then, they are charged to 80% capacity approximately 5 minutes before the engagement stage. The ESM operates the ES as spinning-reserve during the engagement stage as shown in Figure 4. The ES are synergistic in their charge/discharge operations as expected from the design's objective. After the engagement stage, all ES are charged to 80% SOC simultaneously. The effect of ESM in reducing total PGM power ramp rate from an average of 17 MW/s to less than 5 MW/s is shown in Figure 3.12 (a).

The goal of EEM is to reduce cost by saving fuel through optimizing PGM efficiencies. The EEM is active during the cruising stages (stages 1 and 3). The total fuel consumption of the PGM during the cruising stages, with and without EEM are shown in Figure 3.12 (b). The total fuel saving benefit of the EEM is 39.52 U.S. Gal which is about 1.2 % over 45 minutes. The gradual increase in fuel savings from stage 1 to 3 indicate potentially larger benefits in longer studies that span days or months. The EEM is turned off five minutes before stage 2 to allow ESM operation and reactivated five minutes after stage 2; this maneuver increases the overall fuel consumption, because: 1) there is no optimal PGM power allocation when the EEM is off, and 2) ES charging imposes extra load demand.

So far, the hierarchical control's performance was discussed with respect to its designed objectives. The MM benchmark provides a more holistic performance evaluation by calculating a

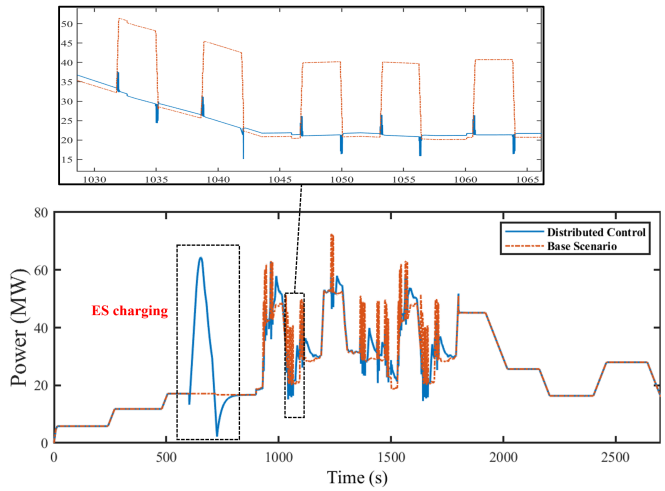

(a)

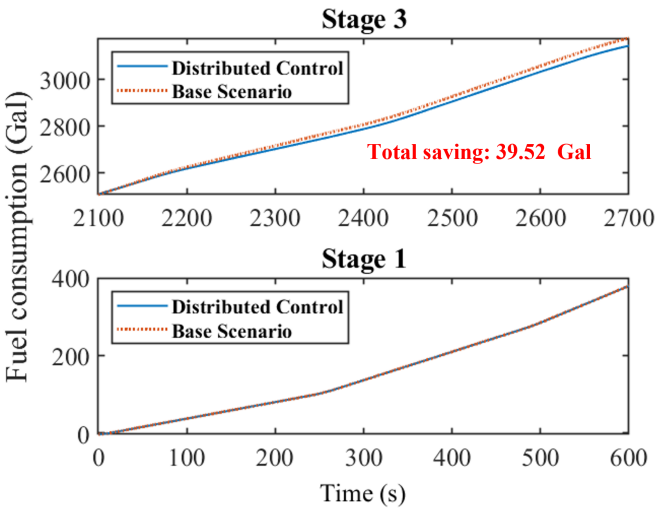

(b)

Figure 3.12: 4-zone DC Navy SPS operation results during the virtual test experiment. (a) The effect of using ESM on the total PGM ramp-rate during the engagement stage. (b) Total fuel consumption savings by the EEM during the cruising modes.

global criterion ($\mathcal{M}$) relative to the DM's preferences. The average $\mathcal{M}$ score during the test is shown in Figure 3.13 (a). Note that $\mathcal{M}$ is the combination of six different metrics normalized with respect to their designated references. Therefore, the most influential factors in $\mathcal{M}$ which are $\hat{M}_1, \hat{M}_2, \hat{M}_5$, and W_{1-6} are shown in Figure 3.13 (b), (c) and (d). The average $\mathcal{M}$ for the scenarios in Table 3.6 are demonstrated using colored contours in Figure 3.14.

Comparing Figure 3.13 with Figure 3.12, it is evident that although the hierarchical control

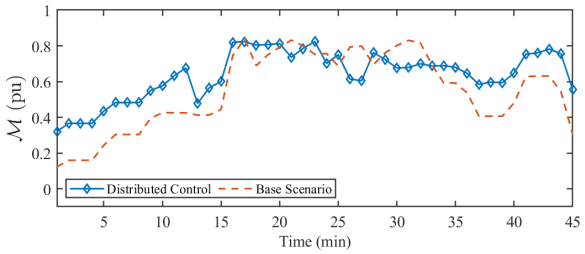

(a)

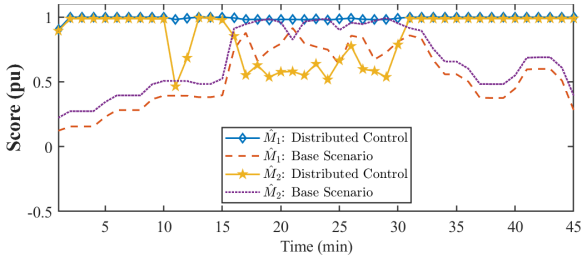

(b)

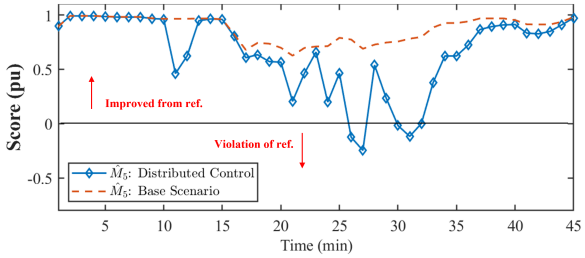

(c)

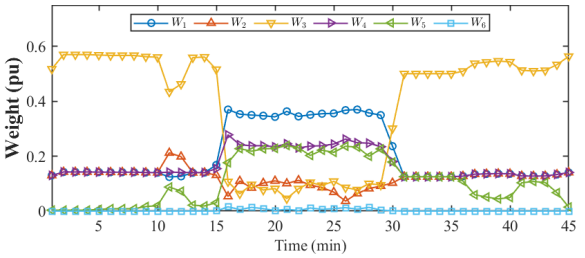

(d)

Figure 3.13: The real-time MM benchmark results during the virtual test experiment of the 4-zone DC Navy SPS.

was able to achieve its designer's performance objectives, the same conclusion cannot be definitively made from the DM's standpoint. The global performance ($\mathcal{M}$) with the candidate control is always higher during the cruising stages than the base scenario. The improved voltage profile ($\hat{M}_1$ and $\hat{M}_2$), and improved PGM efficiency ($\hat{M}_3$) are the main factors in $\mathcal{M}$. However in the engagement stage, utilization of ES increases the maximum current, thus adversely affecting $\hat{M}_2$ and $\hat{M}_5$ in the process.

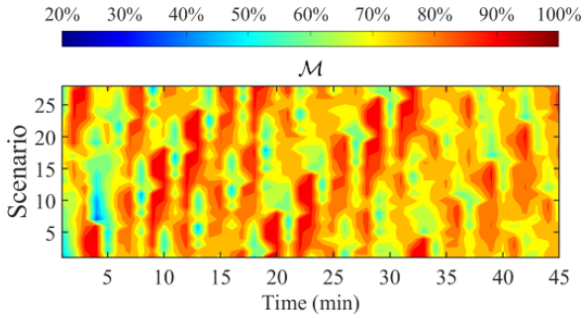

(a)

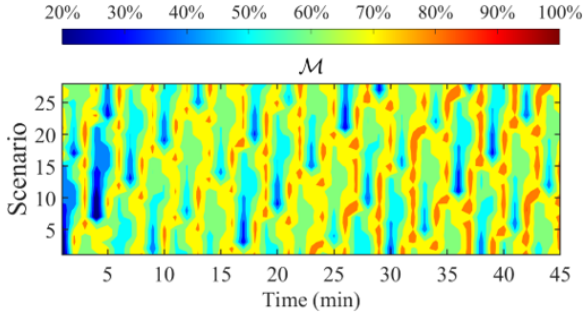

(b)

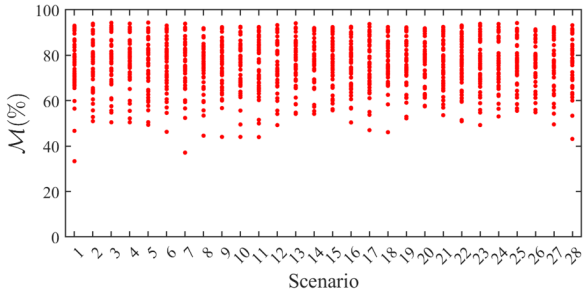

(c)

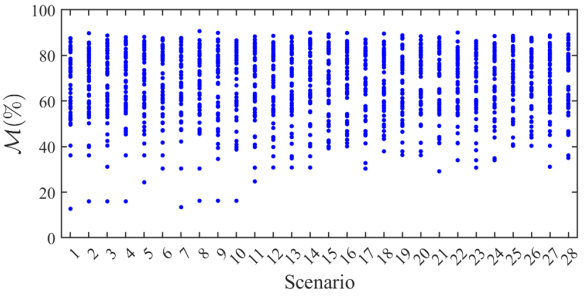

(d)

Figure 3.14: The *a postriori* MM benchmark results for different DM preference scenarios in the 4-zone DC Navy SPS.

This phenomenon describes a performance trade-off between $\hat{M}_2$, $\hat{M}_4$ (PGM ramp rate) and $\hat{M}_5$. It can be seen in Figure 3.13 (c) that $\hat{M}_5$ violates the 500 A DM reservation limit in the final minutes of the engagement stage. Note that 500 A is not necessarily a physical limitation, but rather a DM choice for performance assessment. Additionally, Figure 3.13 (d) shows how each metric is adaptively weighted based on DM preferences.

Statistical analysis of $\mathcal{M}$ are shown in Figure 3.14. The statistical analysis provides insight into the effects of varying DM preferences on the MM benchmark. Thus, if any specific preference results in an overall advantage or disadvantage in $\mathcal{M}$, it can be interpreted as either 1) the highest performing metric corresponds with the highest DM priority, 2) the least performing metric is also least important to the DM, or 3) both. Figure 3.14 (a) and (b) demonstrate the strong (red) and weak (blue) performances of the SPS with distributed control and the base scenario against time and different DM preferences.

The important data in Figure 3.14 (a) and (b) are summarized in Table 3.7. Scenarios 5, 20 and 25 produced the best maximum, minimum and average $\mathcal{M}$, respectively. Figure 3.14 (c) and (d) show that the average standard deviation (Std Dev) of $\mathcal{M}$ with distributed control is 10.58 % compared to 14.93 % in the base scenario. Std Dev of $\mathcal{M}$ is directly proportional to the number of system's transient dynamics. Therefore, it can be deduced from the MM analysis that the distributed control provided better transient response under similar operational circumstances than the base scenario.

Table 3.7: Summary of *a postriori* $\mathcal{M}$ data (with hierarchical control) for different DM preferences in the 4-zone DC Navy SPS.

no.	min/max/avg (%)	no.	min/max/avg (%)	no.	min/max/avg (%)	no.	min/max/avg (%)
1	33.36/93/75.42	8	44.59/91.91/75.84	15	55.76/92.4/76.34	22	50.94/93.1/76.39
2	50.97/93.9/76.09	9	44.05/92.38/75.71	16	50.42/92.56/75.99	23	49.27/93.85/75.87
3	50.49/94.29/76.07	10	44.05/92.54/75.57	17	47.03/93.77/75.71	24	53.05/93.79/76.75
4	50.49/93.94/76.83	11	43.97/92.43/75.19	18	46.13/92.45/76.51	**25**	**55.53/94.19/77.19**
5	**49.37/94.39/75.97**	12	49.25/93.27/75.79	19	52.21/92.29/76.32	26	54.87/91.41/76.83
6	46.28/93.08/75.99	13	54.2/94.1/76.05	**20**	**57.49/91.87/76.47**	27	49.56/92.37/76.07
7	37.12/93.92/75.87	14	54.2/92/76.69	21	53.62/92.49/76.06	28	43.16/93.22/75.98

Chapter 4

MetaMetric: Evolutionary Control in Power and Energy Systems

Nomenclature

DIWA	Dynamic Implicit Weighting Approach
CSA	Crow Search Algorithm
PSO	Particle Swarm Optimization
MOCSA	Multi-Objective Crow Search Algorithm
MOPSO	Multi-Objective Particle Swarm Optimization
MOO	Multi-Objective Optimization
EMO	Evolutionary Multi-objective Optimization
EED	Environmental/Economic Dispatch
DSS	Decision Support System
ROI	Region Of Interest
PF	Pareto optimal Front
DM	Decision-Maker
MM	MetaMetric
VSD	Variable Speed Drive
VFD	Variable Frequency Drive

4.1 Overview

This chapter extends the MM benchmark's application by integrating it into the decision making process of EMO algorithms. Section 4.2 repeats the key equations and concepts that are

necessary to integrate MM into EMO algorithms as their DSS. Section 4.3 reviews CSA as an evolutionary algorithm and introduces a new MOCSA with MM as its DSS. Sections 4.6 and 4.5 introduce two autonomous control example problems where EMO algorithms with MM DSS can be used to solve.

4.2 MetaMetric review

The DIWA preference articulation method and MM global criterion were introduced in Chapter 2, and utilized for *in-situ* performance benchmarking in two case studies in Chapter 3. In this chapter, MM will be used to form a new DSS for EMO algorithms. The goal is to produce a simple, flexible, and preference-oriented DSS that can be integrated into EMO algorithms with relative ease. The relevant equations from Chapter 2 are repeated in this section for the readers' convenience and easier referencing.

Straightforward normalization:

$$M_k := \tilde{f}_k(\mathbf{x}) = \frac{f_k(\mathbf{x}) - Z_k^{lo}}{Z_k^{up} - Z_k^{lo}} \tag{4.1}$$

DIWA:

$$c_k(t) = \frac{1 - M_k(t)}{\text{mean}(1 - M_k(t))} \tag{4.2a}$$

$$W_k'(t) = \min\left(\mu_k^{\max}, \max\left(\mu_k^{\min},\ c_k(t).\mu_k^{\text{avg}}\right)\right) \tag{4.2b}$$

$$W_k(t) = \frac{W_k'(t)}{\sum_{\forall k} W_k'(t)} \tag{4.2c}$$

Table 4.1: DM preference options.

Options	Range $\{\mu^{\min}, \mu^{\text{avg}}, \mu^{\max}\}$ (pu)
Low Importance	{0, 0.125, 0.25}
Medium Importance	{0.25, 0.375, 0.50}
High Importance	{0.50, 0.625, 0.75}
Very High Importance	{0.75, 0.875, 1}

MM criterion:

$$\mathcal{M}(M_k, W_k) = \sum_{k=1}^{K} W_k(t) M_k(t) \tag{4.3a}$$

$$\text{s.t.} \;\; 0 \leq W_k \leq 1 \tag{4.3b}$$

4.3 Crow search algorithm

4.3.1 Introduction

CSA is an evolutionary metaheuristic optimization method that was originally introduced by Askarzadeh [7]. CSA is inspired by the natural behavior of crows in search and preservation of food. Crows in CSA represent feasible solutions to an optimization problem. The CSA's straightforward concept, implementation, and low number of parameters make it and its various augmentations an attractive option in different optimization problems, especially time-constrained autonomous control applications [103, 97, 111, 64, 71, 89]. Figure 4.1 illustrates the concept behind the basic CSA. The CSA's iterative search pattern for a soluion vector $\mathbf{x} := \{x_i \mid i = 1 : N\}$, such that $\mathbf{x} \subset \mathcal{S}$, can be generally formulated as follows.

$$x_i(t+1) = \begin{cases} x_i(t) + r_i.fl(t).\big(x_j^*(t) - x_i(t)\big) & r_j \geq AP(t) \\ x_i^{\text{rand}} & \text{else} \end{cases} \tag{4.4}$$

Where x_j^* is the the so-called "leader" which determines the CSA's search direction. Awareness Probability (AP), and flight length (fl) are the two main parameters of CSA such that they represent the possibility of solution (crow) x_i following leader x_j^*, and its perturbation per iteration, respectively. $r_{i,j} \in [0, 1]$ are uniformly selected random numbers. x_i^{rand} is a randomly generated solution subject to applicable problem constraints.

The primary difference between a single-objective CSA and a MOCSA is the way x_j^* is generated. In single-objective CSA works (for example [103]), the generated population of solutions are evaluated with respect to the sole objective at the end of each iteration. The best solution found is then selected as the leader x_j^* in the subsequent iterations. In MOCSA (see [71, 64, 97]), leader selection is based on the domination operator, and an external archive. In addition to this, the

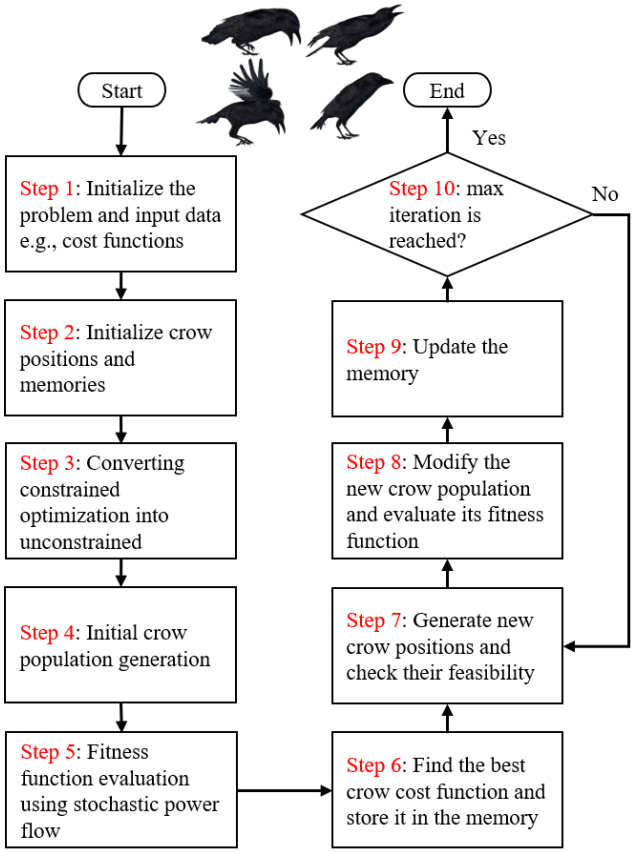

Figure 4.1: The CSA concept flowchart.

authors in [71] proposed some modifications (4.5) to enhance the search focus of the MOCSA, and claim improved convergence speed as a result. In essence, these modifications are designed to narrow down the range of $r_{i,j}$ as the algorithm progresses.

$$b = b^{\min} + (1 - b^{\min}).\frac{T - t}{T} \tag{4.5a}$$

$$\frac{1}{fl}(1 - b) \leq r(t) \leq \frac{1}{fl}(1 + b(fl - 1)) \tag{4.5b}$$

Where $b^{\min}$ is an additional algorithm parameter, denoted the minimum search range correction, and T is total of number of iterations. The problem with the modification in [71] is that it increases the number of parameters in CSA to three. However, this addition reduces one of the main CSA's advantages as an algorithm with minimal parameters, and reduces its robustness.

In [64], a similar but simpler idea to narrow the algorithm's search range is implemented without adding any additional parameters. More specifically, the authors used an Adaptive AP ($AAP = t/T$) to gradually increase the likelihood of solutions following their designated leader in each iteration as the algorithm progresses and better leaders are found. Furthermore, [64] uses chaotic per-unit flight lengths as shown in (4.6) and claim better exploration as a result.

$$fl(t+1) = \mathcal{G}\big(fl(t)\big) \tag{4.6a}$$

$$\mathcal{G}\big(fl(t)\big) = \begin{cases} \frac{1}{0.7} fl(t) & fl(t) < 0.7 \\ \\ \frac{1}{0.3} fl(t).\big(1 - fl(t)\big) & \text{else} \end{cases} \tag{4.6b}$$

However, (4.6) adds two new explicit parameters (0.3 and 0.7 in this case) which may not be suitable for all problems; thus, reducing the algorithm's extendability.

4.3.2 MOCSA with MetaMetric DSS

The fundamental difference of this new DSS for MOCSA is the introduction of a new leader selection mechanic based on the DIWA and MM concepts. Additionally, the Knowles' niching method (adaptive grid algorithm) [78] is employed to maintain a fixed archive size at all times and increase solution diversity. Generally, pressure parameters are used in the Boltzmann distribution to calculate the probability of leader selection among the non-dominated crows in the archive [71].

$$\mathcal{P}_i = \frac{e^{\pm\beta.\epsilon_i}}{\sum e^{\pm\beta.\epsilon_i}} \tag{4.7}$$

Where ϵ_i is the "energy" of the i-th crow, and β is an auxiliary variable known as the "pressure" parameter. The $-$ sign is used when there is an inverse relationship between ϵ_i and $\mathcal{P}_i$, and the $+$ is used when there is direct relationship between ϵ_i and $\mathcal{P}_i$. Two energies are considered for each non-dominated crow stored in the archive: 1) the total number of crows present in their region (diversity) based on the adaptive grid algorithm (ϵ_i^g) [78], and 2) their MM benchmark (ϵ_i^m).

In summary the adaptive grid mechanic functions as follows[1]. After non-dominated crows are filtered from the batch of generated crows in each iteration, they are assigned a "grid location"

[1] In-depth analysis of this method is out-of-scope. Interested readers are encouraged to visit [78] for more details.

in the objective space. Assuming the range of each objective is defined in the feasible space, the grid location can be found by repeatedly bisecting the range of each objective and determining in which half the non-dominated crow resides. The location of the solution is recorded as a binary string of length $2^{l.K}$ where l is the number of bisections (optimization parameter), and K is the number of objectives. Each time a crow in the archive is in the larger half of the prevailing bisection of the space, its corresponding bit in the binary string is set. A map of the grid is also memorized, indicating how many and which non-dominated crows in the archive currently reside there. The recursive subdivision of the objective space and grid location assignment is carried out adaptively to eliminate the need for a niche size parameter. This adaptive method works by calculating the range of the current archive members in the objective space and adjusting the grid so that it covers that range; then, grid locations are recalculated accordingly. ϵ_i^g is the hence the number of crows in the grid location where the i-th crow resides.

The MM criterion (4.3) of the archive members is calculated for each iteration based on straightforward normalization (4.1), and DIWA preference articulation (4.2). Consequentially, ϵ_i^m is the MM score of each crow stored in the archive. The total leader selection probability is the product of the probabilities from each energies' "perspectives" as follows. Note that $\beta = 1$ is assumed at all times in the Boltzmann distribution to reduce the optimization's total parameters.

$$\mathcal{P}_i^g = \frac{e^{-\epsilon_i^g}}{\sum e^{-\epsilon_i^g}} \tag{4.8a}$$

$$\mathcal{P}_i^m = \frac{e^{-\epsilon_i^m}}{\sum e^{-\epsilon_i^m}} \tag{4.8b}$$

$$\mathcal{P}_i = \mathcal{P}_i^g . \mathcal{P}_i^m \tag{4.8c}$$

$$\mathbf{x}^* \text{ is randomly selected based on probability distribution } \mathcal{P}_i \tag{4.8d}$$

A notional example shown in Figure 4.2 illustrates how the leader selection probability is determined from both the diversity and MM perspectives. The proposed MOCSA is depicted in Algorithm 1.

Algorithm 1 MOCSA with MM DSS pseudo code

input: T, l ,crow population (p_c), archive size (n_a), fl, problem constraints, DM opinion
initialize p_c
apply problem constraints
evaluate dominance (Def. 1.3.1)
store non-dominated crows (n_{nd}) in the archive
while $n_{nd} > n_a$ **do**
    apply the adaptive grid algorithm [78]
end while
for $i = 1 : n_a$ **do**
    apply DIWA (Eq. 4.2)
    normalize and calculate MM (Eq. 4.1 and 4.3)
    select the leaders ($\mathbf{x}^*$) from archive (Eq. 4.8)
end for
while $t \leq T$ **do**
    $AAP = \frac{t}{T}$
    for $j = 1 : p_c$ **do**
        apply CSA operator (Eq. 4.4)
        apply problem constraints
        evaluate dominance (Def. 1.3.1)
    end for
    update the archive
    while $n_{nd} > n_a$ **do**
        apply the adaptive grid algorithm [78]
    end while
    for $i = 1 : n_a$ **do**
        apply DIWA (Eq. 4.2)
        normalize and calculate MM (Eq. 4.1 and 4.3)
        update the leaders ($\mathbf{x}^*$) from archive (Eq. 4.8)
    end for
end while
sort the archive based on their MM score
output: the solution in archive with the best MM score

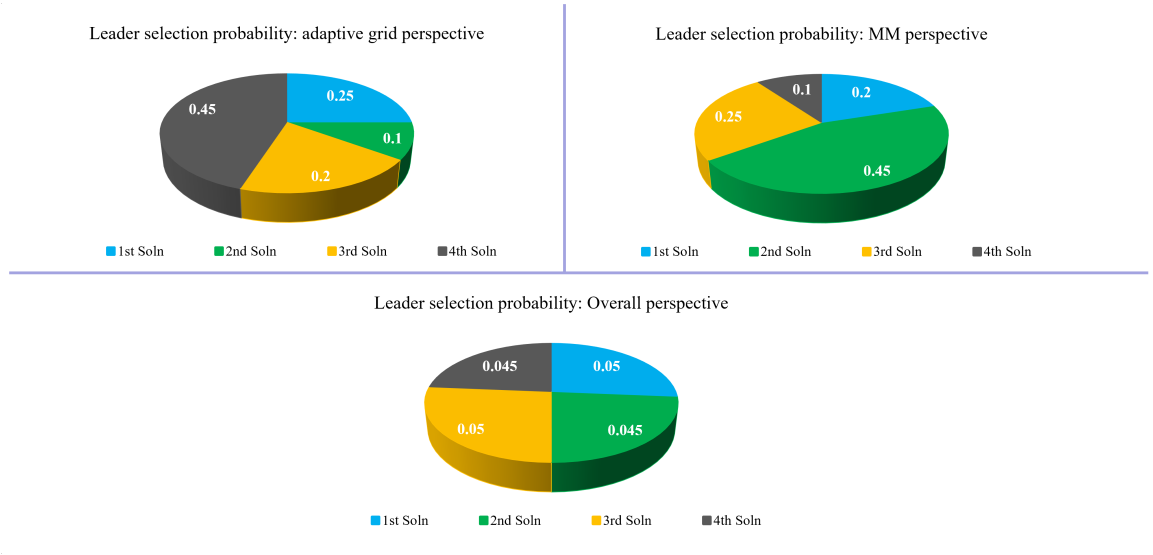

Figure 4.2: A leader crow selection probability example in MOCSA. The solution with the highest selection probability will lead the next iteration.

4.4 Particle swarm optimization

4.4.1 Introduction

PSO was originally introduced by Kennedy *et al* [76] as a single-objective algorithm for continuous non-linear function optimizations and neural network training. PSO is based on two main component methods. More obvious component is its general relationship to artificial life, and to bird flocking, fish schooling, and particularly the swarming theory. It is also related to evolutionary computation, and has both genetic algorithm and evolutionary programming elements into it. Later, various algorithmic augmentations, such as adding chaotic operators, or selection methods were proposed to increase the PSO's effectiveness [5, 85].

The multi-objective extension of PSO, denoted MOPSO, was originally proposed in [26], but despite discussing selecting leader solutions using Pareto dominance and crowding factors, the authors did not include any DM preference information. Similarly, more MOPSO works that were later published focused on improving the underlying algorithm and mitigating problems such as "swarm explosion" that were reported in some problems [123, 106, 98]. In [84], decomposition approach is used to break multiple objectives into a scalar aggregation. Decomposition is essentially a form of DSS that has weighting preference articulation, and seeks to minimize the distance and direction

of solution vectors to the Utopian vector. The biggest problem in decomposition is that the DM is expected to provide multiple explicit parameters such as weight vectors, a penalty factor. Additionally, the Utopian solution vector is not always easily found. Therefore, in this section the MM DSS is integrated into MOPSO to exploit the benefits that were previously shown for MOCSA, and to further demonstrate the MM's application in different EMO algorithms.

4.4.2 MOPSO with MM DSS

Each potential solution vector of the problem in a PSO algorithm is called a "particle" and the population of those solutions is called "swarm". A basic PSO updates the particle $\vec{x}_i$ at the iteration t as follows.

$$\vec{x}_i(t+1) = \vec{x}_i(t) + \vec{v}_i(t+1) \tag{4.9a}$$

$$\vec{v}_i(t+1) = w.\vec{v}_i(t) + C_1 r_1.(\vec{x}_p(t) - \vec{x}_i(t)) + C_2 r_2.(\vec{x}_g - \vec{x}_i(t)) \tag{4.9b}$$

Where $\vec{v}_i$ is called the particle velocity, $\vec{x}_p$ is the best solution at iteration t, and $\vec{x}_g$ is the best solution seen so far memorized in an external archive. w, C_1, and C_2 are inertia weight and control parameters which must be predefined by the DM. $r_1, r_2 \in [0, 1]$ are uniformly distributed random numbers.

Similar to MOCSA, the MM DSS is integrated by calculating the MM criterion and using it as reference to select particle leaders for each iteration. The external archive is subsequently updated considering Pareto dominance and adaptive grid factors. The logical flow of MOPSO with MM DSS is described in Algorithm 2.

Algorithm 2 MOPSO with MM DSS pseudo code

input: T, l ,swarm population (p_s), archive size (n_a), inertia weight (w), problem constraints, DM opinion
initialize p_c
apply problem constraints
evaluate dominance (Def. 1.3.1)
store non-dominated crows (n_{nd}) in the archive
while $n_{nd} > n_a$ **do**
    apply the adaptive grid algorithm [78]
end while
for $i = 1 : n_a$ **do**
    apply DIWA (Eq. 4.2)
    normalize and calculate MM (Eq. 4.1 and 4.3)
    select the leaders ($\mathbf{x}^*$) from archive (Eq. 4.8)
end for
while $t \leq T$ **do**
    for $j = 1 : p_s$ **do**
        apply PSO operator (Eq. 4.9)
        apply problem constraints
        evaluate dominance (Def. 1.3.1)
    end for
    update the archive
    while $n_{nd} > n_a$ **do**
        apply the adaptive grid algorithm [78]
    end while
    for $i = 1 : n_a$ **do**
        apply DIWA (Eq. 4.2)
        normalize and calculate MM (Eq. 4.1 and 4.3)
        update the leaders ($\mathbf{x}^*$) from archive (Eq. 4.8)
    end for
end while
sort the archive based on their MM score
output: the solution in archive with the best MM score

4.5 Example problem 1: Motor current optimization

Electric motor applications that use VSD/VFD require some type of speed control. Speed controls are either open loop or closed loop. Open loop speed control methods propagate an speed/torque/flux reference input into corresponding voltage/current set-points (depending on the downstream switching control method) using mathematical models of the motor under control. As indicated by its name, open loop speed control does not use any feedback information measured from the system. Closed loop speed control in the other hand provides set-points to the switching control based on minimizing the error between reference and measured information. Generally, closed loop methods are preferred over open loop variants due to better accuracy, reliability and robustness, but they are more expensive because of the additional measurement equipment.

The timing constraints are several orders of magnitude smaller in speed control than EED problems. Therefore, most optimization techniques, especially gradient-based, are impractical in speed control applications, and are only useful for offline benchmarks. This problem exacerbates if there are two or more conflicting objectives involved. Considering the electromagnetic torque output and winding ohmic losses as two conflicting objectives that are proportional to the current magnitude (decision variable), the following MOO problem can be formulated.

$$\min \mathbf{f}(I) := \min\{-\tau, P_{cu}\} \tag{4.10a}$$

$$\text{s.t.} \quad \begin{cases} I^{\min} \leq I \leq I^{\max} \\ \tau^{\min} \leq \tau \leq \tau^{*} \end{cases} \tag{4.10b}$$

Where τ is the motor electromagnetic torque magnitude, P_{cu} is the winding ohmic loss, and I is the winding current magnitude. $\tau^{\min}$ is the minimum torque constraint and τ^{*} is the reference torque. $\tau^{\min}$ is calculated as a fraction of τ^{*} as follows.

$$\tau^{\min} = (1 - \alpha)\tau^{*} \tag{4.11}$$

Where α is the ratio of τ^{*} that is available for optimization. For example, $\alpha = 0.2$ means that there is a 20% torque window for optimization. Note that τ^{*} is entirely dependent on the drive

cycle circumstances, and the subsequent speed control commands. τ depends on the design and properties of different motors, and so must be determined on a case-by-case basis.

4.6 Example problem 2: EED

EED is a dual-objective optimization problem that includes the economic and environmental cost of operating power/energy systems. Similar to other MOO problems, EEDs requires some type of DSS to evaluate, sort and output solutions from the PF. Evolutionary algorithms are popular EED methods due to their simplicity, flexibility and practicality. Although generally less accurate than derivative-based optimization approaches, EMO methods provide a balance between performance and speed which is useful in dynamic applications such as EEDs.

So far, MM was introduced as a means for multi-criteria performance evaluation, and a preference-based DSS in EMO algorithms. In this section, the EED problem in power and energy systems is investigated in particular as a suitable application for the proposed DSS. A general form of an EED problem in an AC power system at any given time and its applied constraints is shown in the following.

$$\min \mathbf{f}(\mathbf{P}) := \min\{f_{\mathcal{C}}, f_{\mathcal{E}}\} \tag{4.12a}$$

$$f_{\mathcal{C}} := \sum_{i=1}^{N_g} \Big(\mathcal{U}_i \mathcal{C}_i(P_i)\Big) + \mathcal{C}_{grid} P_{grid} \tag{4.12b}$$

$$f_{\mathcal{E}} := \sum_{i=1}^{N_g} \Big(\mathcal{U}_i \mathcal{E}_i(P_i)\Big) + \mathcal{E}_{grid} P_{grid} \tag{4.12c}$$

$$\text{s.t.} \quad \begin{cases} \mathbf{P}^{\min} \leq \mathbf{P} \leq \mathbf{P}^{\max} \\ \mathbf{V}^{\min} \leq \mathbf{V} \leq \mathbf{V}^{\max} \end{cases} \tag{4.12d}$$

Where:

- $\mathbf{P} := \{P_i \mid \forall i \in \{1, \ldots, N_g\}\}$, and $\mathbf{V} := \{V_j \angle \delta_j \mid \forall j \in \{1, \ldots, N_b\}\}$ are the generated power and bus voltage vectors respectively.
- N_g and N_b are the number of dispatchable power generation units and buses (nodes), respec-

tively.

- $\mathcal{U}_i$ is the On/Off status of power generation units.
- $\mathcal{C}_i(P_i)$ are power generation unit cost functions (usually quadratic).
- $\mathcal{C}_{grid}$ is the per unit cost of purchasing power from outside sources (grid).
- $\mathcal{E}_i(P_i)$ are power generation unit emission functions.
- $\mathcal{E}_{grid}$ is the per unit emission footprint of purchasing power from the grid.

Chapter 5

MetaMetric Control Case Studies

Nomenclature

EV/HEV	Electric/Hybrid-Electric Vehicles
ICE	Internal Combustion Engine
PMSM	Permanent Magnet Synchronous Machines
IPM	Interior Permanent Magnet
NPC	Neutral-Point-Clamped
LPTN	Lumped Parameter Thermal Network
MOCSA	Multi-Objective Crow Search Algorithm
MTPA	Maximum Torque Per Ampere
DSS	Decision Support System
MM	MetaMetric
SVM	Space Vector Modulation
NEMA	National Electrical Manufacturers Association
DRTS	Digital Real-Time Simulation
EED	Economic and Environmental Dispatch
WT	Wind Turbine

5.1 IPMSM traction motor drive

5.1.1 Introduction

The rapid growth of EV/HEV in transportation has created a need for state-of-the-art control methods and technologies that improve their performance and overall efficiency. EV/HEV powertrains replace traditional mechanical propulsion systems in ICE vehicles with one or more electric traction motors [45]. Rise of semiconductor switching devices in the 20th century facilitated the development of advanced control methodologies such as variable speed and variable frequency motor drives. These advanced motor drive systems were particularly useful in the automotive industry to complement and eventually replace mechanical power transmission in vehicles [121, 20].

The sensitive nature of semiconductor devices and high maintenance cost of traction motors, especially permanent magnet types, are challenging issues in EV/HEV. A drive system that can simultaneously consider multiple, often conflicting, control objectives to produce the "best" trade-off operation is helpful in mitigating these challenges. Two important objectives in traction motor drives are: 1) speed/torque response, and 2) thermal cycling/overheating. The former objective looks to maximize performance at any cost, which conflicts the latter's purpose of minimizing thermal side effects. Long term issues such as degradation, thermal fatigue, and component failures which increase maintenance frequency are directly proportional to thermal objectives. Speed/torque response is specifically important in high-intensity applications such as military ground vehicles which require high quality (minimal steady-state error and dynamic overshoot/undershoot) performance to meet their operational demands.

5.1.2 Plant model

Before designing the control structure, the "plant" under control must be appropriately selected and modeled. Different types of traction motors exist for EV/HEV but PMSM, and more specifically IPM variants are advantageous since they have relatively higher power density and efficiency [40, 148]. However, recently some studies suggest switched-reluctance motors as suitable new candidates for traction motors in EV/HEV [60, 104]. A NPC inverter-fed IPM traction motor is chosen in this case study. By neglecting the time-variant properties and assuming that the motor will not operate in the magnetic saturation region, a forth order model can be used to describe the

IPM as given in (5.1). This model is proved to be accurate enough for control design purposes [12].

$$\begin{bmatrix} \dot{i}_d \\ \dot{i}_q \\ \dot{\omega}_m \\ \dot{\theta}_m \end{bmatrix} = \begin{bmatrix} -\frac{R_s}{L_d} & \frac{L_q}{L_d} p\omega_m & 0 & 0 \\ -\frac{L_d}{L_q} p\omega_m & -\frac{R_s}{L_q} & -\frac{\lambda_f}{L_q} p & 0 \\ \frac{3}{2J_{eq}} p(L_d - L_q) i_q & \frac{3}{2J_{eq}} p\lambda_f & -\frac{1}{J_{eq}} \eta & 0 \\ 0 & 0 & 1 & 0 \end{bmatrix} \begin{bmatrix} i_d \\ i_q \\ \omega_m \\ \theta_m \end{bmatrix} + \begin{bmatrix} \frac{1}{L_d} & 0 & 0 \\ 0 & \frac{1}{L_q} & 0 \\ 0 & 0 & -\frac{1}{J_{eq}} \\ 0 & 0 & 0 \end{bmatrix} \begin{bmatrix} v_d \\ v_q \\ \tau_m \end{bmatrix} \tag{5.1}$$

Where i_d, i_q, L_d and L_q are IPM winding currents and inductances in the synchronous frame of reference (dq-axis), respectively. R_s is the average winding resistance per phase. p is the number of pole pairs. λ_f is the PM (field) flux linkage. η is the rotor damping coefficient. ω_m, θ_m and J_{eq} are the mechanical angular speed, rotor angular position and equivalent inertia applied to the shaft, respectively. v_d and v_q are the dq-axis phase voltages at the motor terminals. τ_m is the load torque applied to the shaft. J_{eq} is the equivalent vehicle inertia and will be further discussed in the case study section.

5.1.3 Thermal models

To analytically model and predict thermal states, i.e. temperatures, an equivalent analytical model known as LPTN is used. LPTN utilizes the thermal and electrical circuit similarities to estimate thermal dynamics via equivalent RC circuits. Depending on the LPTN's order, it aggregates multiple heat paths with each other and assumes cylindrical structure and uniform heat distribution in different components. Although LPTN is not the most accurate method for thermal modeling, they are proven to be within 5% error range in the literature [35, 68, 127]. The experimental validation shown by the authors in [68] demonstrate that a third order LPTN can estimate motor temperatures

with a ±3 Kelvin accuracy. The biggest challenge in developing LPTN is to identify and approximate heat paths, thermal resistances and heat capacities of different components [91]. The LPTN method for converter thermal modeling is also well-established in the literature [102, 8]. Due to their relative simplicity and sufficient accuracy, third order LPTNs are used for estimating the converter and motor thermal states. The state-space equations for the converter and motor LPTNs are shown in (5.2-5.3) and (5.4), respectively.

$$\begin{bmatrix} \dot{T}_J \\ \dot{T}_1 \\ \dot{T}_2 \end{bmatrix} = \mathbf{A}_{con} \begin{bmatrix} T_J \\ T_1 \\ T_2 \end{bmatrix} + \mathbf{B}_{con} \begin{bmatrix} P_{L,con} \\ T_p \end{bmatrix} \tag{5.2a}$$

$$\begin{bmatrix} \dot{T}_W \\ \dot{T}_{EW} \\ \dot{T}_{Rot} \end{bmatrix} = \mathbf{A}_{mot} \begin{bmatrix} T_W \\ T_{EW} \\ T_{Rot} \end{bmatrix} + \mathbf{B}_{mot} \begin{bmatrix} P_W \\ P_{EW} \\ P_{Rot} \\ T_C \\ T_E \end{bmatrix} \tag{5.2b}$$

Such that

$$\mathbf{A}_{con} = \begin{bmatrix} -\frac{1}{\mathcal{C}_{th1}\mathcal{R}_{th1}} & \frac{1}{\mathcal{C}_{th1}\mathcal{R}_{th1}} & 0 \\ \frac{1}{\mathcal{C}_{th1}\mathcal{R}_{th1}} & -\frac{\mathcal{R}_{th1}+\mathcal{R}_{th2}}{\mathcal{C}_{th2}\mathcal{R}_{th1}\mathcal{R}_{th2}} & \frac{1}{\mathcal{C}_{th2}\mathcal{R}_{th2}} \\ 0 & \frac{1}{\mathcal{C}_{th3}\mathcal{R}_{th2}} & \frac{\mathcal{R}_{th2}+\mathcal{R}_{th3}}{\mathcal{C}_{th3}\mathcal{R}_{th2}\mathcal{R}_{th3}} \end{bmatrix} \tag{5.3a}$$

$$\mathbf{B}_{con} = \begin{bmatrix} \frac{1}{\mathcal{C}_{th1}} & 0 \\ 0 & 0 \\ 0 & \frac{1}{\mathcal{C}_{th3}\mathcal{R}_{th3}} \end{bmatrix} \tag{5.3b}$$

$$\mathbf{A}_{mot} = \begin{bmatrix} \frac{1}{\mathcal{C}_W} a_{11} & \frac{1}{\mathcal{C}_W} a_{12} & \frac{1}{\mathcal{C}_W} a_{13} \\ \frac{1}{\mathcal{C}_{EW}} a_{21} & -\frac{1}{\mathcal{C}_{EW}} a_{22} & 0 \\ \frac{1}{\mathcal{C}_{Rot}} a_{31} & 0 & \frac{1}{\mathcal{C}_{Rot}} a_{33} \end{bmatrix} \tag{5.4a}$$

$$\mathbf{B}_{mot} = \begin{bmatrix} \frac{1}{\mathcal{C}_W} & 0 & 0 & \frac{1}{\mathcal{C}_W \mathcal{R}_{W-C}} & 0 \\ 0 & \frac{1}{\mathcal{C}_{EW}} & 0 & 0 & 0 \\ 0 & 0 & \frac{1}{\mathcal{C}_{Rot}} & 0 & \frac{1}{\mathcal{C}_{Rot} \mathcal{R}_{Rot-E}} \end{bmatrix} \tag{5.4b}$$

$$a_{11} = -\Big(\frac{1}{\mathcal{R}_{W-C}} + \frac{1}{\mathcal{R}_{W-EW}} + \frac{1}{\mathcal{R}_{W-Rot}}\Big) \tag{5.4c}$$

$$a_{12} = a_{21} = -a_{22} = \Big(\frac{1}{\mathcal{R}_{W-EW}}\Big) \tag{5.4d}$$

$$a_{13} = a_{31} = \Big(\frac{1}{\mathcal{R}_{W-Rot}}\Big) \tag{5.4e}$$

$$a_{33} = -\Big(\frac{1}{\mathcal{R}_{W-Rot}} + \frac{1}{\mathcal{R}_{Rot-E}}\Big) \tag{5.4f}$$

Where T_J, T_1 and T_2 are the temperatures of the switch junction, the first layer and the second layer between the junction and the switch plate, respectively. T_P is the switch plate temperature. $P_{L,con}$ is the total power loss of the switch. T_W, T_{EW} and T_{Rot} are the winding, end-winding and rotor temperatures in the motor, respectively. P_W, P_{EW} and P_{Rot} are the interior winding copper loss plus stator iron loss, exterior (end) winding copper loss and rotor iron loss, respectively. T_C and T_E are the coolant and environment temperatures of the motor. $\mathcal{R}$ and $\mathcal{C}$ represent thermal resistances and heat capacities of different heat paths and components of the converter and motor as shown in Figure 5.1.

5.1.4 Power loss calculation

The inputs to the LPTNs are power losses modeled as heat/current sources. There are two types of converter power loss: 1) switching, and 2) copper (ohmic). Calculating converter losses is straightforward and provided in (5.5)-(5.8) [102]. The parameters necessary to calculate those losses

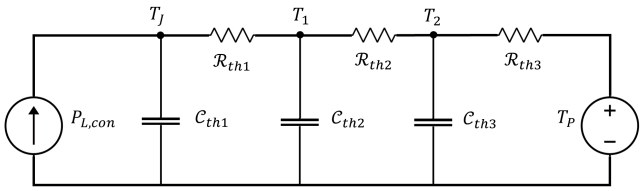

(a) Converter LPTN.

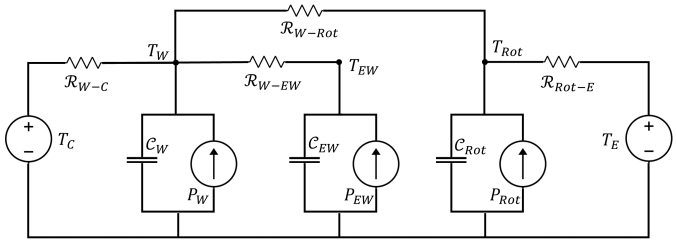

(b) Motor LPTN.

Figure 5.1: The third order LPTNs used for temperature estimation.

are provided in semiconductor switching device datasheets from manufacturers.

$$E_{sw} = \big(E_{on} + E_{off}\big)\Big(\frac{i_D}{i_{ref}}\Big)^{K_i}\Big(\frac{v_{dc}}{v_{ref}}\Big)^{K_v} \big(1 + c_{T,sw}(T_J - T_{J,ref})\big) \tag{5.5}$$

$$E_d = E_{rr}\Big(\frac{i_f}{i_{d,ref}}\Big)^{K_{i,d}}\Big(\frac{v_f}{v_{d,ref}}\Big)^{K_{v,d}} \big(1 + c_{T,d}(T_{J,d} - T_{J,d,ref})\big) \tag{5.6}$$

$$P_{cond,sw} = R_{on} * I_D^2 \tag{5.7}$$

$$P_{cond,d} = V_{SD} * I_F \tag{5.8}$$

Where E_{on}, E_{off} and E_{rr} are the turn-on and off switching energies and diode recovery energy, respectively. i_{ref}, v_{ref}, $T_{J,ref}$ and $T_{J,d,ref}$ are the operational references at which the datasheet information are given for current, voltage, switch junction temperature and diode junction temperature, respectively. $K_{v/v,d}$, $K_{i/i,d}$, $c_{T,sw/d}$ and $c_{T,rr}$ are empirical constants. i_c, i_f, R_{on} and V_{SD} are the drain (collector in IGBT) current, forward current, on-state resistance and source-drain voltage,

respectively.

Calculating motor power losses is more sophisticated than converters, because there are more power loss sources in different parts of the motor such as mechanical friction (shaft and bearings), iron losses (rotor hysteresis, rotor eddy current, stator hysteresis, stator eddy current) and winding copper loss. Motor losses are functions of either current (winding copper loss), speed (mechanical friction) or both (iron losses). To circumvent differential loss calculations during each control cycle, lookup tables are derived offline and integrated into the control algorithm. Such lookup tables are three-dimensional, outputting estimated power losses based on shaft speed and electromagnetic torque indices. Note that electromagnetic torque is directly proportional to winding current. The lookup tables cover the entire torque/speed operating range of the motor but linear interpolation and extrapolation is used for any unspecified indices. The winding copper loss, stator iron loss and rotor iron loss lookup tables are derived using ANSYS Motor-CAD. The iron loss calculation techniques used in ANSYS Motor-CAD are based on a mixture of finite element analysis and analytical models such as the method proposed in [92].

5.1.5 Control strategy

The utilized control strategy has three successive elements: 1) PI speed error controller, 2) MOCSA with MM DSS reference current optimizer, and 3) MTPA control.

The PI controller is intended to generate electromagnetic torque references based on the error between the desired and actual speed values. Common tuning methods such as the Ziegler-Nichols method [152], and some trial-error adjustments are used to set the PI controller gains. The speed controller generates an appropriate torque reference (τ^*) considering the speed error at each time step. The PI speed controller function is as follows.

$$\tau^* = K_P.e_\omega(t) + K_I.\int_{t_0}^{t_1} e_\omega(t)dt \tag{5.9a}$$

$$e_\omega(t) = \omega_m^*(t) - \omega_m(t) \tag{5.9b}$$

Where K_P and K_I are the proportional and integral gains, respectively. ω_m^* is the reference angular speed command requested by the driver or autonomous driving program.

The MOCSA with MM DSS is incorporated into the control strategy as shown in Figure 5.2. MTPA is a control strategy used in PMSM drive systems to achieve maximum torque utilization for a given current reference at any time. MTPA is particularly effective for operation in the field-weakening region [86, 149]. IPMSM in particular have PMs embedded into the rotor structure which generate magnetic saliency. This magnetic saliency produces a reluctance torque because of the resulting difference between L_d and L_q. Maximum efficiency can be achieved in IPMSM by properly selecting a current vector ratio between magnetic torque current (i_q^*) and reluctance torque current (i_d^*) satisfying the total current magnitude (I_m) constraint [83]. There are two modes of operation in IPMSM: 1) constant torque, 2) constant power (field-weakening), which are determined based on rotor speed. If ω_m is less than the base speed ($\omega_m \leq \omega_b$), the IPMSM is in the constant torque mode, and if $\omega_m > \omega_b$, it is in constant power mode. Calculating the appropriate (i_q^*, i_d^*) to achieve MTPA in constant torque and power regions is shown in (5.10).

$$I_m = \sqrt{{i_q^*}^2 + {i_d^*}^2} = \frac{2}{3p\lambda_f}\tau^* \tag{5.10a}$$

$$i_d^* = \begin{cases} \frac{\lambda_f}{4(L_q - L_d)} - \sqrt{\frac{\lambda_f^2}{16(L_q - L_d)^2} + \frac{I_m^2}{2}} & \omega_m \leq \omega_b \\ \frac{-\lambda_f L_d + \sqrt{(\lambda_f L_d)^2 - (L_d^2 - L_q^2)(\lambda_f^2 + L_q^2 I_m^2 - \frac{v_{\max}^2}{\omega_e^2})}}{(L_d^2 - L_q^2)} & \omega_m > \omega_b \end{cases} \tag{5.10b}$$

$$i_q^* = \sqrt{I_m^2 - {i_d^*}^2} \tag{5.10c}$$

Where $v_{\max}$ is the maximum peak fundamental line to neutral voltage supplied to the motor, and is calculated as follows.

$$v_{d0} = -\omega_e L_q i_q \tag{5.11a}$$

$$v_{q0} = \omega_e (L_d i_d + \lambda_f) \tag{5.11b}$$

$$v_{\max} = \sqrt{{v_{d0}}^2 + {v_{q0}}^2} \tag{5.11c}$$

Where v_{d0} and v_{q0} are the d-axis voltage when i_d is zero, and the q-axis voltage when i_q is zero, respectively. $\omega_e = p\omega_m$ is the electrical angular rotor speed.

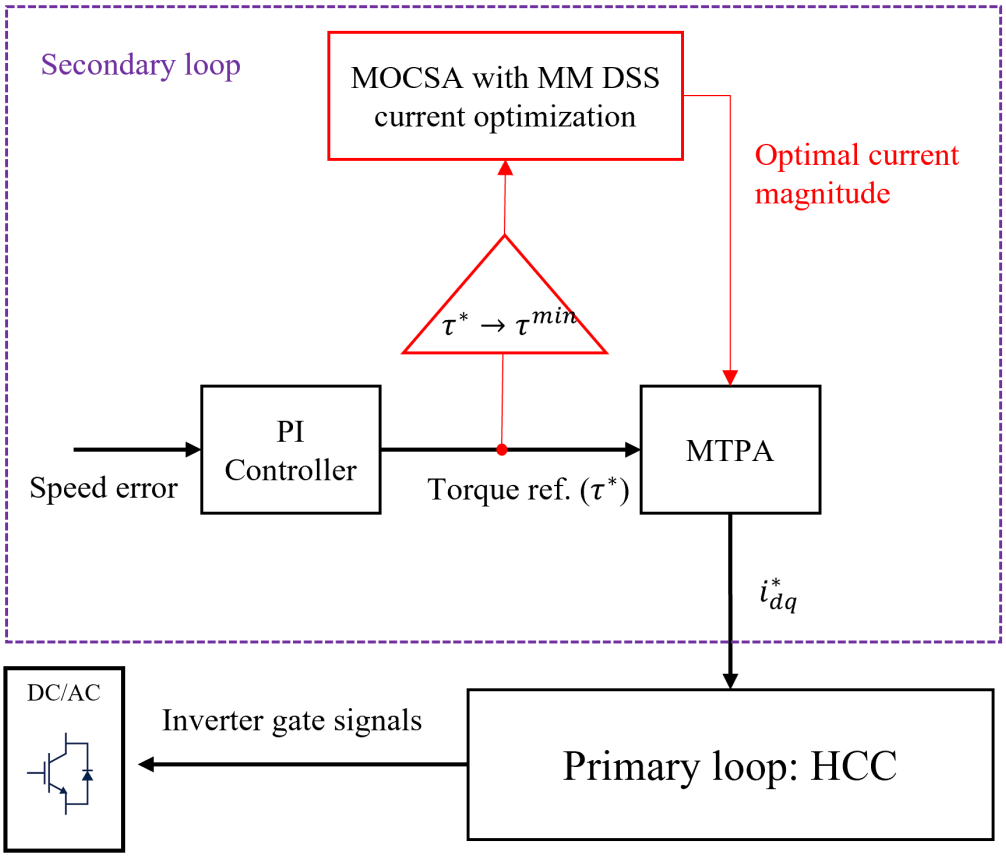

Figure 5.2: The IPMSM control schematic with MOCSA and MM DSS current magnitude optimization.

5.1.6 Modulation scheme

SVM is used to find the optimal gate signals based on the presented control objectives. There are a limited number of possible space vector combinations depending on the topology of the controlled converter. The NPC converter has three legs with a maximum of three states for each leg. Therefore, there are 27 total vectors but nine of them are the same, so the total number is reduced to 19 (Figure 5.3). The converter leg states and the generated voltage in dq-frame is given in (5.12).

$$S_x = \begin{cases} +1(P) & S_{1x},\ S_{2x}:\ \text{ON} \\ 0 & S_{2x},\ S_{3x}:\ \text{ON} \\ -1(N) & S_{3x},\ S_{4x}:\ \text{ON} \end{cases} \tag{5.12}$$

Where S_{ix} is the switching state of the i-th switch in the x-th leg of the converter.

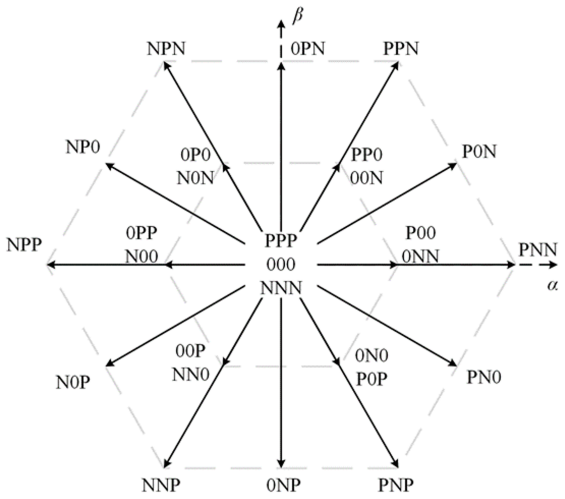

Figure 5.3: Three-level converter voltage vectors.

5.1.7 Example motor and vehicle specifications

To derive the parameters required to use the control methodology presented in the previous section, a series of offline analysis are conducted using the multi-physics software ANSYS Motor-CAD and switching device design software SaberRD. The first step is to design an example IPM traction motor. The example traction motor is a 120 kW 8 pole IPM with a maximum speed of 10,000 rpm. The example IPM and vehicle general specifications are shown in Table 5.2 and Table 5.3, respectively. NEMA has categorized maximum operating motor winding temperatures based on their insulation quality [99]. There are five NEMA insulation classes (A, B, F and H), but most applications are either class B or F. Class F motors have a maximum allowable winding temperature of 155 °C. In a traction motor the total inertia applied to the shaft includes a factor of the overall vehicle mass, wheel radius and gear ratio. The precise value of the vehicle inertia must be experimentally calculated for specific vehicles; however, some numerical approximations are proposed in the literature for an "equivalent" rotational inertia [46]. The equivalent rotational inertia of an average vehicle is given by (5.13).

Table 5.2: Example IPM traction motor specifications

Base speed (n_b)	6500 rpm
Max. speed ($n_{\max}$)	10,000 rpm
Rated power (P_r)	120 kW
Pole pairs (p)	4
Max. winding current mag. ($I_{\max}$)	480 A
Winding resistance (R_s)	0.01267 Ω
dq-axis inductances (L_d, L_q)	0.1901, 0.4528 mH
PM flux linkage (λ_f)	0.07 V.s
NEMA insulation class	F

Table 5.3: Example ground vehicle specifications

Mass (m)	5,000 lbs
Gear ratio (G)	7.938
Rolling resistance coefficient	0.045
Wheel radius (r_w)	15 in

$$J_{eq} = \frac{m_e r_w^2}{G^2} \tag{5.13a}$$

$$m_e = \delta m \tag{5.13b}$$

$$\delta = 1 + 0.04 + 0.0025 G^2 \tag{5.13c}$$

5.1.8 Simulation results

Substituting $I^{\max} = 480$ A in (4.10) for the example 120 kW IPM introduced in this section, the MOCSA with MM DSS (Algorithm 1) is utilized to solve the IPM optimization problem. The results for three different DM preference settings are shown in Figure 5.4. It must be noted that the results shown in Figure 5.4 are independent of any drive cycle requirements, and are meant to show how DM preferences are applied to select the final solution in the problem's entire possible PF. It is evident from Figure 5.4 that the solutions found by MOCSA with MM DSS are superimposed on the algebraically calculated "true" PF of the problem. The reference used to derive the true PF is based on the direct multisearch method which has a proven convergence and robust efficiency in more than 50 MOO test problems with a diverse range of decision variable and objective numbers [29].

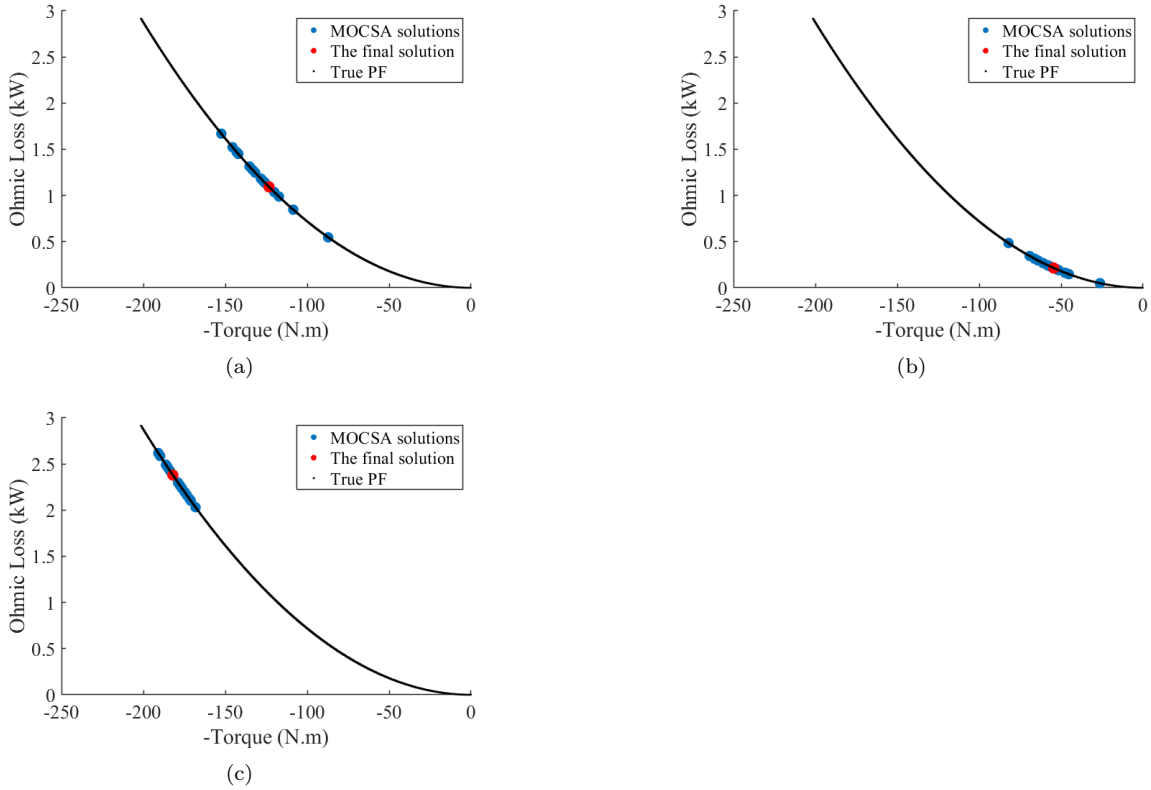

Figure 5.4: The optimization results for the example IPMSM using MOCSA with MM DSS, a) DM preference: medium (torque) - medium (power loss), b) DM preference: medium (torque) - high (power loss), c) DM preference: high (torque) - medium (power loss).

5.1.9 Experimental setup

The real-time experiments are conducted via DRTS using a Speedgoat simulator. The control strategy was modeled and deployed into the simulator's CPU, and the traction motor drive system model was programmed into the Xilinx FPGA device using Speedgoat's HDL compiler in Simulink. The CPU and Xilinx FPGA are connected via peripheral component interconnect express (PCIe) communication. The DRTS setup is illustrated in Figure 5.5.

The WLTC Class 2 standard drive cycle provided by the United Nations is used for real-time testing. The key aspect of this drive cycle that makes it suitable for testing the control system is the variable torque load and speed which challenges the control responsiveness and robustness. The WLTC Class 2 drive cycle is shown in Figure 5.6.

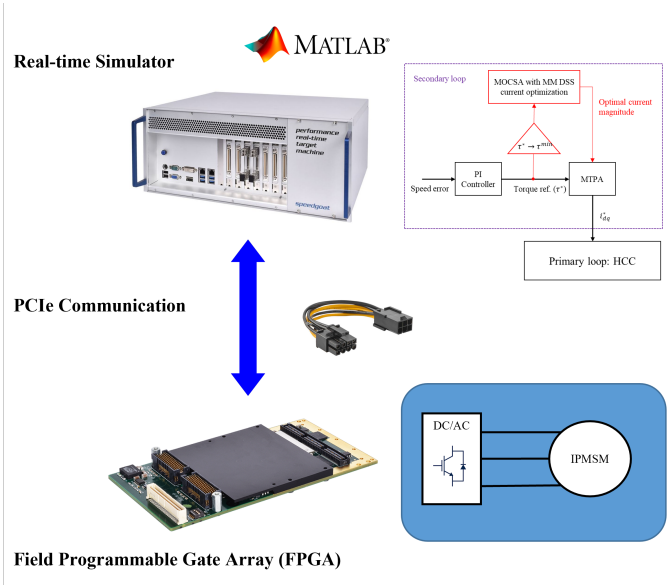

Figure 5.5: DRTS setup schematic, including a Speedgoat real-time simulator and a Xilinx FPGA.

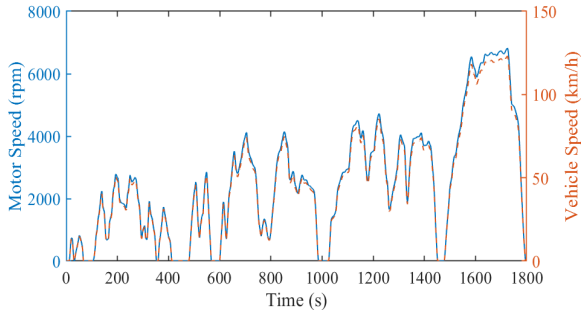

(a)

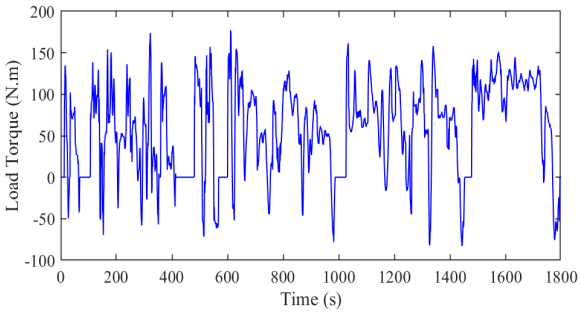

(b)

Figure 5.6: WLTC Class 2 standard driving cycle, (a) speed profile, (b) traction torque profile.

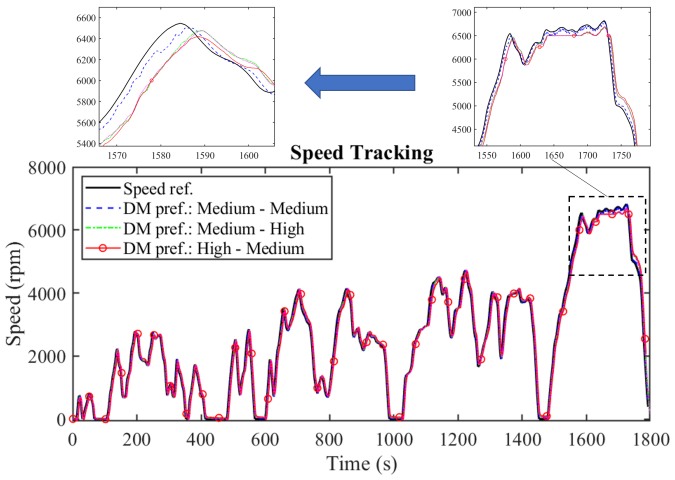

Figure 5.7: The DRTS speed tracking performance for the WLTC class 2 drive cycle.

5.1.10 Real-time results

The real-time experiments are conducted for three different DM preference scenarios, and the WLTC Class 2 drive cycle. Two criteria, i.e., speed tracking performance, and temperature benchmarks, are sufficient to demonstrate the proposed control method's impact on the traction motor's drive system. The average speed tracking performance over the 30 minutes long drive cycle, with and without MOCSA for all DM preference scenarios is illustrated in Figure 5.7. Consequentially, three different temperatures, i.e., end-winding, rotor, and switch junction, were analytically estimated using the LPTN method outlined in subsection 5.1.3. The real-time temperature benchmarks are shown in Figure 5.8. The overall average temperature benchmark improvement and absolute speed error are illustrated in Figure 5.9. Note that the first objective is torque and the second one is power loss in the preference articulation; so, medium-high means torque has medium and power loss has high relative importance for the DM.

The results in Figures 5.7, 5.8 and 5.9 clearly show the trade-off relationship between speed tracking and temperature performance of the traction IPMSM, as a result of the proposed current optimization method. The DM's opinions are also reflected in the performance benchmarks. The high-medium DM preference test generated the least mean absolute speed error at 126.61 rpm, in contrast to 135.12 rpm and 196.63 rpm in medium-medium and medium-high tests, respectively. On the other hand, the mean temperature reductions for the high-medium DM preference scenario are 0.74%, 0.20%, and 0.13% in the end-winding, rotor and switch junction, respectively. As anticipated,

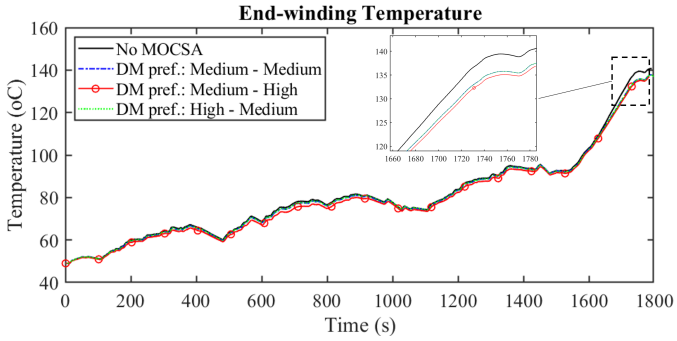

(a)

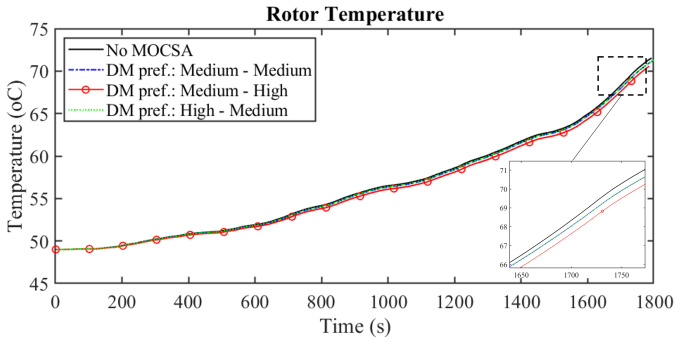

(b)

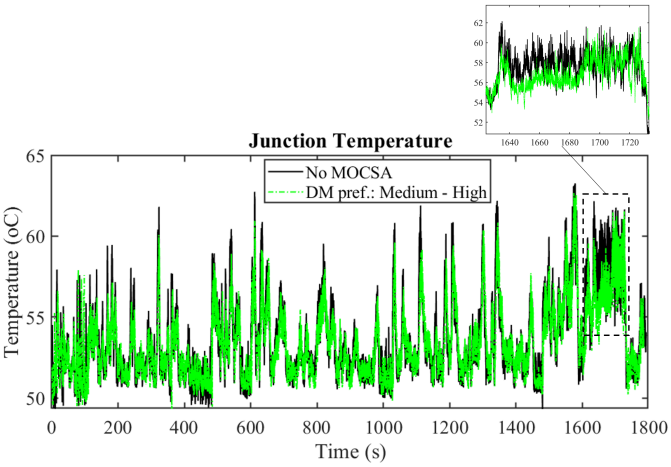

(c)

Figure 5.8: The DRTS temperature benchmark for (a) end-winding, (b) rotor, and (c) switch junction.

the maximum temperature benefits were achieved when the DM chose the medium-high option, with 1.88% average improvement in the end-winding, 0.62% in the rotor and 0.31% in the switch junction.

An important takeaway from the real-time results is that the rotor and junction temperatures were the least sensitive to the applied current optimization regardless of the DM preferences, because:

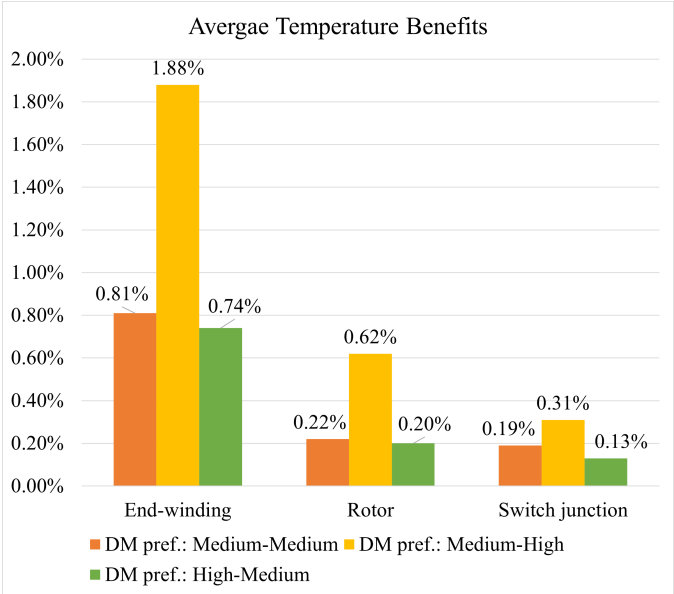

(a)

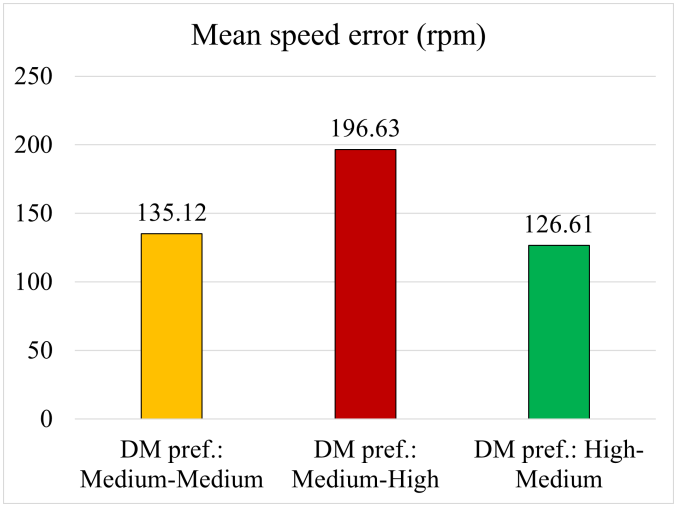

(b)

Figure 5.9: The DRTS average, a) temperature improvements, and b) absolute speed error, for the WLTC class 2 drive cycle.

1. The main loss mechanics in the rotor are eddy currents and hysteresis losses which are speed dependent; thus, the modulated current magnitude does not directly impact its temperature performance.

2. The junction temperature dynamics depend more on the primary-level control actions, which determine the switching frequency and the number of devices that are turned on simultaneously.

However, the rotor is still thermally coupled with the stator through heat convection, and reduced torque output indirectly affects its temperature dynamics. The junction temperature is dependent on the conduction and switching losses. The current magnitude modulated through the inverter as a whole impacts the individual conduction loss of each switch. Switching losses are determined by the gate modulation which in this case is cascaded HCC. On the other hand, the end-winding temperature is directly related to the P_{cu} objective.

5.2 IEEE 33-bus distribution system EED

5.2.1 Introduction

In this case study the EED problem for a notional IEEE 33-bus distribution system with RES and DG integration which was formulated in (4.12) is solved via MOPSO with MM DSS. The overall goal is to optimize operating cost and emission production of the system over 24 hours while maintaining bus voltage levels within acceptable margins; thus, ensuring reliable power delivery to the loads. The power system layout was previously shown in Figure 3.1, which has six dispatchable resources, i.e., utility grid, two 250 kW and three 60 kW DGs. The PV and WT resources provide energy based on weather forecasts, and cost of purchasing power from the utility is pre-scheduled based on the time of the day [95]. IEEE Std. 1547 suggests that the voltage deviation should remain within 5 % for power systems with less than 35 kV voltage levels [1].

5.2.2 Results

The EED optimizations are conducted for three different DM preference scenarios, i.e., medium-medium, high-low, and low-high, with the former being associated with operating cost, and the latter emission. The optimization results in the objective space are shown in Figure 5.10 which illustrate the total daily cost and emission of the IEEE 33-bus system in different DM preference scenarios. Note that there are 144 decision variables (six power sources over 24 hours) corresponding to the illustrated objective values. Similar to the traction problem, the results are compared with points on the true PF that satisfy the conditions described in [29].

A limited number of points on the true PF equal to the MOPSO's final archive size were generated and a distance benchmark was calculated to show how close the MOPSO solutions are to

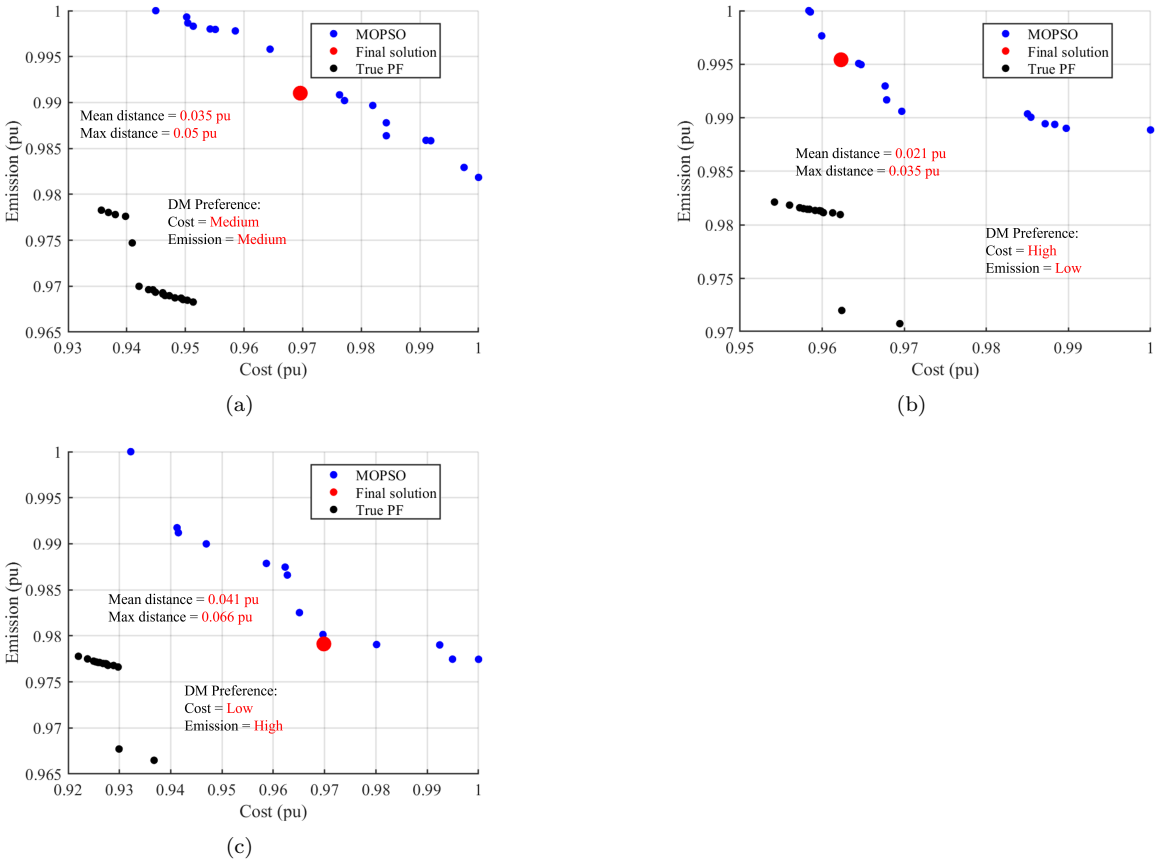

Figure 5.10: The optimization results for the IEEE 33-bus system using MOPSO with MM DSS, a) DM preference: medium (cost) - medium (emission), b) DM preference: high (cost) - low (emission), c) DM preference: low (cost) - high (emission).

the true PF. The average and maximum distance metrics are shown in Figure 5.10, with a maximum overall of 0.066 pu (6.6%) distance from the true PF. On the other hand, the true PF computation takes approximately 65 s to generate solutions while MOPSO finishes the optimization in about 3 s on an Intel Core i7 CPU; that is 21-times faster convergence. Note that both set of solutions have equal sizes to make the comparison fair.

5.2.3 Discussion

Unlike the IPMSM traction problem example where the EMO with MM DSS generated solutions superimposed to the true PF, there are some distance errors between them in the EED example. The traction problem had one non-linear, and one linear objective functions with respect to one decision variable, that had to satisfy two inequality constraints. The EED problem definition in

the IEEE 33-bus system has two linear objectives, there are 144 decision variables, and both decision and objective spaces have inequality constraints. Overall, there is a trade-off between the distance error to the true PF and computation time. In the presented case study, a maximum of 6 % error was observed for 21-times faster computational time.

Chapter 6

Conclusion

This dissertation investigated the role of human decision-makers (DM) in the autonomous control of power and energy systems. There were two major themes in this work:

1. MetaMetric (MM) performance benchmark: a novel approach to evaluate the performance of power and energy systems in real-time was presented. The key aspects of this approach was the consideration of implicit DM opinions in developing the benchmark, and generating one normalized global criterion that represented the system's performance characteristics.

2. MM decision support system (DSS): a natural progression of the MM benchmark, the MM DSS incorporates the preference-based holistic criterion into evolutionary multi-objective optimization algorithms to guide their process.

Multiple different power and energy systems including a ship power system, a terrestrial power distribution system, and a vehicular traction systems were studied as cases to validate the MM benchmark and EMO DSS. crow search algorithm (CSA) and particle swarm optimization (PSO) were studied with MM DSS integration, but the modular nature of the proposed DSS makes it compatible with any other EMO algorithm with minimal adjustments. It is hoped that the findings of this dissertation will be a stepping stone for researchers to further explore mathematical and psychological interrelations in autonomous control systems. Some potential future research are:

1. MM scalarizing function, which is the equivalent of DSS for gradient-based optimization methods.

2. Distinguishing the end-user from DM by introducing an "analyst". The analyst should be an intelligent intermediary between human users and machine processes. Investigating artificial intelligence and machine learning are lucrative potential avenues to develop analysts.

3. Applying many objectives (three or more) with dynamic time constants that are several orders of magnitude different. Model reduction, optimal programming and hierarchical decision processing are in this category.

Appendices

Appendix A Distributed Dual-step Single-perturbation EM Example

Nomenclature

RES	Renewable Energy Sources
DG	Distributed Generation/Generator
EM	Energy Management
ADMM	Alternating Direction Method of Multipliers
N_g	Number of DG
N_r	Number of RES
N_b	Number of buses
μ, λ	Lagrange multipliers
h	Optimization iteration
ρ	Optimization penalty factor
$\vec{y}$	Optimization dual variables
$\vec{z}$	Optimization global consensus variables
α, β, γ	Quadratic cost function coefficients
t_s	Simulation (model) time-step
P, P^L	Active power output and demand, respectively
$\mathcal{C}_{grid}$	Cost of purchasing power from utility
$\mathcal{C}_{fuel}$	Fuel cost
$\mathcal{C}_{res}$	RES power generation cost
$V\angle\delta$	Phase-to-ground rms voltage
$Z\angle\theta$	Impedance magnitude and angle

The EM objective functional and the applied active and reactive power constraints for an AC power system are given as follows.

$$\min J(.) = f(P_{grid}(t)) + \sum_{i=1}^{N_g} f_i(P_i(t)) \tag{1a}$$

$$f_i(P_i(t)) = \mathcal{C}_{fuel}\Big(\alpha_i P_i^2 + \beta_i P_i + \gamma_i\Big) \tag{1b}$$

$$f_j(P_j(t)) = \mathcal{C}_{res,j} P_j(t) \tag{1c}$$

$$f(P_{grid}(t)) = \mathcal{C}_{grid}(t) P_{grid}(t) \tag{1d}$$

s.t.

$$P_i^{\min} \leq P_i(t) \leq P_i^{\max} \quad \forall i \in \{1, 2, \ldots, N_g\} \tag{1e}$$

$$P_j^{\min} \leq P_j(t) \leq P_j^{\max} \quad \forall j \in \{1, 2, \ldots, N_r\} \tag{1f}$$

$$P_{grid}^{\min} \leq P_{grid}(t) \leq P_{grid}^{\max} \tag{1g}$$

$$P_{grid}(t) + \sum_{i=1}^{N_g} P_i(t) + \sum_{j=1}^{N_r} P_j(t) - \sum_{n=1}^{N_b} P_n^L(t) = 0 \tag{1h}$$

Equivalent forms of (1e), (1f), and (1g) are also applied for reactive powers. The cost function parameters, i.e, $\mathcal{C}_{fuel}$, $\mathcal{C}_{grid}$, $\mathcal{C}_{res}$, α, β and γ, are found in [129, 142, 66]. Furthermore, the bus voltage limits are included in the EM as the following optimization constraint.

$$V_n^{\min} \leq |V_n| \leq V_n^{\max} \text{ pu} \quad \forall n \in \{1, 2, \ldots, N_b\} \tag{2a}$$

$$-\delta_n^{\min} \leq \delta_n = \arctan\Big(\frac{\Im\{V_n(t)\}}{\Re\{V_n(t)\}}\Big) \leq \delta_n^{\max} \tag{2b}$$

In the first step, the relaxed optimization problem, i.e., (1a) s.t. (1e), (1f), (1g), and (1h), is solved using the distributed singular perturbation-based technique. The concept behind this technique is to form two time-scale dynamical systems namely the fast dynamical layer and the slow dynamical layer, which have an equilibrium point that satisfies the Karush–Kuhn–Tucker conditions for optimality [141]. The augmented Lagrnagian for the relaxed optimization is as follows (note that

t-dependence notation is neglected for simplicity).

$$
\begin{aligned}
L_1 &= f(\vec{P}) + \mu\Big(\sum_{r=1}^{R} P_r^A + \sum_{n=1}^{N_b} P_n^B\Big) \\
&+ \sum_{r=1}^{R} \lambda_r^{\max}\big(P_r^A - P_r^{A,\max}\big) + \sum_{r=1}^{R} \lambda_r^{\min}\big(-P_r^A + P_r^{A,\min}\big) \\
&+ \frac{\rho_1}{2}\Big\|\sum_{r=1}^{R} P_r^A + \sum_{n=1}^{N_b} P_n^B\Big\|_2^2
\end{aligned}
\tag{3}
$$

Where $\vec{P} = [P_1, P_2, \ldots, P_{N_g}, \ldots, P_{N_r}, \ldots P_{grid}]^T$. Also, $P_r^A \subseteq P_r$ are dispatchable generation powers in region $r \in \{1, 2, \ldots, R\}$, i.e. DG and/or the purchased power from the utility grid; and P_n^B is the algebraic sum of the RES active power generation and the load demand at bus n (non-dispatchable quantities).

The second step applies the ADMM algorithm in (4) to the narrowed search space after the reconfiguration of constraints based on the first step's results.

$$
\begin{aligned}
&\min\big(f(\vec{x}) + g(\vec{z})\big) \\
&\text{s.t.} \quad \mathbf{A}\vec{x} + \mathbf{B}\vec{z} = \mathbf{c}
\end{aligned}
\tag{4a}
$$

$$
\begin{aligned}
L_2(\vec{x}, \vec{y}, \vec{z}) = f(\vec{x}) + g(\vec{z}) + \vec{y}^T(\mathbf{A}\vec{x} + \mathbf{B}\vec{z} - \mathbf{c}) \\
+ \frac{\rho_2}{2}\Big\|\mathbf{A}\vec{x} + \mathbf{B}\vec{z} - \mathbf{c}\Big\|_2^2
\end{aligned}
\tag{4b}
$$

$$
\vec{x}^{(h+1)} = \text{argmin } L_2\big(\vec{x}, \vec{z}^{(h)}, \vec{y}^{(h)}\big) \tag{4c}
$$

$$
\vec{z}^{(h+1)} = \text{argmin } L_2\big(\vec{x}^{(h+1)}, \vec{z}, \vec{y}^{(h)}\big) \tag{4d}
$$

$$
\vec{y}^{(h+1)} = \vec{y}^{(h)} + \rho_2\big(\mathbf{A}\vec{x} + \mathbf{B}\vec{z} - \mathbf{c}\big) \tag{4e}
$$

s.t.

$$\vec{x} = \left[V^{\mathbb{C}}_{1,\kappa_1} \; V^{\mathbb{C}}_{1,\kappa_2} \; V^{\mathbb{C}}_{2,\kappa_1} \; V^{\mathbb{C}}_{2,\kappa_2} \; \dots \; V^{\mathbb{C}}_{R,\kappa_1} \; V^{\mathbb{C}}_{R,\kappa_2} \right]^T \tag{5a}$$

$$\mathbf{A} = \Big[a_{ij} \Big]_{4l \times d} \left\{ a_{ij} > 0 \;\; \forall V^{\mathbb{C}}_{r,\kappa_2}, \text{ else } a_{ij} = 0 \right\} \tag{5b}$$

$$\mathbf{B} = -\mathbf{I}_{4l \times 4l} \tag{5c}$$

$$\mathbf{c} = 0 \;\; \text{and} \;\; g(\vec{z}) = 0 \;\; \text{and} \;\; \rho > 0 \tag{5d}$$

Where d is the dimension of $\vec{x}$, and l is the number of edges connecting bordering regions. The elements of $\vec{x}$ are complex bus voltages. Note that κ_1 index is the set of all buses in region r that have neighbors in other regions, and κ_2 index is the set of those neighbors.

Appendix B Distributed Hierarchical Control Example in SPS

Nomenclature

ES	Energy Storage
ESM	Energy Storage Management
EEM	Efficiency Energy Management
PGM	Power Generation Module
SOC	State Of Charge
DM	Decision-Maker
MPC	Model Predictive Control
ADMM	Alternating Direction Method of Multipliers
CSA	Crow Search Algorithm
MRAC	Model Reference Adaptive Control

B.1 Energy storage management

The ESM's main goal is to coordinate ES modules as spinning-reserve such that they reduce the ramp-rate stress imposed by pulse load demands on PGM. This goal is achieved by scheduling ES charge/discharge cycles at appropriate times. To this end, a distributed optimization problem is formulated to determine the optimal consensus SOC for ES modules. The consensus SOC for charging cycles is defined by the DM. The discrete equations describing the ES are as follows.

$$\sum_{i=1}^{N_{ES}} E_i^{ES}(k+1) = \sum_{i=1}^{N_{ES}} E_i^{ES}(k) + T_s \sum_{i=1}^{N_{ES}} P_i^{ES}(k) \tag{6a}$$

$$\sum_{i=1}^{N_{ES}} P_i^{ES}(k+1) = \sum_{i=1}^{N_{ES}} P_i^{ES}(k) + T_s \sum_{i=1}^{N_{ES}} r_i^{ES}(k) \tag{6b}$$

Where T_s is the sampling time, E_i^{ES} is the ES energy, P_i^{ES} is the ES power and r^{ES} is the ES ramp-rate. Equations (6a) and (6b) can be augmented in terms of their difference as shown in (7a) and (7b).

$$\Delta E_i^{ES}(k+1) = \Delta E_i^{ES}(k) + T_s\ \Delta P_i^{ES}(k) \tag{7a}$$

$$\Delta P_i^{ES}(k) = P_i^{ES}(k) - P_i^{ES}(k-1) = T_s \; r_i^{ES}(k-1) \tag{7b}$$

Let $\vec{x}(k) = \begin{bmatrix}\Delta E_i^{ES}(k) & E_i^{ES}(k)\end{bmatrix}^T$ be the state vector; thus, by combining (6a) and (6b) into (7a), the state-space equation is formulated as follows.

$$\vec{x}(k+1) = A \; \vec{x}(k) + B \; \Delta P_i^{ES} \tag{8a}$$

$$E_i^{ES}(k) = C \; \vec{x}(k) \tag{8b}$$

$$A = \begin{bmatrix} 1 & 0 \\ 1 & 1 \end{bmatrix}, B = \begin{bmatrix} T_s \\ 0 \end{bmatrix}, C = \begin{bmatrix} 0 & 1 \end{bmatrix} \tag{8c}$$

Next, the MPC for N_p prediction horizon and N_c control steps is formulated in (9).

$$\bar{E}_i^{ES} = G \; \vec{x}(k) + \Phi \; \Delta \bar{P}_i^{ES} \tag{9}$$

Where

$$\bar{E}_i^{ES} = \begin{bmatrix} E_i^{ES}(k+1) \; E_i^{ES}(k+2) \; \ldots \; E_i^{ES}(k+N_p) \end{bmatrix} \tag{10a}$$

$$\Delta \bar{P}_i^{ES} = \begin{bmatrix} \Delta P_i^{ES}(k+1) \; \Delta P_i^{ES}(k+2) \; \ldots \; \Delta P_i^{ES}(k+N_p) \end{bmatrix} \tag{10b}$$

$$G = \begin{bmatrix} CA \\ CA^2 \\ \vdots \\ CA^{N_p} \end{bmatrix} \tag{10c}$$

$$\Phi = \begin{bmatrix} CB & 0 & \ldots & 0 \\ CAB & CB & \ldots & 0 \\ \vdots & \vdots & \ddots & \vdots \\ CA^{N_p-1}B & CA^{N_p-2}B & \ldots & CA^{N_p-N_c}B \end{bmatrix} \tag{10d}$$

The MPC objective function is formulated in (11a) with the applied constraints in (11b)-(11f) to satisfy two objectives: 1) manage each ES to reach a desired state ($E_i^{*,ES}$), and 2) meet the load

demand without violating the generator ramp-rate limits.

$$J(\Delta\bar{P}_i^{ES}) = \left\| \bar{E}_i^{*,ES} - \bar{E}_i^{ES} \right\|_2^2 + \left(\Delta\bar{P}_i^{ES}\right)^T \, I_{_{N_c \times N_c}} \, \Delta\bar{P}_i^{ES} \tag{11a}$$

$$A_{ieq} \, \Delta\bar{P}_i^{ES} \leq b_{ieq} \tag{11b}$$

$$A_{ieq} = \begin{bmatrix} 1 & 0 \\ 0 & 1 \end{bmatrix} \tag{11c}$$

$$b_{ieq} = T_s \Big[-r_{\min}^{ES} \quad r_{\max}^{ES} \Big]^T \tag{11d}$$

$$r_{\min}^{ES} = -r_{\min}^{GEN} - r^L \tag{11e}$$

$$r_{\max}^{ES} = r_{\max}^{GEN} - r^L \tag{11f}$$

Where $r_{\min}^{GEN}$, $r_{\max}^{GEN}$ and r^L are the minimum and maximum generator ramp-rate, and load demand ramp-rate, respectively. The objective function (11a) is solved by a two-step process, incorporating ADMM and MPC [13, 18]. More details about the two-step MPC-ADMM algorithm and its application in the SPS can be found in [57, 43].

B.2 Efficiency energy management

The purpose of EEM is to reduce PGM operational cost by finding their optimal power output at each time-step. First, an optimization objective function is formulated based on the PGM quadratic cost functions (12), and the appropriate constraints are applied. Then, a meta-heuristic optimization solver, denoted as CSA [7] is used in a distributed manner to solve the problem.

$$C_i(P_i) = \underbrace{\left(\alpha + \beta P_i + \varsigma P_i^2 + \vartheta P_i^3\right) P_i}_{i=\{1,2,3\}} \tag{12a}$$

$$C_i(P_i) = \underbrace{\left(\alpha' + \beta' P_i + \varsigma' P_i^2 + \vartheta' P_i^3\right) P_i}_{i=\{4,5\}} \tag{12b}$$

$$i = \{ \underbrace{1,2,3}_{\text{MPGM}}, \underbrace{4,5}_{\text{APGM}} \} \tag{12c}$$

$$\begin{bmatrix} \alpha & \beta & \varsigma & \vartheta \\ \alpha' & \beta' & \varsigma' & \vartheta' \end{bmatrix} = \begin{bmatrix} 87.52 & -1.8689 & 0.0597 & -0.0006845 \\ 82.62 & -6.942 & 0.663 & 0 \end{bmatrix} \tag{12d}$$

Subsequently, the optimisation objective function and its constraints are derived in (13). Note that (13) utilises parameters from neighbouring PGM to create a distributed formulation.

$$\min(J(.)) = \Big(C_i(\bar{P}_i) + \sum_{j\neq i}^{\forall j} f_i(\bar{P}_{ji}) + g_i(\bar{Z}_{ji})\Big) \tag{13a}$$

$$\sum_{j\neq i}^{\forall i,j} \big(\bar{P}_{ji} + \bar{P}_i\big) = \bar{P}^L \tag{13b}$$

$$P_{ji}^{\min} \leq \sum_{i\neq j}^{\forall j} \bar{P}_{ji} \leq P_{ji}^{\max} \tag{13c}$$

$$\bar{P}_{ji} - \bar{Z}_{ji} = 0 \tag{13d}$$

$$P_i^{\min} \leq \bar{P}_i \leq P_i^{\max} \tag{13e}$$

$$i, j = \big\{1, 2, 3, 4, 5\big\} \tag{13f}$$

Where $\bar{P}_i$, $\bar{P}_{ji}$ and $\bar{P}^L$ are the PGM power, the j^{th} neighboring PGM power, and the total load demand, prediction vectors. $\bar{Z}_{ji}$ is the consensus variable, representing the global variable of what $\bar{P}_{ji}$ should be. P_i, P_{ji} and P^L are predicted over N_p' horizon (N_p' is not necessarily equal to N_p) as follows.

$$\bar{P}_i = \big[P_i(k+1)\ ,\ P_i(k+2)\ ,\ \ldots\ ,\ P_i(k+N_p')\big]^T \tag{14a}$$

$$\bar{P}_{ji} = \big[P_{ji}(k+1)\ ,\ P_{ji}(k+2)\ ,\ \ldots\ ,\ P_{ji}(k+N_p')\big]^T \tag{14b}$$

$$\bar{P}^L = \big[P^L(k+1)\ ,\ P^L(k+2)\ ,\ \ldots\ ,\ P^L(k+N_p')\big]^T \tag{14c}$$

Then, the augmented Lagrangian for (13) is solved for the following parameters utilizing

CSA.

$$\bar{P}_{ji}(h+1) = \text{argmin}\Bigg(f_i(\bar{P}_{ji}(h)) + \frac{\rho}{2}.\big\|\bar{P}_{ij}(h)+ \bar{Z}_{ji}(h) + \bar{\Upsilon}_{ji}(h)\big\|_2^2 \Bigg) \tag{15a}$$

$$\bar{Z}_{ji}(h+1) = \text{argmin}\Bigg(\sum_{j\neq i}^{\forall j} g_i(\bar{Z}_{ji}) + \frac{\rho}{2}.\big\|\bar{P}_{ij}(h+1)+ \bar{Z}_{ji}(h) + \bar{\Upsilon}_{ji}(h)\big\|_2^2 \Bigg) \tag{15b}$$

$$\bar{\Upsilon}_{ji}(h+1) = \bar{\Upsilon}_{ji}(h) + \bar{P}_{ij}(h+1) - \bar{Z}_{ji}(h+1) \tag{15c}$$

where h, ρ, and $\bar{\Upsilon}_{ji}$ are the optimization iteration index, the penalty factor, and the scaled dual variable, respectively. Equations in (15) demonstrate that local CSA solvers find the optimal $\bar{P}_i$ for each PGM, then share it with the neighboring solvers to find a global solution.

B.3 Power management

The PM methodology used in this paper is based on MRAC for droop compensation of PGM in DC microgrids like SPS to achieve superior bus voltage profile [119, 107, 133]. The fundamental principal of MRAC is to create an ideal reference plant to modify the real plant using control parameters so that it emulates its reference. Then, adaptive control laws that satisfy the Lyapunov stability criterion are developed for the control parameters. The MRAC for droop control has two loops: 1) the adaptive current-control loop that compensates the internal droop resistance of each PGM (R_{droop}), and 2) the adaptive voltage-control loop compensating the internal V^* to maintain nominal voltages at the port and starboard buses. Additionally, an identification plant is added to estimate the plant model and improve the control outputs. The state-space equations for a first-order estimation of the PGM, its reference plant, and the identification model are given in (16a)-(16c),

respectively.

$$\dot{x}_p(k) = a_p x_p(k) + b_p u(k) \tag{16a}$$

$$\dot{x}_r(k) = a_r x_r(k) + b_r u_r(k) \tag{16b}$$

$$\dot{\hat{x}}_p(k) = a_r \hat{x}_p(k) + \Big[\hat{a}_p(k) - a_r\Big] x_p(k) + \hat{b}_p u(k) \tag{16c}$$

Where a_p, b_p, a_r and b_r are the plant and the reference model parameters. $u_r(k)$ is the reference model input. The plant input $u(k)$ is modified via two control parameters (θ and γ) determined by the following adaptive laws.

$$u(k) = \gamma u_r(k) + \theta x_p(k) \tag{17a}$$

$$\dot{\theta} = -\text{sgn}(b_p)\Big[e_c x_p + \epsilon_\theta\Big] \tag{17b}$$

$$\dot{\gamma} = -\text{sgn}(b_p)\Big[e_c u_r + \epsilon_\gamma\Big] \tag{17c}$$

$$\dot{\hat{a}}_p = \hat{e} x_p(k) - \epsilon_\theta \tag{17d}$$

$$\dot{\hat{b}}_p = \hat{e} u(k) - \theta\epsilon_\theta - \gamma\epsilon_\gamma \tag{17e}$$

$$\epsilon_\theta = \hat{a}_p + \hat{b}_p\theta - a_r \tag{17f}$$

$$\epsilon_\gamma = \hat{b}_p\gamma - b_m \tag{17g}$$

Where e_c, $\hat{e}$, ϵ_θ and ϵ_γ are the control, identification, closed-loop θ and closed-loop γ errors, respectively. The modified reference voltage input to the PGM after MRAC is described in (18a) and (18b) for the port and starboard busses, respectively.

$$V_{P,i}^{**} = V_i^* + DV_{P,i} - I_{P,i}(R_{droop,i} + \Delta R_{P,i}) \tag{18a}$$

$$V_{S,i}^{**} = V_i^* + DV_{S,i} - I_{S,i}(R_{droop,i} + \Delta R_{S,i}) \tag{18b}$$

Where $I_{P/S}$ and $\Delta R_{P/S}$ are the PGM generator winding currents and the droop compensations, respectively.

Bibliography

[1] Ieee standard for interconnection and interoperability of distributed energy resources with associated electric power systems interfaces. *IEEE Std 1547-2018 (Revision of IEEE Std 1547-2003)*, pages 1–138, 2018.

[2] Ieee recommended practice for monitoring electric power quality. *IEEE Std 1159-2019 (Revision of IEEE Std 1159-2009)*, pages 1–98, 2019.

[3] Emissions by Plant and by Region, Oct 2019.

[4] Mohammed A Abido. Environmental/economic power dispatch using multiobjective evolutionary algorithms. *IEEE transactions on power systems*, 18(4):1529–1537, 2003.

[5] P.J. Angeline. Using selection to improve particle swarm optimization. In *1998 IEEE International Conference on Evolutionary Computation Proceedings. IEEE World Congress on Computational Intelligence (Cat. No.98TH8360)*, pages 84–89, 1998.

[6] A. Anvari-Moghaddam, T. Dragicevic, Lexuan Meng, Bo Sun, and J. M. Guerrero. Optimal planning and operation management of a ship electrical power system with energy storage system. In *IECON 2016 - 42nd Annual Conference of the IEEE Industrial Electronics Society*, pages 2095–2099, 2016.

[7] Alireza Askarzadeh. A novel metaheuristic method for solving constrained engineering optimization problems: Crow search algorithm. *Computers & Structures*, 169:1–12, 2016.

[8] P.E. Bagnoli, C. Casarosa, M. Ciampi, and E. Dallago. Thermal resistance analysis by induced transient (trait) method for power electronic devices thermal characterization. i. fundamentals and theory. *IEEE Transactions on Power Electronics*, 13(6):1208–1219, 1998.

[9] Ameen M Bassam, Alexander B Phillips, Stephen R Turnock, and Philip A Wilson. Development of a multi-scheme energy management strategy for a hybrid fuel cell driven passenger ship. *International Journal of Hydrogen Energy*, 42(1):623–635, 2017.

[10] Slim Bechikh, Rituparna Datta, and Abhishek Gupta. *Recent advances in evolutionary multi-objective optimization*, volume 20. Springer, 2016.

[11] Slim Bechikh, Marouane Kessentini, Lamjed Ben Said, and Khaled Ghédira. Preference incorporation in evolutionary multiobjective optimization: A survey of the state-of-the-art. In *Advances in Computers*, volume 98, pages 141–207. Elsevier, 2015.

[12] M Boussak. Implementation and experimental investigation of sensorless speed control with initial rotor position estimation for interior permanent magnet synchronous motor drive. *IEEE Transactions on Power Electronics*, 20(6):1413–1422, 2005.

[13] Stephen Boyd, Neal Parikh, Eric Chu, Borja Peleato, and Jonathan Eckstein. Distributed optimization and statistical learning via the alternating direction method of multipliers. *Foundations and Trends® in Machine Learning*, 3(1):1–122, 2010.

[14] Jürgen Branke, , Kalyanmoy Deb, Kaisa Miettinen, and Roman Slowiński. *Multiobjective optimization: Interactive and evolutionary approaches*, volume 5252. Springer Science & Business Media, 2008.

[15] Jürgen Branke and Kalyanmoy Deb. Integrating user preferences into evolutionary multi-objective optimization. In *Knowledge incorporation in evolutionary computation*, pages 461–477. Springer, 2005.

[16] Jürgen Branke, Thomas Kaußler, and Harmut Schmeck. Guidance in evolutionary multi-objective optimization. *Advances in engineering software*, 32(6):499–507, 2001.

[17] K. L. Butler-Purry and N. D. R. Sarma. Self-healing reconfiguration for restoration of naval shipboard power systems. *IEEE Transactions on Power Systems*, 19(2):754–762, 2004.

[18] Eduardo F Camacho and Carlos Bordons Alba. *Model predictive control*. Springer science & business media, 2013.

[19] Stephan C. Carlson. Metric space, Apr 2017.

[20] C.C. Chan and K.T. Chau. An overview of power electronics in electric vehicles. *IEEE Transactions on Industrial Electronics*, 44(1):3–13, 1997.

[21] Vira Chankong and Yacov Y Haimes. *Multiobjective decision making: theory and methodology*. Courier Dover Publications, 2008.

[22] Abraham Charnes, William W Cooper, and Robert O Ferguson. Optimal estimation of executive compensation by linear programming. *Management science*, 1(2):138–151, 1955.

[23] Abraham Charnes and William Wager Cooper. Management models and industrial applications of linear programming. *Management science*, 4(1):38–91, 1957.

[24] Abraham Charnes and William Wager Cooper. Goal programming and multiple objective optimizations: Part 1. *European journal of operational research*, 1(1):39–54, 1977.

[25] O. Ciftci, M. Mehrtash, and A. Kargarian. Data-driven nonparametric chance-constrained optimization for microgrid energy management. *IEEE Transactions on Industrial Informatics*, 16(4):2447–2457, 2020.

[26] CA Coello Coello and Maximino Salazar Lechuga. Mopso: A proposal for multiple objective particle swarm optimization. In *Proceedings of the 2002 Congress on Evolutionary Computation. CEC'02 (Cat. No. 02TH8600)*, volume 2, pages 1051–1056. IEEE, 2002.

[27] A. M. Cramer, X. Liu, Y. Zhang, J. D. Stevens, and E. L. Zivi. Early-stage shipboard power system simulation of operational vignettes for dependability assessment. In *2015 IEEE Electric Ship Technologies Symposium (ESTS)*, pages 382–387, 2015.

[28] M. Cupelli, F. Ponci, G. Sulligoi, A. Vicenzutti, C. S. Edrington, T. El-Mezyani, and A. Monti. Power flow control and network stability in an all-electric ship. *Proceedings of the IEEE*, 103(12):2355–2380, 2015.

[29] Ana Luísa Custódio, JF Aguilar Madeira, A Ismael F Vaz, and Luís Nunes Vicente. Direct multisearch for multiobjective optimization. *SIAM Journal on Optimization*, 21(3):1109–1140, 2011.

[30] Kalyanmoy Deb. Multi-objective evolutionary algorithms: Introducing bias among pareto-optimal solutions. In *Advances in evolutionary computing*, pages 263–292. Springer, 2003.

[31] Kalyanmoy Deb. Multi-objective optimisation using evolutionary algorithms: an introduction. In *Multi-objective evolutionary optimisation for product design and manufacturing*, pages 3–34. Springer, 2011.

[32] Kalyanmoy Deb, Amrit Pratap, Sameer Agarwal, and TAMT Meyarivan. A fast and elitist multiobjective genetic algorithm: Nsga-ii. *IEEE transactions on evolutionary computation*, 6(2):182–197, 2002.

[33] Kalyanmoy Deb, Abbadi Raji Reddy, and Gulshan Singh. Optimal scheduling of casting sequence using genetic algorithms. *Materials and Manufacturing Processes*, 18(3):409–432, 2003.

[34] Kalyanmoy Deb, Rahul Tewari, Mayur Dixit, and Joydeep Dutta. Finding trade-off solutions close to kkt points using evolutionary multi-objective optimization. In *2007 IEEE Congress on Evolutionary Computation*, pages 2109–2116. IEEE, 2007.

[35] Georgios D Demetriades, Hector Zelaya de la Parra, Erik Andersson, and Håkan Olsson. A Real-Time Thermal Model of a Permanent-Magnet Synchronous Motor. *IEEE Transactions on Power Electronics*, 25(2):463–474, 2010.

[36] N Doerry. Next generation integrated power systems (ngips) for the future fleet. In *IEEE Electric Ship Technology Symposium*, Baltimore, 2009. IEEE.

[37] N Doerry and J Davis. Integrated Power System for Marine Applications. *American Society of Naval Engineers*, 106(3):77–90, 1994.

[38] Christopher J. Doktorcik. *Modeling and simulation of a hybrid ship power system.* PhD thesis, Purdue University, December 2011.

[39] Stacey L Dolan and Garvin A Heath. Life Cycle Greenhouse Gas Emissions of Utility-Scale Wind Power. *Journal of Industrial Ecology*, 16(s1):S136–S154, 2012.

[40] David G. Dorrell, Andrew M. Knight, Mircea Popescu, Lyndon Evans, and David A. Staton. Comparison of different motor design drives for hybrid electric vehicles. In *2010 IEEE Energy Conversion Congress and Exposition*, pages 3352–3359, 2010.

[41] Stefan Droste, Thomas Jansen, and Ingo Wegener. On the analysis of the (1+ 1) evolutionary algorithm. *Theoretical Computer Science*, 276(1-2):51–81, 2002.

[42] Carlos A Bana e Costa and Jean-Claude Vansnick. Macbeth—an interactive path towards the construction of cardinal value functions. *International transactions in operational Research*, 1(4):489–500, 1994.

[43] Chris S Edrington, Gokhan Ozkan, Behnaz Papari, David E Gonsoulin, Dallas Perkins, Tuyen V Vu, and Hesan Vahedi. Distributed energy management for ship power systems with distributed energy storage. *Journal of Marine Engineering & Technology*, 19(sup1):31–44, 2020.

[44] Christopher S. Edrington, Tuyen Vu, Hesan Vahedi, David E Gonsoulin, Dallas Perkins, Behnaz Papari, Gokhan Ozkan, K Schoder, H Ravindra, and M Stanovich. Demonstration and Evaluation of Large-scale Distributed Control for Integrated Power and Energy MVDC Systems on Ships. In *Advanced Machinery Technology Symposium*, Philadelphia, PA, 2018. IEEE.

[45] Ali Emadi, Young Joo Lee, and Kaushik Rajashekara. Power Electronics and Motor Drives in Electric, Hybrid Electric, and Plug-In Hybrid Electric Vehicles. *IEEE Transactions on Industrial Electronics*, 55(6):2237–2245, 2008.

[46] Poria Fajri, Reza Ahmadi, and Mehdi Ferdowsi. Equivalent vehicle rotational inertia used for electric vehicle test bench dynamic studies. In *IECON Proceedings (Industrial Electronics Conference)*, pages 4115–4120, 2012.

[47] Eduardo Fernandez, Edy Lopez, Sergio Bernal, Carlos A Coello Coello, and Jorge Navarro. Evolutionary multiobjective optimization using an outranking-based dominance generalization. *Computers & Operations Research*, 37(2):390–395, 2010.

[48] Eduardo Fernandez, Edy Lopez, Fernando Lopez, and Carlos A Coello Coello. Increasing selective pressure towards the best compromise in evolutionary multiobjective optimization: The extended nosga method. *Information Sciences*, 181(1):44–56, 2011.

[49] José Rui Figueira, Salvatore Greco, and Roman Słowiński. Building a set of additive value functions representing a reference preorder and intensities of preference: Grip method. *European Journal of Operational Research*, 195(2):460–486, 2009.

[50] Peter C Fishburn. Exceptional paper—lexicographic orders, utilities and decision rules: A survey. *Management science*, 20(11):1442–1471, 1974.

[51] David B Fogel. *Artificial intelligence through simulated evolution*. Wiley-IEEE Press, 1998.

[52] Carlos M Fonseca, Peter J Fleming, et al. Genetic algorithms for multiobjective optimization: Formulation discussion and generalization. In *ICGA*, number July, pages 416–423. Citeseer, 1993.

[53] Viviane Grunert da Fonseca, Carlos M Fonseca, and Andreia O Hall. Inferential performance assessment of stochastic optimisers and the attainment function. In *International Conference on Evolutionary Multi-Criterion Optimization*, pages 213–225. Springer, 2001.

[54] Vasilis M Fthenakis, Hyung Chul Kim, and Erik Alsema. Emissions from Photovoltaic Life Cycles. *Environmental Science & Technology*, 42(6):2168–2174, 2008.

[55] Saul Gass and Thomas Saaty. The computational algorithm for the parametric objective function. *Naval research logistics quarterly*, 2(1-2):39–45, 1955.

[56] D. E. Gonsoulin, T. V. Vu, F. Diaz, H. Vahedi, D. Perkins, and C. S. Edrington. Coordinating multiple energy storages using mpc for ship power systems. In *2017 IEEE Electric Ship Technologies Symposium (ESTS)*, pages 551–556, 2017.

[57] David Gonsoulin, Gokhan Ozkhan, Behnaz Papari, and Chris S Edrington. Effects of varying ramp rate and amount of es. In *Conference Proceedings of INEC*, volume 2, page 4, 2018.

[58] Salvatore Greco, Vincent Mousseau, and Roman Słowiński. Ordinal regression revisited: multiple criteria ranking using a set of additive value functions. *European Journal of Operational Research*, 191(2):416–436, 2008.

[59] Yacov Haimes. On a bicriterion formulation of the problems of integrated system identification and system optimization. *IEEE transactions on systems, man, and cybernetics*, 1(3):296–297, 1971.

[60] Shouyi Han, Kaikai Diao, and Xiaodong Sun. Overview of multi-phase switched reluctance motor drives for electric vehicles. *Advances in Mechanical Engineering*, 13(9):16878140211045195, 2021.

[61] Ali Haseltalab, Rudy R Negenborn, and Gabriel Lodewijks. Multi-Level Predictive Control for Energy Management of Hybrid Ships in the Presence of Uncertainty and Environmental Disturbances**This research is supported by the project ShipDrive: A Novel Methodology for Integrated Modelling, Control, and Optimization of Hybrid Ship Systems (project 13276) of the Dutch Technology Foundation STW. *IFAC-PapersOnLine*, 49(3):90–95, 2016.

[62] Linjun He, Hisao Ishibuchi, Anupam Trivedi, Handing Wang, Yang Nan, and Dipti Srinivasan. A survey of normalization methods in multiobjective evolutionary algorithms. *IEEE Transactions on Evolutionary Computation*, 25(6):1028–1048, 2021.

[63] Meisam Hemmati, Nima Amjady, and Mehdi Ehsan. System modeling and optimization for islanded micro-grid using multi-cross learning-based chaotic differential evolution algorithm. *International Journal of Electrical Power & Energy Systems*, 56:349–360, 2014.

[64] Salvador Hinojosa, Diego Oliva, Erik Cuevas, Gonzalo Pajares, Omar Avalos, and Jorge Gálvez. Improving multi-criterion optimization with chaos: a novel multi-objective chaotic crow search algorithm. *Neural Computing and Applications*, 29(8):319–335, 2018.

[65] P. H. Hoang, C. S. Edrington, B. Papari, G. Ozkan, and H. Ahn. Distributed constrained optimization over networked systems via a singular perturbation method and application to economic dispatch. In *2020 Clemson University Power Systems Conference (PSC)*, pages 1–6, 2020.

[66] Phuong H. Hoang, Gokhan Ozkan, Payam R. Badr, Behnaz Papari, Christopher S. Edrington, Mustafa Alparslan Zehir, Barry Hayes, Laura Mehigan, Dlzar Al Kez, and Aoife M. Foley. A dual distributed optimal energy management method for distribution grids with electric vehicles. *IEEE Transactions on Intelligent Transportation Systems*, pages 1–12, 2021.

[67] Jeffrey Horn, Nicholas Nafpliotis, and David E Goldberg. A niched pareto genetic algorithm for multiobjective optimization. In *Proceedings of the first IEEE conference on evolutionary computation. IEEE world congress on computational intelligence*, pages 82–87. IEEE, 1994.

[68] T Huber, W Peters, and J Böcker. A low-order thermal model for monitoring critical temperatures in permanent magnet synchronous motors. In *7th IET International Conference on Power Electronics, Machines and Drives (PEMD 2014)*, pages 1–6, 2014.

[69] Hisao Ishibuchi, Yusuke Nojima, et al. On the effect of normalization in moea/d for multi-objective and many-objective optimization. *Complex & Intelligent Systems*, 3(4):279–294, 2017.

[70] Eric Jacquet-Lagreze and Jean Siskos. Assessing a set of additive utility functions for multicriteria decision-making, the uta method. *European journal of operational research*, 10(2):151–164, 1982.

[71] Armin Javidi, Eysa Salajegheh, and Javad Salajegheh. Optimization of weight and collapse energy of space structures using the multi-objective modified crow search algorithm. *Engineering with Computers*, pages 1–18, 2021.

[72] Z. Jin, G. Sulligoi, R. Cuzner, L. Meng, J. C. Vasquez, and J. M. Guerrero. Next-generation shipboard dc power system: Introduction smart grid and dc microgrid technologies into maritime electrical netowrks. *IEEE Electrification Magazine*, 4(2):45–57, 2016.

[73] F. D. Kanellos. Optimal power management with ghg emissions limitation in all-electric ship power systems comprising energy storage systems. *IEEE Transactions on Power Systems*, 29(1):330–339, 2014.

[74] Phillip Kaye, Raymond Laflamme, and Michele Mosca. *An introduction to quantum computing*. OUP Oxford, 2006.

[75] Ralph L Keeney, Howard Raiffa, and Richard F Meyer. *Decisions with multiple objectives: preferences and value trade-offs*. Cambridge university press, 1993.

[76] J. Kennedy and R. Eberhart. Particle swarm optimization. In *Proceedings of ICNN'95 - International Conference on Neural Networks*, volume 4, pages 1942–1948 vol.4, 1995.

[77] M. M. S. Khan, M. O. Faruque, and A. Newaz. Fuzzy logic based energy storage management system for mvdc power system of all electric ship. *IEEE Transactions on Energy Conversion*, 32(2):798–809, 2017.

[78] Joshua D Knowles and David W Corne. Approximating the nondominated front using the pareto archived evolution strategy. *Evolutionary computation*, 8(2):149–172, 2000.

[79] Eva Krockow. How many decisions do we make each day? *Psychology Today*, Sep 2018.

[80] Kexing Lai and Mahesh S Illindala. A distributed energy management strategy for resilient shipboard power system. *Applied Energy*, 228:821–832, 2018.

[81] R. H. Lasseter and P. Paigi. Microgrid: a conceptual solution. In *2004 IEEE 35th Annual Power Electronics Specialists Conference (IEEE Cat. No.04CH37551)*, volume 6, pages 4285–4290 Vol.6, June 2004.

[82] Gwo-Ching Liao. Solve environmental economic dispatch of smart microgrid containing distributed generation system–using chaotic quantum genetic algorithm. *International Journal of Electrical Power & Energy Systems*, 43(1):779–787, 2012.

[83] Steve Lim. Sensorless-foc with flux-weakening and mtpa for ipmsm motor drives. Technical report, Texas Instruments, 2018.

[84] Qiuzhen Lin, Jianqiang Li, Zhihua Du, Jianyong Chen, and Zhong Ming. A novel multi-objective particle swarm optimization with multiple search strategies. *European Journal of Operational Research*, 247(3):732–744, 2015.

[85] Bo Liu, Ling Wang, Yi-Hui Jin, Fang Tang, and De-Xian Huang. Improved particle swarm optimization combined with chaos. *Chaos, Solitons & Fractals*, 25(5):1261–1271, 2005.

[86] Qian Liu and Kay Hameyer. High-performance adaptive torque control for an ipmsm with real-time mtpa operation. *IEEE Transactions on Energy Conversion*, 32(2):571–581, 2017.

[87] Alexander V Lotov, Vladimir A Bushenkov, and Georgy K Kamenev. *Interactive decision maps: Approximation and visualization of Pareto frontier*, volume 89. Springer Science & Business Media, 2004.

[88] Mariano Luque, Kaisa Miettinen, Petri Eskelinen, and Francisco Ruiz. Incorporating preference information in interactive reference point methods for multiobjective optimization. *Omega*, 37(2):450–462, 2009.

[89] Sina Makhdoomi and Alireza Askarzadeh. Optimizing operation of a photovoltaic/diesel generator hybrid energy system with pumped hydro storage by a modified crow search algorithm. *Journal of Energy Storage*, 27:101040, 2020.

[90] F. Y. Melhem, O. Grunder, Z. Hammoudan, and N. Moubayed. Energy management in electrical smart grid environment using robust optimization algorithm. *IEEE Transactions on Industry Applications*, 54(3):2714–2726, 2018.

[91] PH Mellor, D Roberts, and DR Turner. Lumped parameter thermal model for electrical machines of tefc design. In *IEE Proceedings B (Electric Power Applications)*, volume 138, pages 205–218. IET, 1991.

[92] P.H. Mellor, R. Wrobel, and D. Holliday. A computationally efficient iron loss model for brushless ac machines that caters for rated flux and field weakened operation. In *2009 IEEE International Electric Machines and Drives Conference*, pages 490–494, 2009.

[93] Kaisa Miettinen. *Nonlinear multiobjective optimization*, volume 12. Springer Science & Business Media, 2012.

[94] Kaisa Miettinen, Marko M Mäkelä, and Katja Kaario. Experiments with classification-based scalarizing functions in interactive multiobjective optimization. *European Journal of Operational Research*, 175(2):931–947, 2006.

[95] Amjad Anvari Moghaddam, Alireza Seifi, Taher Niknam, and Mohammad Reza Alizadeh Pahlavani. Multi-objective operation management of a renewable mg (micro-grid) with back-up micro-turbine/fuel cell/battery hybrid power source. *energy*, 36(11):6490–6507, 2011.

[96] Faisal A Mohamed and Heikki N Koivo. System modelling and online optimal management of microgrid using mesh adaptive direct search. *International Journal of Electrical Power & Energy Systems*, 32(5):398–407, 2010.

[97] Zahra Movahediyan and Alireza Askarzadeh. Multi-objective optimization framework of a photovoltaic-diesel generator hybrid energy system considering operating reserve. *Sustainable Cities and Society*, 41:1–12, 2018.

[98] Antonio J Nebro, Juan José Durillo, Jose Garcia-Nieto, CA Coello Coello, Francisco Luna, and Enrique Alba. Smpso: A new pso-based metaheuristic for multi-objective optimization. In *2009 IEEE Symposium on computational intelligence in multi-criteria decision-making (MCDM)*, pages 66–73. IEEE, 2009.

[99] NEMA. NEMA Insulation Classes, 2004.

[100] Taher Niknam, Rasoul Azizipanah-Abarghooee, and Mohammad Rasoul Narimani. An efficient scenario-based stochastic programming framework for multi-objective optimal micro-grid operation. *Applied Energy*, 99:455–470, 2012.

[101] Daniel Nugent and Benjamin K Sovacool. Assessing the lifecycle greenhouse gas emissions from solar PV and wind energy: A critical meta-survey. *Energy Policy*, 65:229–244, 2014.

[102] Gökhan Özkan, Phuong Hoang, Payam Ramezani Badr, Chris Edrington, and Behnaz Papari. Real-time thermal management for two-level active rectifier with finite control set model predictive control. *International Journal of Electrical Power & Energy Systems*, 131:107057, 2021.

[103] Behnaz Papari, Chris S. Edrington, Indranil Bhattacharya, and Ghadir Radman. Effective energy management of hybrid ac–dc microgrids with storage devices. *IEEE Transactions on Smart Grid*, 10(1):193–203, 2019.

[104] Mahesh A Patel, Kamran Asad, Zeel Patel, Mohit Tiwari, Purv Prajapati, Hitesh Panchal, M Suresh, Ralli Sangno, and Mohammd Israr. Design and optimisation of slotted stator tooth switched reluctance motor for torque enhancement for electric vehicle applications. *International Journal of Ambient Energy*, 0(0):1–6, 2021.

[105] D. Paul. A history of electric ship propulsion systems [history]. *IEEE Industry Applications Magazine*, 26(6):9–19, 2020.

[106] Wei Peng and Qingfu Zhang. A decomposition-based multi-objective particle swarm optimization algorithm for continuous optimization problems. In *2008 IEEE international conference on granular computing*, pages 534–537. IEEE, 2008.

[107] D. Perkins, T. Vu, H. Vahedi, and C. S. Edrington. Distributed power management implementation for zonal mvdc ship power systems. In *IECON 2018 - 44th Annual Conference of the IEEE Industrial Electronics Society*, pages 3401–3406, 2018.

[108] K Rahbar, J Xu, and R Zhang. Real-Time Energy Storage Management for Renewable Integration in Microgrid: An Off-Line Optimization Approach. *IEEE Transactions on Smart Grid*, 6(1):124–134, jan 2015.

[109] Gintaras V Reklaitis, A Ravindran, and Kenneth M Ragsdell. *Engineering optimization: Methods and applications*. Wiley New York, 1983.

[110] Jon T. Richardson, Mark R. Palmer, Gunar E. Liepins, and Mike Hilliard. Some guidelines for genetic algorithms with penalty functions. In *Proceedings of the Third International Conference on Genetic Algorithms*, page 191–197, San Francisco, CA, USA, 1989. Morgan Kaufmann Publishers Inc.

[111] Rizk M Rizk-Allah, Aboul Ella Hassanien, and Adam Slowik. Multi-objective orthogonal opposition-based crow search algorithm for large-scale multi-objective optimization. *Neural Computing and Applications*, 32(17):13715–13746, 2020.

[112] Richard S Rosenberg. Simulation of genetic populations with biochemical properties: Ii. selection of crossover probabilities. *Mathematical Biosciences*, 8(1-2):1–37, 1970.

[113] Richard S Rosenberg. Stimulation of genetic populations with biochemical properties: I. the model. *Mathematical Biosciences*, 7(3-4):223–257, 1970.

[114] Bernard Roy. The outranking approach and the foundations of electre methods. In *Readings in multiple criteria decision aid*, pages 155–183. Springer, 1990.

[115] Bernard Roy. *Multicriteria methodology for decision aiding*, volume 12. Springer Science & Business Media, 1996.

[116] Bernard Roy and Vincent Mousseau. A theoretical framework for analysing the notion of relative importance of criteria. *Journal of Multi-Criteria Decision Analysis*, 5(2):145–159, 1996.

[117] Stefan Ruzika and Margaret M Wiecek. Approximation methods in multiobjective programming. *Journal of optimization theory and applications*, 126(3):473–501, 2005.

[118] Thomas L Saaty. The analytic hierarchy and analytic network processes for the measurement of intangible criteria and for decision-making. In *Multiple criteria decision analysis*, pages 363–419. Springer, 2016.

[119] Shankar Sastry and Marc Bodson. *Adaptive control: stability, convergence and robustness*. Courier Corporation, 2011.

[120] J David Schaffer. Some experiments in machine learning using vector evaluated genetic algorithms. Technical report, Vanderbilt Univ., Nashville, TN (USA), 1985.

[121] Antonio Sciarretta and Lino Guzzella. Control of hybrid electric vehicles. *IEEE Control Systems Magazine*, 27(2):60–70, 2007.

[122] Q. Shen, B. Ramachandran, S. K. Srivastava, M. Andrus, and D. A. Cartes. Power and energy management in integrated power system. In *2011 IEEE Electric Ship Technologies Symposium*, pages 414–419, 2011.

[123] Margarita Reyes Sierra and Carlos A Coello Coello. Improving pso-based multi-objective optimization using crowding, mutation and-dominance. In *International conference on evolutionary multi-criterion optimization*, pages 505–519. Springer, 2005.

[124] E. Skjong, R. Volden, E. Rødskar, M. Molinas, T. A. Johansen, and J. Cunningham. Past, present, and future challenges of the marine vessel's electrical power system. *IEEE Transactions on Transportation Electrification*, 2(4):522–537, 2016.

[125] Nidamarthi Srinivas and Kalyanmoy Deb. Muiltiobjective optimization using nondominated sorting in genetic algorithms. *Evolutionary computation*, 2(3):221–248, 1994.

[126] Ralph E Steuer. Multiple criteria optimization. *Theory, computation and applications*, 1986.

[127] Tianfu Sun, Jiabin Wang, Antonio Griffo, and Bhaskar Sen. Active Thermal Management for Interior Permanent Magnet Synchronous Machine (IPMSM) Drives Based on Model Predictive Control. *IEEE Transactions on Industry Applications*, 54(5):4506–4514, 2018.

[128] Ruoli Tang, Xin Li, and Jingang Lai. A novel optimal energy-management strategy for a maritime hybrid energy system based on large-scale global optimization. *Applied Energy*, 228:254–264, 2018.

[129] Michael Taylor, Pablo Ralon, Harold Anuta, and Sonia Al-Zoghoul. Renewable Power Generation Costs in 2019. *International Renewable Energy Agency (IRENA)*, pages 12–13, June 2020.

[130] Lothar Thiele, Kaisa Miettinen, Pekka J Korhonen, and Julian Molina. A preference-based evolutionary algorithm for multi-objective optimization. *Evolutionary computation*, 17(3):411–436, 2009.

[131] T. V. Vu, D. Gonsoulin, F. Diaz, C. S. Edrington, and T. El-Mezyani. Predictive control for energy management in ship power systems under high-power ramp rate loads. *IEEE Transactions on Energy Conversion*, 32(2):788–797, 2017.

[132] T. V. Vu, D. Gonsoulin, D. Perkins, F. Diaz, H. Vahedi, and C. S. Edrington. Predictive energy management for mvdc all-electric ships. In *2017 IEEE Electric Ship Technologies Symposium (ESTS)*, pages 327–331, 2017.

[133] Tuyen V Vu, Dallas Perkins, Fernand Diaz, David Gonsoulin, Chris S Edrington, and Touria El-Mezyani. Robust adaptive droop control for DC microgrids. *Electric Power Systems Research*, 146:95–106, 2017.

[134] M. Weiming. Development of vessel integrated power system. In *2011 International Conference on Electrical Machines and Systems*, pages 1–12, 2011.

[135] Daniel Weisser. A guide to life-cycle greenhouse gas (GHG) emissions from electric supply technologies. *Energy*, 32(9):1543–1559, 2007.

[136] Margaret M. Wiecek. Model-based decision support methodology with environmental applications. *Interfaces*, 32(2):84–86, Mar 2002. Copyright - Copyright Institute for Operations Research and the Management Sciences Mar/Apr 2002; Last updated - 2021-09-10; CODEN - INFAC4.

[137] Andrzej P Wierzbicki. A mathematical basis for satisficing decision making. *Mathematical modelling*, 3(5):391–405, 1982.

[138] Andrzej P Wierzbicki. On the completeness and constructiveness of parametric characterizations to vector optimization problems. *Operations-Research-Spektrum*, 8(2):73–87, 1986.

[139] Andrzej P. Wierzbicki. On the role of intuition in decision making and some ways of multicriteria aid of intuition. *Journal of Multi-Criteria Decision Analysis*, 6(2):65–76, 1997.

[140] Andrzej P Wierzbicki. Reference point approaches. In *Multicriteria decision making*, pages 237–275. Springer, 1999.

[141] Hsien-Chung Wu. The Karush–Kuhn–Tucker optimality conditions in multiobjective programming problems with interval-valued objective functions. *European Journal of Operational Research*, 196(1):49–60, 2009.

[142] J. Wu, T. Yang, D. Wu, K. Kalsi, and K. H. Johansson. Distributed optimal dispatch of distributed energy resources over lossy communication networks. *IEEE Transactions on Smart Grid*, 8(6):3125–3137, 2017.

[143] Bing Yan, Peter B Luh, Guy Warner, and Peng Zhang. Operation and design optimization of microgrids with renewables. *IEEE Transactions on Automation Science and Engineering*, 14(2):573–585, 2017.

[144] Po-Lung Yu. A class of solutions for group decision problems. *Management science*, 19(8):936–946, 1973.

[145] Lofti Zadeh. Optimality and non-scalar-valued performance criteria. *IEEE transactions on Automatic Control*, 8(1):59–60, 1963.

[146] Bijan Zahedi, Lars E Norum, and Kristine B Ludvigsen. Optimized efficiency of all-electric ships by dc hybrid power systems. *Journal of Power Sources*, 255:341–354, 2014.

[147] Milan Zeleny. *Multiple criteria decision making Kyoto 1975*, volume 123. Springer Science & Business Media, 2012.

[148] Mounir Zeraoulia, Mohamed El Hachemi Benbouzid, and Demba Diallo. Electric motor drive selection issues for hev propulsion systems: A comparative study. *IEEE Transactions on Vehicular Technology*, 55(6):1756–1764, 2006.

[149] Weiwei Zhang, Fei Xiao, Jilong Liu, Zhiqin Mai, and Chaoran Li. Maximum torque per ampere control for ipmsm traction system based on current angle signal injection method. *Journal of Electrical Engineering & Technology*, 15(4):1681–1691, 2020.

[150] Z. Zhang, C. Guan, and Z. Liu. Real-time optimization energy management strategy for fuel cell hybrid ships considering power sources degradation. *IEEE Access*, 8:87046–87059, 2020.

[151] Bo Zhao, Xuesong Zhang, Jian Chen, Caisheng Wang, and Li Guo. Operation optimization of standalone microgrids considering lifetime characteristics of battery energy storage system. *IEEE transactions on sustainable energy*, 4(4):934–943, 2013.

[152] John G Ziegler, Nathaniel B Nichols, et al. Optimum settings for automatic controllers. *trans. ASME*, 64(11), 1942.

[153] Eckart Zitzler, Dimo Brockhoff, and Lothar Thiele. The hypervolume indicator revisited: On the design of pareto-compliant indicators via weighted integration. In *International Conference on Evolutionary Multi-Criterion Optimization*, pages 862–876. Springer, 2007.

[154] Eckart Zitzler and Lothar Thiele. Multiobjective evolutionary algorithms: a comparative case study and the strength pareto approach. *IEEE transactions on Evolutionary Computation*, 3(4):257–271, 1999.

[155] Eckart Zitzler, Lothar Thiele, Marco Laumanns, Carlos M Fonseca, and Viviane Grunert Da Fonseca. Performance assessment of multiobjective optimizers: An analysis and review. *IEEE Transactions on evolutionary computation*, 7(2):117–132, 2003.

[156] Nasibeh Zohrabi, Jian Shi, and Sherif Abdelwahed. An overview of design specifications and requirements for the MVDC shipboard power system. *International Journal of Electrical Power & Energy Systems*, 104:680–693, 2019.